Spermatoproteasome-deficient mice are proficient in meiotic DNA repair but defective in meiotic exit

Laura Gómez-H[1], Natalia Felipe-Medina[1], Yazmine B. Condezo[1], Rodrigo Garcia-Valiente[1], Isabel Ramos[1], Ignasi Roig[3], Manuel Sánchez-Martín[4], Dirk de Rooij[5], Elena Llano[1,2#], Alberto M. Pendas[1#].

[1] Instituto de Biología Molecular y Celular del Cáncer (CSIC-Universidad de Salamanca), 37007 Salamanca, Spain. [2] Departamento de Fisiología y Farmacología, Universidad de Salamanca, 37007 Salamanca, Spain. [3] Genome Integrity and Instability Group, Institut de Biotecnologia i Biomedicina, Universitat Autònoma de Barcelona, Cerdanyola del Vallès, Spain. [4] Departamento de Medicina, Universidad de Salamanca, 37007 Salamanca, Spain. [5] Reproductive Biology Group, Division of Developmental Biology, Department of Biology, Faculty of Science, Utrecht University, Utrecht 3584CM, The Netherlands.

[#] *To whom Correspondence should be addressed*

Abstract

Meiotic recombination generates crossovers which are essential to ensure genome haploidization. The ubiquitin proteasome system regulates meiotic recombination through its association to the synaptonemal complex, a 'zipper'-like structure that holds homologs and provides the structural framework for meiotic recombination. Here we show that the testis-specific α4s subunit (PSMA8) of the spermatoproteasome is located at the synaptonemal complex and is essential for the assembly of its activator PA200. Accordingly, synapsis-deficient mice show delocalization of PSMA8 from the synaptonemal complex. Genetic analysis of *Psma8*-deficient mice shows normal meiotic DNA repair, crossing over formation and an increase of spermatocytes at metaphase I and metaphase II which either enter into apoptosis or slip to give rise to an early spermatid arrest and infertility. Thus, spermatoproteasome-dependent histone degradation is dispensable for meiotic recombination. We show that PSMA8 deficiency alters the proteostasis of several key meiotic players such as acetylated histones, SYCP3, SYCP1, CDK1 and TRIP13 which in turn leads to an aberrant meiotic exit and early spermatid arrest prior to the histone displacement process that take place subsequently.

Introduction

Intracellular protein contents are controlled through their rates of synthesis and degradation. In the cytosol and nucleus of eukaryotic cells, most of this degradation is carried out by the ubiquitin-proteasome system (UPS). The proteasome is a highly conserved protease complex that eliminates proteins typically labeled with ubiquitin by ATP-driven proteolysis (Collins & Goldberg, 2017). All the proteasome complexes have a cylindrical catalytic core particle (CP) and different numbers of regulatory particles (RP) that regulate the access to the CP by capping it at either end (Schmidt et al, 2005). Based on its sedimentation coefficients, the 26S proteasome is formed by one CP (20S) and one or two RP (19S). The CP is composed of seven α-type subunits (α1- α7) and seven β-type subunits (β1- β7, three of which are catalytically active) arranged as a cylinder of four heptameric rings (α1-7, β1-7, β1-7, α1-7) (Collins & Goldberg, 2017; Murata et al, 2009). The two central β rings contain the proteolytic activity sites within a central chamber and the two alpha rings serve as a gate for substrate entry (Murata et al, 2009).

The 19S proteasome activator or RP is composed of 20 subunits and its association with the CP is ATP-dependent. However, there are four additional proteasome activators, the 11S regulator PA28α/β/γ (PSME1, PSME2 and PSME3) and the PA200 (PSME4) regulator that stimulate protein degradation by binding to the CP without ATP hydrolysis and independently of ubiquitin (Finley, 2009). Most proteasomes are comprised of one or two RP in combination with a CP but hybrid proteasomes enclosing a RP in one end of the CP and an activator on the other are also possible (Cascio et al, 2001).

This heterogeneity is further increased due to the existence of mammalian paralogs for the genes encoding the β1, β2 and β5 subunits which are expressed in the immunological system and constitutes the so called immunoproteasome (Griffin et al, 1998) . In addition, there is a meiotic paralog of the α4 gene (*Psma7*) that encodes a protein with a very high identity to α4 named α4s which is encoded by *Psma8* (Uechi et al, 2014). The differences between α4s/PSMA8 and α4/PSMA7 are located in the outer surface of the CP, suggesting that it provides substrate specificity (Uechi et al, 2014). In addition, the ubiquitous subunit PA200 (highest expression in the male germline) is the main activator of the proteasome in the mammalian testis (spermatoproteasome) and play its main role in spermatogenesis. Genetic depletion of *Pa200* in the mouse abolishes acetylation-dependent degradation of

somatic core histones during DNA double-strand breaks repair and delays core histone disappearance in elongated spermatids (Khor et al, 2006; Qian et al, 2013).

From a classical point of view, it is assumed that the rate of the protein ubiquitylation determines the rate of proteasome-dependent digestion (Collins & Goldberg, 2017). The resulting proteolytic products are short peptides most of which are digested by cytosolic peptidases to amino acids which are recycled by the cell for further protein synthesis (Kisselev et al, 1999). However, the proteolytic activity of the proteasome is also precisely regulated by the association of their CP and RP with E3 ubiquitin ligases and deubiquitinating enzymes (DUB) which edit their potential substrates (Inobe & Matouschek, 2014). The classical targets of the UPS are misfolded or damaged proteins with an abnormal conformations or short lived regulatory proteins, whose concentration is regulated by fine-tuning of their synthesis and degradation kinetics (Belle et al, 2006; Guo et al, 2016). Examples of the later proteins are cyclins in cell cycle control or the ZMM complex (also known as the synapsis initiation complex) in homologous recombination (Glotzer et al, 1991; Meyer & Rape, 2014; Rao et al, 2017). Functionally, the UPS is involved in a diverse array of biological processes, including protein quality control, apoptosis, immune response, cell-cycle regulation, DNA repair, and meiotic recombination.

Meiosis is a fundamental process in sexually reproducing species that generates new combinations between maternal and paternal genomes. During meiosis, two successive rounds of chromosome segregation follow a single round of replication, which leads to the production of haploid gametes from diploid progenitors (Zickler & Kleckner, 2015). This reduction in chromosome number is achieved by differences in chromosome dynamics during meiosis as compared with mitosis such as suppression of sister centromere separation (Kim et al, 2015) and also the physical connections between homologs by chiasmata. To generate these chiasmata the homologs; i) self-induce DSBs, ii) use as repair template the homolog non-sister chromatid, iii) find each other in the nucleus (pairing), iv) intimately associate (synapse) their proteinaceous core structures or axial elements (AEs) that scaffold the chromosomal DNA content, and, finally, v) connect physically through the assembly of the synaptonemal complex (SC) which provides the structural framework for all these processes to take place (Baudat et al, 2013). In yeast and mouse, the UPS regulates meiotic recombination in meiocytes via its physical association to the AEs (Ahuja et al, 2017; Rao et

al, 2017). Through the RNF212 (E3 sumo ligase)-Hei10 (E3 ubiquitin ligase) pathway, the UPS regulates the proteostatic turnover of the ZMM (Shinohara et al, 2008), which is required for efficient synapsis and crossover (Rao et al, 2017).

Given our interest in meiotic recombination and fertility (Caburet et al, 2014; Gomez et al, 2016; Llano et al, 2014) and bearing in mind the existence of a specific proteasome (i.e. spermatoproteasome) in the male germline and the pivotal role that the USP plays in meiosis, we now have explored the functional analysis of the spermatoproteasome *in vivo* through the PSMA8 subunit of the mouse. We show that PSMA8 is located at the SC and is essential for the assembly of its activator PA200. Our results show that synapsis-deficient mice show a delocalization of PSMA8 from the SC and that male mice lacking PSMA8 (and thus also PA200) show normal meiotic DNA repair despite of abnormal acetylation-dependent degradation of histones. In addition, mutant male mice show an increase of spermatocytes at metaphase I and metaphase II which either enter into apoptosis or escape to give rise to fully arrested early round spermatids leading to male infertility. Finally, we show that PSMA8 deficiency provokes an alteration of the proteostasis of several key meiotic players such as SYCP3, SYCP1, CDK1 and TRIP13 leading to an aberrant meiotic exit and deficient spermiogenesis with an early arrest in the development of round spermatid which is apparently unrelated with the classical histone displacement taking place later at mid round spermatid.

Results

Alpha4S/*Psma8* is expressed in spermatocytes and decorates the LEs

Analysis of *Psma8* mRNA expression in mouse tissues by RT-qPCR (Fig 1A) revealed that it is almost exclusively transcribed in testis (in agreement with the GTEx database (Consortium, 2015) and previous studies (Uechi et al, 2014)). We examined the expression of PSMA8 by western blot analysis of testis extracts at various postnatal ages during the first wave of spermatogenesis, which progresses more synchronously than in adult mice. The expression of PSMA8 (using a specific antibody against PSMA8 C-term, see Fig 1A (Uechi et al, 2014)), started on P12 and increased from P14 to P20 peaking at P16 (late pachytene-early diplotene). We also used an anti-PSMA8-R2 antibody raised against the whole recombinant PSMA8 protein (Fig 1B and EV1) and showed the expression of both PSMA7 (already detected at P8 when meiosis has not started) and PSMA8 (Fig 1B). In addition, we also analysed testis cell lines (including spermatogonium GC1-spg, Leydig cell TM3, and Sertoli cell TM4) showing ubiquitous expression of PSMA7 and only positive PSMA8 expression in whole testis which indicate that PSMA8 expression is restricted to cells undergoing meiosis.

To explore the subcellular localization of PSMA8, we employed the R2 antibody (PSMA7/8). Double immunolabelling of PSMA8 with the AE protein SYCP3 and with SYCP1, the transverse protein essential for synapsis (Fig 1C-D and EV2), showed that PSMA7/8 (R2 antibody) was detected from zygotene (start synapsis) to pachytene along the fully synapsed LEs where SYCP1 is localized. On the XY bivalent only the pseudoautosomal region (PAR) is synapsed and this region labeled positive for PSMA7/8 (Fig 1D). As desynapsis progresses through diplotene, PSMA7/8 was only observed at the still synapsed regions (Fig EV2). The specific C-term antibody did not produce any labelling by IF, preventing its use for this application. In order to validate the localization of PSMA8 independently of PSMA7, we *in vivo* electroporated an expression plasmid encoding GFP-PSMA8 in the mouse testis (Gomez et al, 2016). After 48 hours, the GFP-PSMA8 co-localized with SYCP3 along the synapsed LEs at pachytene (Fig 1E), corroborating its localization to the chromosomal axes of mouse spermatocytes. This result agrees with the

cytological localization of the proteasome to the LEs of the chromosomes (Rao et al, 2017). Altogether, our results indicate a specific meiotic function of the CP of the spermatoproteasome during mouse male meiosis.

PSMA8 loading is dependent on synapsis.

To investigate the possible dependence of PSMA8 localization on the degree of chromosome synapsis, we analysed spermatocytes of mice deficient for *Six6os1* (Gomez et al, 2016) and *Rec8* (Bannister et al, 2004). These meiotic mutants display different synaptic defects, from mild to more severe. Interestingly, in *Rec8*-deficient mice, where there is no true synapsis between homologues but instead in some pachynema-like cells there is "auto-synapsis" between sister chromatids (Xu et al, 2005), PSMA8 is also present at these atypical synapsed-like regions (Fig 2). However, in mice lacking the novel central element protein SIX6OS1, in which AEs completely fail to synapse in a pachytene-like stage with most homologs aligned but physically separated (Gomez et al, 2016), PSMA8 was not detected onto the LEs. Instead, a wide and disperse labelling appears decorating the chromatin of the axes (Fig 2). Together, our results indicate that PSMA8 localization to the CE is consequently dependent on the assembly of the SC either between the homologous chromosomes or the sister chromatids.

The interdependency of the transverse filament and central element proteins for the proper assembly of the SC is evidenced by the lack of loading of any of the central element subunits in the synapsis-less *Six6os1* or *Syce1* mutants (Bolcun-Filas et al, 2009; Gomez et al, 2016) . Thus, we expect delocalization of the spermatoproteasome from the LEs in the mouse mutants of the central element proteins such as SYCP1, SYCE1, SYCE2, SYCE3 and TEX12 with unexplored functional consequences for their corresponding meiotic arrest.

Purification of PSMA8 interacting proteins

The composition of the CPs and their RPs, has previously been shown by mass-spectrometry analysis of crude preparation of proteasomes from the whole testis (Bousquet-Dubouch et al, 2009). In order to gain further insight into the composition of the spermatoproteasome and specially their proteasome-interacting proteins, we purified PSMA8 interacting proteins by a single step affinity chromatography procedure using

Sepharose-bound to the antibody R1, which detects endogenous PSMA8 (in addition to PSMA7) under the fixative conditions of the chromosome spreads. As a proof of concept the most prevalent protein detected was PSMA8 followed by PSMA7 (two orders of magnitude lower; Table EV1), suggesting a moderate specificity of the R1 antibody (for PSMA8 vs PSMA7) under more native conditions than in western blot and IF. Most of the canonical subunits of the CP and RP were present within the more than 596 proteins of the PSMA8 proteome (Table EV1, using a conservative cut off, see methods). In agreement with previous results, among the two activators of the spermatoproteasome detected (PA200 and pa28γ), PA200 was the most abundant (Qian et al, 2013). In contrast with previous observations, we were not able to detect neither pa28α and pa28β nor the inducible catalytic subunits of the immunoproteasome (β1i, β2i and β5i) (Qian et al, 2013). Of interest, we detected several novel potential candidate proteasome interacting proteins (PIPs) with high confidence (Table EV2). Among ubiquitin ligases and USPs, we detected known PIPs such as chaperones HSP90-β, HSP90AB, HSP70a2, and PAC1 (PSMC1), E3 ligases like SKP1, RBX, CAND1, and USP7, USP14 and USP47. The absence of known PIPs of the 20S proteasome such as UCH37 (UCHL5) and RPN13 (ADRM1) and RPN14 (PAAF1) is noteworthy. Among new PIPs we detected, were chaperones like CCT6b and CCT2, ubiquitin ligases like TRIP12, NEDD4, TRIM36 and RAD18 (USP7), and new USPs like USP9X, USP34, USP5 and USP47. Altogether, this list of novel proteins with the potential ability to edit the ubiquitin code of the interactome of the spermatoproteasome reflects the complexity of the spermatoproteasome system.

Interestingly, we identified proteins *a priori* unrelated to the UPS such as SYCP1, TRIP13 (pachytene checkpoint), CDK1 (cyclin dependent kinase 1), SMC6 or SMC4 (subunit of the condensin complexes). Furthermore, there were proteins with important meiotic functions or involved in spermatogenesis such as DAZL (deleted in azoospermia), SPAG1 (Sperm-associated antigen 1), SPATA5 / SPATA20 (Spermatogenesis-associated protein 5 / 20), the tudor domain proteins TDRD1, TDRD6 and TDRD9, MAEL (reppresor of transposable elements) and RNF17 (see below). These PIPs could represent proteins captured during the Ub-dependent targeted degradation as has been previously described (Verma et al, 2000) and/or proteins interacting via the Ubiquitin-independent proteasomal

degradation (UIPD) as has been shown for other subunits of the CP and especially the related subunit α4/PSMA7 (Sanchez-Lanzas & Castano, 2014).

Finally, we studied the proteins enriched in the IP through its functional (gene ontology, GO) and pathway analysis (KEGG). The results of the top GO and KEGG over-representation test were related to the proteasome complex, proteasomal catabolic process and to ribonucleoproteins. Pathway analysis were linked to spermatogenesis, cell cycle, and meiosis (Appendix).

Mice lacking PSMA8 are infertile

To study the role of PSMA8 we generated a targeted mutation in exon 1-intron1 of the murine *Psma8* gene by CRISPR/Cas9 genome editing (Fig 3A). The predicted best null mutation was selected by PCR sequencing of the targeted region of the *Psma8* gene (Fig 3B). The selected founder was crossed with wild-type (WT) C57BL/6J. Heterozygotes were crossed to yield homozygous mutant mice (knock-out, KO) which were identified by PCR (Fig 3B). Homozygous mutant mice showed no PSMA8 protein expression by western blot when analysed using two independent polyclonal antibodies raised against the whole recombinant PSMA8 protein (Figs 3C and EV1). When we analysed PSMA8 expression on mutant spermatocytes by IF (R2 antibody, Fig 3D) we obtained a weaker signal (51% less; 4.22±1,9 WT vs 2.05±1.7 KO) in the synapsed LEs of the spermatocytes in comparison with the wild type control, likely representing the PSMA7 detected by the R2 Ab (observed also in the WB; Fig 3C). These results indicate that the generated mutation is a null allele of the *Psma8* gene (herein $Psma8^{-/-}$).

Mice lacking PSMA8 did not display any obvious abnormalities but male mice were sterile. Indeed, genetic ablation of *Psma8* leads to a reduction of the testis weight (63.09% lighter; N=6) and to the absence of spermatozoa in the epididymides (Fig 4A-B). Histological analysis of adult $Psma8^{-/-}$ testes revealed the presence of apparently normal numbers of spermatogonia, spermatocytes, Sertoli cells and Leydig cells (Fig 4B). Mouse seminiferous tubules can be classified from stage I to XII by determining the groups of associated germ cell types in histological sections. Following these criteria, the spermatogenic process in the mutant testes proceeds normal up to the diplonema spermatocytes in epithelial stage XI. Spermatocytes in meiotic divisions were seen to occur at epithelial stage XII but our counts

by squashed analysis of seminiferous tubules revealed the presence of increased numbers of these cells compared to in WT testes (Fig 4C), suggesting a delay in the completion of the meiotic divisions. Together with meiotic divisions, massive numbers of apoptotic cells can be seen that from their size are most likely round spermatids. Indeed, seminiferous tubules in PSMA8 deficient testes contain few if any normal round spermatids and the ones present were often apoptotic, no elongating spermatids were observed (Fig 4B). FACs analysis of whole cells from seminiferous tubules was carried out to verify this conclusion. The results obtained sustained the presence of the haploid compartment in *Psma8*$^{-/-}$ testes (Fig 4D). Taken together, we conclude that the PSMA8 deficiency causes a delay during the meiotic divisions with a relative accumulation of spermatocytes at metaphase I/II and that the resulting round spermatids enter apoptosis soon after their formation, leading to non-obstructive azoospermia (NOA) and consequently to infertility. We verified the arrest by lack of immunolabelling with TNP1 and TNP2 (Fig EV3A-B), two transition proteins involved in the replacement of histones by protamines at later stages of spermiogenesis (Barral et al, 2017). We also analysed the presence of H2AL2 (absent from mutant spermatids, see Fig EV3C), a transition histone essential for the first replacement of histones by TNP1 and TNP2 before protamine incorporation (Barral et al, 2017).

The core subunit PSMA8 co-immunoprecipitates PA200 (Table EV1), an activator of the spermatoproteasome that mediates the acetylation-dependent (ubiquitin independent) degradation of histones in response to DNA damage (Qian et al, 2013). Given the stoichiometric relationship between the CP and RP, we analysed the expression of PA200 by western blot. We observed a complete loss of expression in *Psma8*-deficient mice (undetectable signal, Fig 5A). Similar to PSMA8, PA200 decorates also the LEs of the wild type spermatocytes (Fig 5B). Accordingly, we did not detect PA200 in the LEs of mutant spermatocytes. These results indicate that PSMA8 is necessary or promotes the assembly of PA200 to the CP. Thus the *Psma8* mutation is functionally a double mutant of both PSMA8 and pa200 subunits thus constituting a spermatoproteasome-null mouse mutant.

Psma8 deficient spermatocytes show normal DSB repair, synapsis/desynapsis but have abnormal metaphases I and II.

Metaphase I accumulation can occur either because of a difficulty to enter anaphase or because of abnormal events during meiotic prophase I in *Psma8*$^{-/-}$ spermatocytes leads to a checkpoint mediated delay. Given that *pa200*-deficient mice show defects in somatic DNA repair and acetylation-dependent degradation of histones, we tested meiosis progression, DSB processing, and synapsis in *Psma8*$^{-/-}$ spermatocytes.

To evaluate the role of PSMA8 in meiotic progression and DNA repair, we initially analysed the assembly/disassembly of the SC by monitoring the distribution of the TF protein SYCP1 as co-labelling of SYCP3 and SYCP1 highlights regions of synapsis in wild type testes. We did not observe differences in the synapsis and chromosome behaviour from zygotene to pachytene and during the desynapsis process from diplotene to diakinesis (Fig EV4). The fraction of spermatocytes in metaphase I was increased (1.56±0.6% WT vs 6.7±0.5 KO; increase 77% Table EV3) as well as the number of cells in stage XII and both were apoptotic by Caspase or TUNEL staining (Fig 6A-B). However, the accumulation of metaphase I was not an arrest since we observed cells at the interkinesis stage (by DAPI staining) and also at metaphase II (0.92±1.0 WT vs 8.32±3.3 KO; increase 89%), though a fraction of them were also apoptotic (Table EV3) and showed aberrant labelling of SYCP3 in their centromeres (no SYCP3 labelling is observed in metaphase II chromosomes in wild type cells, Fig 6C). Finally, aberrant round spermatids were observed showing a very fragmented heterochromatin after DAPI staining (Fig 6D). We could no detect any further stage of spermiogenesis in the chromosome spreads (lack of elongating spermatids by immunolabelling for transition proteins, Fig EV3A-C) nor in the histological sections (Fig 4B) indicating that the PSMA8 deficiency leads to an arrest at early round spermatid.

We next studied the kinetics of DSB repair during meiosis. Meiotic DSBs are generated by the nuclease SPO11 and are then resected to form ssDNA ends that invade into the homologous chromosome. DSBs are marked by the presence of phosphorylated H2AX (γ-H2AX) (Rogakou et al, 1998), which is catalyzed by ATM during a first wave (leptotene) and ATR during the following waves (Jiang et al, 2018). The γ-H2AX distribution in mutant spermatocytes resembles that of wild-type cells in early prophase I (leptonema, WT

82.2±19.6 and KO 81.6±26.7) (Table EV4). As synapsis proceeds to pachytene (similarly in the spermatocytes from *Psma8*$^{-/-}$; see Figs 7A and EV5A), γ-H2AX staining diminished in the autosomes of both wild type and mutant spermatocytes (WT 1.3±0.8 and KO 1.2±0.6, respectively, Figs 7A and EV5A) and appeared mainly at the sex body. From diplotene to diakinesis, γ-H2AX labelling is further decreased in the spermatocytes of both genotypes (Fig EV5A). We next analysed if DSBs were processed properly during early stages of recombination. To do that we first studied the distribution of RAD51, a recombinase that promotes homologous strand invasion at the early recombination nodules (Mimitou & Symington, 2009). In wild-type zygonema spermatocytes, RAD51 assembles on numerous foci along the AEs/LEs and finally disappears towards pachytene, with the exception of the unsynapsed sex AEs (Figs 7B and EV5B). We did not observe differences in the number of foci between wild type and *Psma8* deficient spermatocytes from leptotene to late pachytene (Table EV4). Because defective DNA repair finally abrogates crossing over formation (Dai et al, 2017), we then analysed the foci distribution of MLH1, a mismatch repair protein (marker of crossover sites) that functions in the resolution of joint molecules at the end of crossover formation (Moens et al, 2007). We observed a similar value in the KO (24.9±2.5 foci) in comparison with the wild-type (23.3±2.4 foci; Fig 7C). These results indicate that the repair of meiotic DSBs and synapsis/desynapsis proceeds normally during prophase I in the absence of PSMA8 and is not responsible for the observed metaphase I accumulation.

PSMA8 deficiency abolishes H4ac turnover from late prophase to round spermatid

During spermatogenesis most of the histones are replaced by basic transition proteins, and ultimately by protamines facilitating chromatin compaction. Hyperacetylation of core histones during this process, and specially acetylation of H4, is supposed to play a pivotal role in the initiation of the histone displacement and chromatin ultracondensation (Pivot-Pajot et al, 2003; Shang et al, 2007). In addition, H4ac participates in meiotic DNA repair, chromatin-wide expansion of H2AX phosphorylation and the formation of crossovers during male meiosis (Jiang et al, 2018).

To understand the acetylated-dependent degradation of histones by spermatoproteasome, we measured the acetylation status of three core histones H2acK5, H3ac and H4ac in chromosome spreads by double IF for SYCP3 and the corresponding acetylated histones (Fig

8A-C). This procedure enables a more precise staging of the spermatocytes and a more precise way to quantitate the signals than with the peroxidase immunostaining (IHC) of testis sections (Qian et al, 2013). As expected, the loss of PSMA8 (and pa200) leads to the accumulation of H2acK5, H3ac and H4ac though to a different degree, being the most affected H2acK5, a fact that has been linked to defects in somatic DNA repair.

The results show that the levels of H2acK5, H3ac and H4ac are moderated from pachytene to diakinesis with a relative increase of all of them during the later stages of prophase I in the *Psma8*$^{-/-}$ (see Fig. 8A-C and EV6-EV8). We did not detect further staining of H2acK5 and H3ac between late diakinesis spermatocytes and round spermatids in the wild type and arrested spermatids in the mutant cells. In contrast, H4ac also labeled metaphase I chromosomes (whole chromosomes and especially centromeres), interkinesis nuclei and arrested round spermatids, with greater intensity in the mutant cells than in the wild type (Fig 8C).

A role of H4ac in the three waves of H2AX phosphorylation has been recently revealed (Jiang et al, 2018). Despite the slight accumulation of H4ac in mutant prophases, we did not observe defects in this process through the comparison of γ-H2AX staining between WT and *Psma8*-deficient spermatocytes (leptonema and zygonema) including the expansion of γ-H2AX staining to the chromatin of the sex body (in pachynema) by a DMC1-mediated ATR phosphorylation mechanism. This result further support the notion that loss of acetylation-dependent degradation of histones through the spermatoproteasome has no physiological impact onto the meiotic recombination process. In early and round spermatid the only acetylated histone showing labelling is H4ac. Accordingly, H4ac is the only acetylated histone showing an accumulation in the arrested spermatid from spermatoproteasome-deficient mice (Figs 8C and EV8).

Histone displacement, through histone ac-dependent degradation, occurs in round spermatids during the middle of their elongating development (Rathke et al, 2014) and mice lacking pa200 (*Psme4*$^{-/-}$) are fertile (subfertile) and their spermatocytes are not arrested at any stage and generate functional spermatozoa (Khor et al, 2006). The presence of the malformed spermatids in the *Psme4*$^{-/-}$ tubules has been explained by the accumulation of acetylated histones (histone displacement) which in turns leads to a delay in the

disappearance of the core histones provoking apoptosis (Qian et al, 2013). This is in contrast with the infertility and aberrant transition from metaphase I to early round spermatid stage in the *Psma8* mutant. Thus, this phenotype is more severe and cannot be attributed to accumulation of acetylated histones in spermatids (H4Kac) that could provoke defects in the canonical histone displacement process during mid spermiogenesis.

PSMA8 deficiency is more severe than the pa200 single mutant and that in pa200 and pa28γ double mutant which do not arrest their spermatogenesis despite being infertile *in vivo* but not *in vitro* (spermatozoa are not motile but can fertilize *in vitro*, (Huang et al, 2016)). Thus, this genetic analysis shows that the PSMA8-dependent CP has biochemical functions independently of the activators pa200 and pa28γ. Our proteomic analysis together with others (Uechi et al, 2014) further support this notion and indicate that the PSMA8-containing CP can be associated with other regulators such as the 19S subunit, expanding its substrate promiscuity.

Proteasomal activity in the *Psma*8-deficient mice

We next investigated the biochemical activity of the testis extracts lacking spermatoproteasomes by measuring the chymotrypsin-like activity (corresponding to the catalytic subunit β1), caspase like activity (corresponding to the β5) and the trypsin-like activity (β3) by a standard fluorogenic assay (Gomes et al, 2009) in the presence and absence of SDS (activated proteasome). The results show that the proteasome activity in the *Psma8*-deficient testis extracts is not noticeably down-regulated in comparison with the WT testis extracts. The trypsin-like activity (ARR) was the only proteolytic function with a slight reduction in the KO (see Fig 9A).

Overall, these results point show that the spermatoproteasome-deficient testis does not have a drastic reduction of its general proteasome activity, which is likely due to the presence of Pa28α (*Psme1*), β (*Psme2*) and Pa28γ (*Psme3*) and/or 19S RP complexed to PSMA7-dependent CP given that *Psme1*, *Psme2* and *Psme3* (and the *Rpt1-14*) genes are actively transcribed in mouse spermatocytes (see dataset1 in (da Cruz et al, 2016)).

To ascertain the degree of activity *in vivo*, we first investigated the steady state levels of protein ubiquitination and acetylation (targeted substrates of spermatoproteasome) in testis

during mouse meiosis. By way of IF, we analysed chromosome spreads of spermatocytes using ubiquitin antibodies (Figs 9B and EV9). Contrary to the expected, the results show a slight decrease in the mutant spermatocytes at pachytene and diplotene stages (first stage with relevant labelling, [Fig 9B (upper panel) and EV9]. Similar results were obtained by western blot against ubiquitin from whole extracts of testis (Fig 9C). Because the existing crosstalk between the SUMOylation and the ubiquitylation pathway in the context of protein degradation and its relevance in for crossing over designation and chromosome cohesion (Ding et al, 2018; Rao et al, 2017), we also analysed the pattern of whole sumoylation (SUMO1 and SUMO2/3) during prophase I by IF (Figs 9B and EV10). The results show similar levels of sumoylation in the *Psma8*-deficient spermatocytes (Fig EV10) with the exception of a slight decrease of SUMO2/3 in the late diplotene. These results are in contrast with the observed increase in the sumoylation state of cultured spermatocytes treated with the proteasome inhibitor MG132 (Rao et al, 2017) and suggest a more specific function of the spermatoproteasome in the protein degradation pathway.

Finally, we also roughly evaluated the state of acetylated proteins by western blot, given the acetylated-dependent degradation of histones by PSMA8-containing spermatoproteasomes (Fig 9C). Though the pattern of bands obtained in the western blots are not identical between wild type and mutant extracts (due also to the absence of large spermatids and spermatozoa in the mutant), overall the amount of acetylated signal detected was moderately increased in the *Psma8* mutants (Fig 9C). Altogether, our results indicate that *Psma8*-deficient mice do not show an accumulation of ubiquitinated (rather a slight decrease is observed) or acetylated proteins in their testis and suggest a specific function of the spermatoproteasome in the controlled degradation of proteins during the spermatogenesis.

Interactors of PSMA8 in mouse testis

We reasoned that additional substrates might accumulate in the absence of a functional spermatoproteasome. We focused our attention on potential proteins immunoprecipitated with anti-PSMA8 in testis extracts that in principle could explain the meiotic phenotype. Among the list of interactors, we focused on the intermediate filament SYCP1. Because SYCP1 mutant mice are infertile, but otherwise healthy (de Vries et al,

2005), we analysed in more detail the interaction of SYCP1 with PSMA8 and its localization during meiosis (Fig 10). We co-transfected *Sycp1* with *Psma8* in HEK293T cells and we obtained co-IP between SYCP1 and PSMA8 (Fig 10A).

Despite the observation that SYCP1 is properly loaded to the synapsed LEs concomitant with chromosome synapsis from zygotene to pachytene and also removed from desynapsed regions (Fig EV3) we only observed an abnormal accumulation of SYCP1 around *Psma8*-deficient metaphase I. This pattern of SYCP1 is never observed in wild type controls (see Fig 10B). However, the widespread labelling surrounding the whole spermatocyte suggests defective degradation with unknown functional consequences in the progression of meiosis.

Because the IP procedure could capture proteins interacting via the UIPD (Sanchez-Lanzas & Castano, 2014), we carried out a validation approach of additional meiotic candidate interactors by co-IP with PSMA8 making use of the same heterologous system of HEK293T cells. These include TEX30, PIWIL1, PIWIL2 and CDK1. All protein-protein interaction assays carried out were negative (Fig EV11) with the exception of the cyclin dependent kinase CDK1 (see Fig 11A). Because of the relevance of CDK1 in metaphase transition and to validate it as a candidate interactor, we first determined by western blot and IF the expression levels of CDK1. The results clearly show that there is more CDK1 (but not the related kinase CDK2 (Fig 11B-C) in the centromeres of metaphase I chromosome from mutant cells (Fig 11B; 19.7±13.4 KO vs 9.6±5.4 WT; increased of 49,2 %). Similar results were obtained by western blot of whole testis extracts (Fig 11D). In order to determine if the increase expression of CDK1 correspond to its active or inactive phosphorylated form, we made use of an antibody against CDK1-tyr15-p (inactivating modification, Fig 11E). The results show no differences in the labelling at the centromeres of the metaphase I chromosomes. Overall these results indicate that there is more active CDK1 in the mutant metaphase I cells. We also analysed the expression levels of the endogenous separase inhibitor securin (PTTG1), a well-known substrate of the proteasome through the E3 ubiquitin ligase Anaphase Promoting Complex/Cyclosome (APC/C). Securin overexpression also delays anaphase I entry in mouse oocytes (Marangos & Carroll, 2008). Our analysis by IF and western blot show similar levels of PTTG1 (Fig 11F), which validates the specific

accumulation of CDK1 in mutant spermatocytes. Taken together, we suggest that loss of PSMA8 provokes an increase in CDK1 levels at metaphase I which would lead to the observed delay and accumulation of metaphase I / metaphase II that finally results in apoptotic plates.

The role of CDK1 in metaphase-anaphase transition is complex and has a multifaceted function. CDK1 inhibits and activates APC/C by promoting the Spindle assembly checkpoint (SAC) and by a SAC-independent mechanism. The balance between this opposing functions determines cyclin B1 destruction and separase activation giving rise to cohesin cleavage and anaphase onset (Hellmuth et al, 2015). Experimentally, in mouse oocytes *in vivo,* it has been observed that high CDK1 levels can lead to SAC activation (Rattani et al, 2014).

Because CDK1 activates APC/C^{Cdc20} as well as the SAC, it has both positive and negative effects on APC/C^{Cdc20} activity (Rattani et al, 2014). Based on the normal expression levels of PTTG1 in *Psma8*$^{-/-}$ metaphase I cells in comparison with the control, it can be argued that there is no precocious APC activation in the *Psma8*-deficient cells (Fig 11F). Given that in oocytes CDK1 activation of the SAC is dominant over the activation of APC^{Cdc20} (Rattani et al, 2014), we suggest that the prior effect is acting in the *Psma8*-deficient spermatocytes. Establishing how CDK1 promotes the SAC is still unresolved in oocytes and even more unknown in spermatocytes.

To investigate the structural basis of the PSMA8 localization in the SC and bearing in mind the accumulation of SYCP1 in the spermatocytes lacking PSMA8, we used a candidate gene approach to identify additional putative interactors of PSMA8. We co-transfected *Psma8* with cDNAs encoding each of the known central element proteins (SIX6OS1, SYCE1, SYCE2, SYCE3, and TEX12), transverse filament protein SYCP1, AE protein SYCP3 (Figs 10A, 12A and Fig EV11). As positive controls we used the well-known interaction between SYCE2 and TEX12 (Davies et al, 2012). Surprisingly, we detected co-immunoprecipitation between PSMA8 with SIX6OS1, SYCP1 and SYCE3. Because SYCP3 form filamentous structures in the cytoplasm of transfected cells named polycomplexes (Winkel et al, 2009), co-expression of an interacting protein with SYCP3 may lead to its

recruitment to the polycomplexes (Gomez et al, 2016), an indication of protein interaction. We obtained self assembled higher structures when *Psma8* was co-transfected with *Sycp3* (Fig 12B). This SYCP3-dependent cytological interaction was no observed when *Psma7* was co-transfected, further validating the specificity of the interaction given the extensive protein indentity between both PSMA8 and PSMA7. Because of the high complex structures of transfected SYCP3 we were not able to IP SYCP3 (either using a tag or antibodies against the protein) preventing reciprocal co-IP experiments with PSMA8. In order to validate this interaction *in vivo*, we analysed in detail SYCP3 in mouse mutant spermatocytes. We observed SYCP3 aggregates in the nuclei of the *Psma8*-deficient spermatocytes during metaphase I (Fig 12C). This accumulation of SYCP3 is later on manifested in the *Psma8*$^{-/-}$ metaphases I/II by an abnormal SYCP3 labelling of the kinetochores of the metaphase II chromosomes (WT metaphase II never show SYCP3 labelling, Fig 12C). Interestingly, it has been previously shown that cultured spermatocytes chemically treated with the proteasome inhibitor MG132 form SYCP3 aggregates (Rao et al, 2017). Altogether, our results suggest that SYCP3 is being targeted for degradation by the spermatoproteasome and that in the absence of PSMA8 its accumulation could be mediating in part the arrest and apoptosis of the spermatocytes.

Because overexpressed PSMA8 is able to incorporate into the CP of the somatic proteasome (Uechi et al, 2014), our results should be interpreted in terms of proteasome/spermatoproteasome interactions with the SC proteins and not exclusively to direct interaction with PSMA8. The relationship of the spermatoproteasome with the SC has not been previously analysed in detail in mammals and our results support the idea of a physical anchorage or recruitment to the SC especially through SYCP3, possibly facilitated or mediated by SYCP1, SIX6OS1 and SYCE3 as their most relevant structural partners. Supporting this notion, the Zip1 transverse filament protein of the yeast SC, is the subunit that participates in the recruitment of the proteasome to the SC (Ahuja et al, 2017) which suggests an evolutionary conservation of the mechanism.

TRIP13 levels are increased in *Psma8*-deficient spermatocytes

Among the "captured" proteins with PSMA8 in the IP, we chose to study TRIP13, a pleiotropic AAA-ATPase (AAA-ATPases associated with diverse cellular activities) (Pch2 in yeast) that participates in meiotic DNA repair and chromosome synapsis through HORMAD interaction and somatic SAC proficiency through MAD2 interaction (Bolcun-Filas et al, 2014; Roig et al, 2010; Wojtasz et al, 2009; Yost et al, 2017). We first conducted IF analysis of TRIP13 in *Psma8*-deficient and WT spermatocytes (not analysed before). The results (using two independent antibodies) show a sharp labelling of the telomeres starting at zygotene where two dots corresponding to the telomeres are observed faintly. As synapsis progresses, the two dots become more intense and get very closed or even appear as a single dot at pachytene (Figs 13A and EV12). A very faint labelling could also be observed at the axes of the autosomes and XY. From diplotene to dyakinesis the labelling at the telomeres decreases (Figs 13A and EV12). However, the intensity of the labelling during prophase I was enhanced in the mutant (5.2±1.5 in pachynema and 4.1±1.4 in late diplonema) in comparison with the wild type (2.9±1.4 in pachynema and 2.3± 1.1 in late diplonema; Fig 13A). Finally, at metaphase I a faint labelling appears at the sister kinetochores of the *Psma8*-deficient spermatocytes which is never observed in the wild type, resembling somatic cells (Wang et al, 2014). These results suggest that TRIP13 is accumulating in the absence of a functional spermatoproteasome.

We next confirmed by co-IP experiments in transfected HEK293T cells that TRIP13-GFP is able to co-immunoprecipitate with Flag-PSMA8 (Fig 13B), further supporting the results obtained in the testis IP experiment and mass spectrometry.

Because HORMADs are one type of the several downstream effectors of TRIP13, we also analysed the distribution and expression of HORMAD1 and HORMAD2, two proteins involved in several processes of meiotic DNA repair and synapsis surveillance mechanisms (Daniel et al, 2011; Wojtasz et al, 2012). We did not observe differences in the expression levels and/or distribution of HORMAD1/2 in the mutant as compared to the WT spermatocytes (Fig EV13A-B), which is indicative of a normal DNA repair and synapsis.

The functional consequences of an increased expression/stability of TRIP13 has not been determined and cannot be predicted due to the many *in vivo* processes in which TRIP13, through other downstream effectors such as p31 (comet) and MAD2, play a role in meiosis.

Nonetheless, it has been shown in the worm *C. elegans* that in the absence of TRIP13, MAD2 recruitment to the kinetochores was delayed and that in addition to its role in checkpoint silencing, TRIP13 also contributes to spindle checkpoint activation (Nelson et al, 2015). Thus, it can be postulated that an excess of TRIP13 would increase MAD2 loading to kinetochores delaying mitotic exit as we have observed in the meiosis of the *Psma8*-deficient spermatocytes.

Discussion

We have shown that the genetic depletion of one structural α-subunit of the spermatoproteasome leads to male mouse infertility. Despite of the proteasome being one of only three tissue-specific proteasomes present in mammalians (together with the immunoproteasome and the thymoproteasome), little is known about its biochemical and physiological function. The groundbreaking work from the Qiu lab showing the acetyl-histone preference of the pa200 subunit of the spermatoproteasome (Qian et al, 2013) yielded novel insight in the field of proteasome-dependent degradation of non-ubiquitylated proteins. However, we have shown that the plasticity of the composition of the spermatoproteasome can explain the mild phenotype of the genetic depletion of pa200 (males are fertile), given the existence of other regulators (activators that can be associated to the CP). Thus, the genetic depletion of the *Psma8* gene generates a more severe male phenotype (it is in fact a double mutant of *Psma8* and pa200) in which it can be ascertained an essential role of the spermatoproteasome during spermatogenesis. Our results show that spermatoproteasome-deficiency provokes severe defects in protein turnover of key meiotic players that affect metaphase I / II exit but not the complex process of meiotic recombination that takes place during the prophase I (crossover). By using a candidate approach of PIPs, we have identified CDK1 and TRIP13 as being the crucial proteins that have an abnormal expression pattern during metaphase I in *Psma8*$^{-/-}$ deficient spermatocytes. Given the key roles in all aspects of mitotic/meiotic division that CDK1 and TRIP13 play (including SAC activation), the

accumulation of aberrant metaphase I /II spermatocytes in *Psma8*$^{-/-}$ deficient mice is to be expected.

Another group of proteins found to be deregulated in the spermatoproteasome-deficient mice are the SC structural proteins SYCP1 and SYCP3. The exact contribution of the accumulation of SYCP1 in the cytoplasm of *Psma8*$^{-/-}$ spermatocytes (only detectable in squashed spermatocytes) cannot be experimentally analysed. However, the coiled-coil structure and self-assemblies abilities of SYCP1 strongly suggest a functionally detrimental consequence. Similarly, the presence of SYCP3 in metaphase I spermatocytes and the resulting accumulation at the kinetochores of metaphase II cells, where no SYCP3 is observed in wild type cells, also suggest a functional consequence in the meiotic accumulation and its entrance in apoptosis which is even more pronounced in metaphase II than in metaphase I (Table EV3).

Finally, and as expected from the previous work on pa200 function, *Psma8*-deficient spermatocytes also accumulated acetylated histones. However, given the arrest of very early round spermatids during *Psma8*-deficient spermatogenesis where massive acetylation of histones has yet to occur and only a relatively small accumulation of H4ac is observed, it is difficult to argue histone displacement as the molecular mechanism underlying the spermatogenic defect.

The spermatoproteasome through its complex interactome would serve as a hub for the fine tuning coordination of several fundamental key molecules of the spermatogenic process such as analysed during the present work (SYCP1, TRIP13, CDK1 and acetyl-histones). Our data suggest that deregulation of proteostasis of several meiotic proteins leads to the observed chaotic end of meiosis and the spermatogenic arrest. Thus, we favor an explanation in which the joint contribution of several pathways is responsible for the observed infertility.

From an organismal point of view, *Psma8* transcription is mainly restricted to the testis (Fig 1A). However, as is the case with several other testis genes (named cancer testis genes (Bruggeman et al, 2018)), its expression may be deregulated in some human tumors. Accordingly, *PSMA8* is expressed in Burkitt lymphoma cell lines (i.e. Daudi or Toledo), large B-cell lymphoma and cutaneous melanoma (www.cbioportal.org). The observed

PSMA8 upregulation seems to be mediated by a MYC-dependent transcription binding site present in the proximity of the transcription start site (TSS) of the human *PSMA8* gene (Planello et al, 2014; Rouillard et al, 2016). In addition, this TSS is regulated by DNA methylation by DNMT3B, a methyl transferase involved in lymphomagenesis (Hlady et al, 2012). Thus, we suggest that this MYC binding site is responsible for the overexpression of Psma8 in Myc-dependent tumors such as Burkitt lymphomas and cutaneous melanoma (TCGC). Also in relation with human disease, protein degradation is one of the top cellular functions found in an unbiased differential proteomic profiling of spermatozoa proteins from infertile men with varicocele (Agarwal et al, 2015). In this analysis, PSMA8 is among the top 7 in the list of proteins that are differentially expressed, suggesting a causal role in the severity of the disease.

Taken together, and bearing in mind the PSMA8 dependency of the mouse male germline, we suggest that the spermatoproteasome may be an effective target for male contraception and for the treatment of human malignancies.

Acknowledgements

We wish to express our sincere thanks to Drs. Liu (Univ of Toledo, USA), A. Toth (Dresden Univ. Germany), J. Schimenti (Cornell Univ, USA), and S. Khochbin (Univ. of Grenoble, France) for providing antibodies (TRIP13, Hormad1, Hormad2, H2AL2) and reagents (plasmid and mice). This work was supported by BFU2017-89408-R. LGH and NFM are supported by European Social Fund/JCyLe grants (EDU/1083/2013 and EDU/310/2015) and YBC by a FPI grant from the MINECO. IR was supported by BFU2016-80370-P. The proteomic analysis was performed in the Proteomics Facility of Centro de Investigación del Cáncer, Salamanca, Grant PRB3 (IPT17/0019 - ISCIII-SGEFI / ERDF).

Material and Methods

Immunocytology. Testes were detunicated and processed for spreading using a conventional "dry-down" technique or squashing. Antibody against the C-term of PSMA8 was a gift from Dr. Murata (Univ of Tokyo, Japan) and has been previously described (Uechi et al, 2014). Rabbit polyclonal antibodies against PSMA8 were developed by ProteintechTM (R1 and R2) against a fusion protein of poly-His with full length PSMA8 (pET vector) of mouse origin (see Fig EV1 for validation) and was used to validate the immunofluorescence and western

results. The primary antibodies used for immunofluorescence were rabbit αSYCP1 IgG ab15090 (1:200) (Abcam), rabbit anti-γH2AX (ser139) IgG #07-164 (1:200) (Millipore), ACA or purified human α-centromere proteins IgG 15-235 (1:5, Antibodies Incorporated), mouse αMLH1 51-1327GR (1:5, BD Biosciences), mouse αSYCP3 IgG sc-74569 (1:100), rabbit αRAD51 PC130 (1:50, Calbiochem), Mouse αCDK1 sc-54 (1:20 IF; 1:1000 wb, Santa Cruz), rabbit αCDK1 Tyr15p #4539 (1:10, Cell Signaling), rabbit αCDK2 sc-6248 (1:20, Santa Cruz), rabbit αPTTG1 serum K783 (1:20 IF, 1:1000 wb), rabbit αTRIP13 19602-1-AP (1:20, Proteintech), rabbit αTNP1 and αTNP2 (1:60, from Dr. Stephen Kistler), rabbit αH2AL2 (1:100, from Dr. Saadi Khochbin), rabbit αPa200 (1:20, Bethyl A303-880A), rabbit α-Caspase3 #9661 (1:30, Cell Signaling), rabbit αH2AacK5 ab45152 (1:20, Abcam), Rabbit αH3ac (K9 and K14) #06-599 (1:20, Millipore), Rabbit αH4ac (K5, K8, K12 and K16) #06-598 (1:20, Millipore), Rabbit αAc-Lys #06-933 (1:1000 wb, Upstate), Mouse αUbiquitin 11023 (1:20 IF, 1:1000 wb, QED Bioscience), Mouse αSUMO1 21C7 (1:40, ThermoFisher), Mouse αSUMO2/3 8A2 (1:30, Medimabs), Rabbit αHORMAD1 and αHORMAD2 (1:50, from Dr. Attila Toth). TUNEL staining of chromosome spreads was performed with the *in situ* cell death detection kit (Roche).

Cell lines. The HEK293, GC1-spg, leydig TM3, and sertoli TM4 cell lines were directly purchased at the ATCC and cultured in standard cell media.

Proteasome assay. The 26S proteasome assay was carried out in a total volume of 250 µl in 96 well plates with 2 mM ATP in 26S buffer using 100 µg of protein supernatants from whole extracts of mouse testis. Fluorescently labeled substrates employed were: succinyl-Leu-Leu-Val-Tyr-7-amino-4-methylcoumarin (Suc-LLVY-AMC), Z-Ala-Arg-Arg-AMC (Z-ARR-AMC, Bachem), and Z-Leu-Leu-Glu-AMC (Z-LLE-AMC) for the detection of the chymotrypsin- (β5 catalytic subunit), trypsin- (β2 catalytic subunit) and caspase- (β1 catalytic) like activity measurements respectively. The final concentration of substrate in each assay was 100 µM.

Histology. For histological analysis of adult testes, mice were perfused and their testes were processed into serial paraffin sections and stained with hematoxylin-eosin or were fixed in Bouin´s fixative and stained with Periodic acid–Schiff (PAS) and hematoxylin.

In vivo electroporation of testis. Testes were freed from the abdominal cavity and 10 µl of DNA solution (50 µg) mixed with 1µl of 10×FastGreen (Sigma Aldrich F7258) was injected in the rete testis with a DNA embryo microinjection tip. After a period of 1 h following the injection, testes were held between electrodes and four electric pulses were applied (35 V for 50 ms each pulse) using a CUY21 BEX electroporator.

MS/MS data analysis. Raw MS data were analized using MaxQuant (v. 1.5.7.4) and Perseus (v. 1.5.6.0) programmes (Cox & Mann, 2008). Searches were generated versus the Mus musculus proteome (UP000000589, May 2017 release) and Maxquant contaminants. All FDRs were of 1%. Variable modifications taken into account were oxidation of M, acetylation of the N-term and ubiquitylation remnants di-Gly and LRGG, while fixed modifications included considered only carbamidomethylation of C. The maximum number of modifications allowed per peptide was of 5. For the case of the protein group of CDK1 to 3, experimental results showed that the protein detected was CDK1.

For the PSMA8 antibodies R1 and R2, ratios of their respective iBAQ intensity versus the correspondent iBAQ intensity in the control sample were calculated. Proteins with ratio higher or equal to 5 and two or more unique peptides for at least one RP antibody were selected for ulterior analysis. Aditionally, in order to avoid filtering rare proteins, those with at least one unique peptide and one peptide for both Rabbit antibodies (R1 and R2) and none for anti-IgG were also selected for further analysis.

Functional and pathway analysis. GO and KEGG over-representation tests were performed using the R package *clusterProfiler* (Yu et al, 2012) using standard parameters except for a FDR cutoff of 0.01. KEGG pathways where some key genes (TRIP13, CDK1, SYCP1, DDX4, SYCP3, SYCE3, SIX6OS1) operate and the role of the co-immunoprecipitated proteins were studied using the R package *pathview* (Brouwer et al, 2013).

Immunoprecipitation and western blotting. 200 µg of antibody R1 and R2 were bound to 100 ul of sepharose beads slurry (GE Healthcare). Testis extracts were prepared in 50mM Tris Hcl (pH8), 500mM NaCl, 1mM EDTA 1% tritonX100. 20 mg of proteins extracts were incubated o/n with the sepharose beads. Protein-bound beads were packed into columns and washed in extracting buffer for three times. Protein were eluted in 100 mM glycine pH3. The whole immunoprecipitation of PSMA8 was performed in a buffer lacking ATP and glycerol to increase the stringency of the interactors and regulators/activators subunits.
HEK293T cells were transiently transfected and whole cell extracts were prepared and cleared with protein G Sepharose beads (GE Healthcare) for 1 h. The antibody was added for 2 h and immunocomplexes were isolated by adsorption to protein G-Sepharose beads o/n. After washing, the proteins were eluted from the beads with 2xSDS gel-loading buffer 100mM Tris-Hcl (pH 7), 4% SDS, 0.2% bromophenol blue, 200mM β-mercaptoethanol and 20% glycerol, and loaded onto reducing polyacrylamide SDS gels. The proteins were detected by western blotting with the indicated antibodies. Immunoprecipitations were performed using mouse αFlag IgG (5µg; F1804, Sigma-Aldrich), mouse αGFP IgG (4 µg; CSB-MA000051M0m, Cusabio), rabbit αMyc Tag IgG (4µg; #06-549, Millipore), mouse αHA.11 IgG MMS- (5µL, aprox. 10µg/1mg prot; 101R, Covance), ChromPure mouse IgG (5µg/1mg prot; 015-000-003), ChomPure rabbit IgG (5µg/1mg prot.; 011-000-003, Jackson ImmunoResearch), ChomPure goat IgG (5µg/1mg prot.; 005-000-003, Jackson

ImmunoResearch). Primary antibodies used for western blotting were rabbit αFlag IgG (1:2000; F7425 Sigma-Aldrich), goat αGFP IgG (sc-5385, Santa Cruz) (1:3000), rabbit αHA IgG (H6908, Sigma-Aldrich) (1:1.000), mouse αMyc obtained from hybridoma cell myc-1-9E10.2 ATCC (1:5). Secondary horseradish peroxidase-conjugated α-mouse (715-035-150, Jackson ImmunoResearch), α-rabbit (711-035-152, Jackson ImmunoResearch), or α-goat (705-035-147, Jackson ImmunoResearch) antibodies were used at 1:5000 dilution. Antibodies were detected by using ImmobilonTM Western Chemiluminescent HRP Substrate from Millipore.

Generation of plasmids. Full-length cDNAs encoding PSMA8, PSMA7, CDK1, SYCP1 and SYCP3, SYCE2, TEX12, TEX30, PIWIL1 and PIWIL2 were RT-PCR amplified from murine testis RNA. Full-length cDNAs were cloned into the EcoRV pcDNA3-2XFlag or SmaI pEGFP-C1 expression vectors under the CMV promoter. In frame cloning was verified by sanger sequencing.

Cell lines and transfections. HEK293T cell line was transfected with Lipofectamine (Invitrogen) or Jetpei (PolyPlus). Cell lines were tested for mycoplasma contamination (Mycoplasma PCR ELISA, Sigma).

Production of CRISPR/Cas9-Edited Mice. Psma8-gRNAs G71 5'- GGGCATACT CCACTTGGAAA -3' G84 5'-ACCGCGGTAAGCTGCTCCCC-3' targeting exon 1 and intron 1 were predicted at crispr.mit.edu. Psma8-sgRNAs were produced by cloning annealed complementary oligos at the BbsI site of pX330 (#42230, Addgene), generating PCR products containing a T7 promoter sequence that were purified (NZYtech), and then in vitro transcribed with the MEGAshortscript™ T7 Transcription Kit (Life Technologies). The plasmid pST1374-NLS-flag-linker-Cas9 (#44758; Addgene) was used for generating Cas9 mRNA. After linearization with AgeI, it was transcribed and capped with the mMESSAGE mMACHINE T7 Transcription Kit (AM1345; Life Technologies). RNAs were purified using the RNeasy® Mini Kit (Qiagen). RNAs (100 ng/µl Cas9 and 50ng/µl each guide RNA) were microinjected into B6/CBA F2 zygotes (hybrids between strains C57BL/6J and CBA/J)(Singh et al, 2015) at the Transgenic Facility of the University of Salamanca. Edited founders were identified by PCR amplification (Taq polymerase, NZYtech) with primers flanking exons 1 and intron 1 (Primer F 5`-CTTCTCGGTATGACAGGGCAATC-3' and R 5'- ACTCTACCTCCACTGCCAACCTG-3') and either direct sequenced or subcloned into pBlueScript (Stratagene) followed by Sanger sequencing. The wild-type and mutant allele were 222 bp and 166 bp long, respectively. The selected founder was crossed with wild-type C57BL/6J to eliminate possible unwanted off-targets. *Psma8*$^{+/-}$ heterozygous mice were re-sequenced and crossed to give rise to *Psma8*$^{-/-}$ homozygous. Genotyping was performed by analysis of the PCR products of genomic DNA with primers F and R. Mouse mutants for *Rec8* and *Six6os1* have been previously developed (Bannister et al, 2004; Gomez et al, 2016). Mice were housed in a temperature-controlled facility (specific pathogen free, spf) using

individually ventilated cages, standard diet and a 12 h light/dark cycle, according to EU laws at the "Servicio de Experimentación Animal, SEA". Mouse protocols were approved by the Ethics Committee for Animal Experimentation of the University of Salamanca (USAL). We made every effort to minimize suffering and to improve animal welfare. Blinded experiments were not possible since the phenotype was obvious between wild-type and Psma8 deficient mouse for all of the experimental procedures used. No randomization methods were applied since the animals were not divided in groups/treatments. The minimum size used for each analysis was two animals/genotype. The mice analysed were between 2 and 4 months of age, except in those experiments where is indicated.

Author contributions

LGH with the help of NFM, YBC and ELC performed the characterization of the mutant mice including the cytological and biochemical analysis. MSM carried out the Cas9 injections and the testes electroporation. RGV carried out the bioinformatics proteomic analysis. IsR carried out infertility phenotyping of mutant mice. IgR provided unpublished information and antibodies of TRIP13. DdR performed the histological analysis of the phenotype of the mutant mice. AMP and ELC designed the experiments and wrote the paper with the input of the remaining authors (DdR).

References

Agarwal A, Sharma R, Durairajanayagam D, Cui Z, Ayaz A, Gupta S, Willard B, Gopalan B, Sabanegh E (2015) Differential proteomic profiling of spermatozoal proteins of infertile men with unilateral or bilateral varicocele. *Urology* **85:** 580-588

Ahuja JS, Sandhu R, Mainpal R, Lawson C, Henley H, Hunt PA, Yanowitz JL, Borner GV (2017) Control of meiotic pairing and recombination by chromosomally tethered 26S proteasome. *Science* **355:** 408-411

Bannister LA, Reinholdt LG, Munroe RJ, Schimenti JC (2004) Positional cloning and characterization of mouse mei8, a disrupted allelle of the meiotic cohesin Rec8. *Genesis* **40:** 184-194

Barral S, Morozumi Y, Tanaka H, Montellier E, Govin J, de Dieuleveult M, Charbonnier G, Coute Y, Puthier D, Buchou T, Boussouar F, Urahama T, Fenaille F, Curtet S, Hery P, Fernandez-Nunez N, Shiota H, Gerard M, Rousseaux S, Kurumizaka H, Khochbin S (2017) Histone Variant H2A.L.2 Guides Transition Protein-Dependent Protamine Assembly in Male Germ Cells. *Molecular cell* **66:** 89-101 e108

Baudat F, Imai Y, de Massy B (2013) Meiotic recombination in mammals: localization and regulation. *Nature reviews Genetics* **14:** 794-806

Belle A, Tanay A, Bitincka L, Shamir R, O'Shea EK (2006) Quantification of protein half-lives in the budding yeast proteome. *Proceedings of the National Academy of Sciences of the United States of America* **103:** 13004-13009

Bolcun-Filas E, Hall E, Speed R, Taggart M, Grey C, de Massy B, Benavente R, Cooke HJ (2009) Mutation of the mouse Syce1 gene disrupts synapsis and suggests a link between synaptonemal complex structural components and DNA repair. *PLoS genetics* **5:** e1000393

Bolcun-Filas E, Rinaldi VD, White ME, Schimenti JC (2014) Reversal of female infertility by Chk2 ablation reveals the oocyte DNA damage checkpoint pathway. *Science* **343:** 533-536

Bousquet-Dubouch MP, Baudelet E, Guerin F, Matondo M, Uttenweiler-Joseph S, Burlet-Schiltz O, Monsarrat B (2009) Affinity purification strategy to capture human endogenous proteasome complexes diversity and to identify proteasome-interacting proteins. *Molecular & cellular proteomics : MCP* **8:** 1150-1164

Brouwer CA, Postma A, Hooimeijer HL, Smit AJ, Vonk JM, van Roon AM, van den Berg MP, Dolsma WV, Lefrandt JD, Bink-Boelkens MT, Zwart N, de Vries EG, Tissing WJ, Gietema JA (2013) Endothelial damage in long-term survivors of childhood cancer. *Journal of clinical oncology : official journal of the American Society of Clinical Oncology* **31:** 3906-3913

Bruggeman JW, Koster J, Lodder P, Repping S, Hamer G (2018) Massive expression of germ cell-specific genes is a hallmark of cancer and a potential target for novel treatment development. *Oncogene*

Caburet S, Arboleda VA, Llano E, Overbeek PA, Barbero JL, Oka K, Harrison W, Vaiman D, Ben-Neriah Z, Garcia-Tunon I, Fellous M, Pendas AM, Veitia RA, Vilain E (2014) Mutant cohesin in premature ovarian failure. *The New England journal of medicine* **370:** 943-949

Cascio P, Hilton C, Kisselev AF, Rock KL, Goldberg AL (2001) 26S proteasomes and immunoproteasomes produce mainly N-extended versions of an antigenic peptide. *The EMBO journal* **20:** 2357-2366

Collins GA, Goldberg AL (2017) The Logic of the 26S Proteasome. *Cell* **169:** 792-806

Consortium GT (2015) Human genomics. The Genotype-Tissue Expression (GTEx) pilot analysis: multitissue gene regulation in humans. *Science* **348:** 648-660

Cox J, Mann M (2008) MaxQuant enables high peptide identification rates, individualized p.p.b.-range mass accuracies and proteome-wide protein quantification. *Nature biotechnology* **26:** 1367-1372

da Cruz I, Rodriguez-Casuriaga R, Santinaque FF, Farias J, Curti G, Capoano CA, Folle GA, Benavente R, Sotelo-Silveira JR, Geisinger A (2016) Transcriptome analysis of highly purified mouse spermatogenic cell populations: gene expression signatures switch from meiotic-to postmeiotic-related processes at pachytene stage. *BMC genomics* **17:** 294

Dai J, Voloshin O, Potapova S, Camerini-Otero RD (2017) Meiotic Knockdown and Complementation Reveals Essential Role of RAD51 in Mouse Spermatogenesis. *Cell reports* **18:** 1383-1394

Daniel K, Lange J, Hached K, Fu J, Anastassiadis K, Roig I, Cooke HJ, Stewart AF, Wassmann K, Jasin M, Keeney S, Toth A (2011) Meiotic homologue alignment and its quality surveillance are controlled by mouse HORMAD1. *Nature cell biology* **13:** 599-610

Davies OR, Maman JD, Pellegrini L (2012) Structural analysis of the human SYCE2-TEX12 complex provides molecular insights into synaptonemal complex assembly. *Open biology* **2:** 120099

de Vries FA, de Boer E, van den Bosch M, Baarends WM, Ooms M, Yuan L, Liu JG, van Zeeland AA, Heyting C, Pastink A (2005) Mouse Sycp1 functions in synaptonemal complex assembly, meiotic recombination, and XY body formation. *Genes & development* **19:** 1376-1389

Ding Y, Kaido M, Llano E, Pendas AM, Kitajima TS (2018) The Post-anaphase SUMO Pathway Ensures the Maintenance of Centromeric Cohesion through Meiosis I-II Transition in Mammalian Oocytes. *Current biology : CB* **28:** 1661-1669 e1664

Finley D (2009) Recognition and processing of ubiquitin-protein conjugates by the proteasome. *Annual review of biochemistry* **78:** 477-513

Glotzer M, Murray AW, Kirschner MW (1991) Cyclin is degraded by the ubiquitin pathway. *Nature* **349:** 132-138

Gomes AV, Young GW, Wang Y, Zong C, Eghbali M, Drews O, Lu H, Stefani E, Ping P (2009) Contrasting proteome biology and functional heterogeneity of the 20 S proteasome complexes in mammalian tissues. *Molecular & cellular proteomics : MCP* **8:** 302-315

Gomez HL, Felipe-Medina N, Sanchez-Martin M, Davies OR, Ramos I, Garcia-Tunon I, de Rooij DG, Dereli I, Toth A, Barbero JL, Benavente R, Llano E, Pendas AM (2016) C14ORF39/SIX6OS1 is a

constituent of the synaptonemal complex and is essential for mouse fertility. *Nature communications* **7:** 13298

Griffin TA, Nandi D, Cruz M, Fehling HJ, Kaer LV, Monaco JJ, Colbert RA (1998) Immunoproteasome assembly: cooperative incorporation of interferon gamma (IFN-gamma)-inducible subunits. *The Journal of experimental medicine* **187:** 97-104

Guo X, Wang X, Wang Z, Banerjee S, Yang J, Huang L, Dixon JE (2016) Site-specific proteasome phosphorylation controls cell proliferation and tumorigenesis. *Nature cell biology* **18:** 202-212

Hellmuth S, Pohlmann C, Brown A, Bottger F, Sprinzl M, Stemmann O (2015) Positive and negative regulation of vertebrate separase by Cdk1-cyclin B1 may explain why securin is dispensable. *The Journal of biological chemistry* **290:** 8002-8010

Hlady RA, Novakova S, Opavska J, Klinkebiel D, Peters SL, Bies J, Hannah J, Iqbal J, Anderson KM, Siebler HM, Smith LM, Greiner TC, Bastola D, Joshi S, Lockridge O, Simpson MA, Felsher DW, Wagner KU, Chan WC, Christman JK, Opavsky R (2012) Loss of Dnmt3b function upregulates the tumor modifier Ment and accelerates mouse lymphomagenesis. *The Journal of clinical investigation* **122:** 163-177

Huang L, Haratake K, Miyahara H, Chiba T (2016) Proteasome activators, PA28gamma and PA200, play indispensable roles in male fertility. *Scientific reports* **6:** 23171

Inobe T, Matouschek A (2014) Paradigms of protein degradation by the proteasome. *Current opinion in structural biology* **24:** 156-164

Jiang H, Gao Q, Zheng W, Yin S, Wang L, Zhong L, Ali A, Khan T, Hao Q, Fang H, Sun X, Xu P, Pandita TK, Jiang X, Shi Q (2018) MOF influences meiotic expansion of H2AX phosphorylation and spermatogenesis in mice. *PLoS genetics* **14:** e1007300

Khor B, Bredemeyer AL, Huang CY, Turnbull IR, Evans R, Maggi LB, Jr., White JM, Walker LM, Carnes K, Hess RA, Sleckman BP (2006) Proteasome activator PA200 is required for normal spermatogenesis. *Molecular and cellular biology* **26:** 2999-3007

Kim J, Ishiguro K, Nambu A, Akiyoshi B, Yokobayashi S, Kagami A, Ishiguro T, Pendas AM, Takeda N, Sakakibara Y, Kitajima TS, Tanno Y, Sakuno T, Watanabe Y (2015) Meikin is a conserved regulator of meiosis-I-specific kinetochore function. *Nature* **517:** 466-471

Kisselev AF, Akopian TN, Castillo V, Goldberg AL (1999) Proteasome active sites allosterically regulate each other, suggesting a cyclical bite-chew mechanism for protein breakdown. *Molecular cell* **4:** 395-402

Llano E, Gomez HL, Garcia-Tunon I, Sanchez-Martin M, Caburet S, Barbero JL, Schimenti JC, Veitia RA, Pendas AM (2014) STAG3 is a strong candidate gene for male infertility. *Human molecular genetics* **23:** 3421-3431

Marangos P, Carroll J (2008) Securin regulates entry into M-phase by modulating the stability of cyclin B. *Nature cell biology* **10:** 445-451

Meyer HJ, Rape M (2014) Enhanced protein degradation by branched ubiquitin chains. *Cell* **157:** 910-921

Mikolcevic P, Isoda M, Shibuya H, del Barco Barrantes I, Igea A, Suja JA, Shackleton S, Watanabe Y, Nebreda AR (2016) Essential role of the Cdk2 activator RingoA in meiotic telomere tethering to the nuclear envelope. *Nature communications* **7:** 11084

Mimitou EP, Symington LS (2009) Nucleases and helicases take center stage in homologous recombination. *Trends in biochemical sciences* **34:** 264-272

Moens PB, Marcon E, Shore JS, Kochakpour N, Spyropoulos B (2007) Initiation and resolution of interhomolog connections: crossover and non-crossover sites along mouse synaptonemal complexes. *Journal of cell science* **120:** 1017-1027

Murata S, Yashiroda H, Tanaka K (2009) Molecular mechanisms of proteasome assembly. *Nature reviews Molecular cell biology* **10:** 104-115

Nelson CR, Hwang T, Chen PH, Bhalla N (2015) TRIP13PCH-2 promotes Mad2 localization to unattached kinetochores in the spindle checkpoint response. *The Journal of cell biology* **211:** 503-516

Pivot-Pajot C, Caron C, Govin J, Vion A, Rousseaux S, Khochbin S (2003) Acetylation-dependent chromatin reorganization by BRDT, a testis-specific bromodomain-containing protein. *Molecular and cellular biology* **23:** 5354-5365

Planello AC, Ji J, Sharma V, Singhania R, Mbabaali F, Muller F, Alfaro JA, Bock C, De Carvalho DD, Batada NN (2014) Aberrant DNA methylation reprogramming during induced pluripotent stem cell generation is dependent on the choice of reprogramming factors. *Cell regeneration* **3:** 4

Qian MX, Pang Y, Liu CH, Haratake K, Du BY, Ji DY, Wang GF, Zhu QQ, Song W, Yu Y, Zhang XX, Huang HT, Miao S, Chen LB, Zhang ZH, Liang YN, Liu S, Cha H, Yang D, Zhai Y, Komatsu T, Tsuruta F, Li H, Cao C, Li W, Li GH, Cheng Y, Chiba T, Wang L, Goldberg AL, Shen Y, Qiu XB (2013) Acetylation-mediated proteasomal degradation of core histones during DNA repair and spermatogenesis. *Cell* **153:** 1012-1024

Rao HB, Qiao H, Bhatt SK, Bailey LR, Tran HD, Bourne SL, Qiu W, Deshpande A, Sharma AN, Beebout CJ, Pezza RJ, Hunter N (2017) A SUMO-ubiquitin relay recruits proteasomes to chromosome axes to regulate meiotic recombination. *Science* **355:** 403-407

Rathke C, Baarends WM, Awe S, Renkawitz-Pohl R (2014) Chromatin dynamics during spermiogenesis. *Biochimica et biophysica acta* **1839:** 155-168

Rattani A, Vinod PK, Godwin J, Tachibana-Konwalski K, Wolna M, Malumbres M, Novak B, Nasmyth K (2014) Dependency of the spindle assembly checkpoint on Cdk1 renders the anaphase transition irreversible. *Current biology : CB* **24:** 630-637

Rogakou EP, Pilch DR, Orr AH, Ivanova VS, Bonner WM (1998) DNA double-stranded breaks induce histone H2AX phosphorylation on serine 139. *The Journal of biological chemistry* **273:** 5858-5868

Roig I, Dowdle JA, Toth A, de Rooij DG, Jasin M, Keeney S (2010) Mouse TRIP13/PCH2 is required for recombination and normal higher-order chromosome structure during meiosis. *PLoS genetics* **6**

Rouillard AD, Gundersen GW, Fernandez NF, Wang Z, Monteiro CD, McDermott MG, Ma'ayan A (2016) The harmonizome: a collection of processed datasets gathered to serve and mine knowledge about genes and proteins. *Database : the journal of biological databases and curation* **2016**

Sanchez-Lanzas R, Castano JG (2014) Proteins directly interacting with mammalian 20S proteasomal subunits and ubiquitin-independent proteasomal degradation. *Biomolecules* **4:** 1140-1154

Schmidt M, Haas W, Crosas B, Santamaria PG, Gygi SP, Walz T, Finley D (2005) The HEAT repeat protein Blm10 regulates the yeast proteasome by capping the core particle. *Nature structural & molecular biology* **12:** 294-303

Shang E, Nickerson HD, Wen D, Wang X, Wolgemuth DJ (2007) The first bromodomain of Brdt, a testis-specific member of the BET sub-family of double-bromodomain-containing proteins, is essential for male germ cell differentiation. *Development* **134:** 3507-3515

Shinohara M, Oh SD, Hunter N, Shinohara A (2008) Crossover assurance and crossover interference are distinctly regulated by the ZMM proteins during yeast meiosis. *Nature genetics* **40:** 299-309

Singh P, Schimenti JC, Bolcun-Filas E (2015) A mouse geneticist's practical guide to CRISPR applications. *Genetics* **199:** 1-15

Uechi H, Hamazaki J, Murata S (2014) Characterization of the testis-specific proteasome subunit alpha4s in mammals. *The Journal of biological chemistry* **289:** 12365-12374

Verma R, Chen S, Feldman R, Schieltz D, Yates J, Dohmen J, Deshaies RJ (2000) Proteasomal proteomics: identification of nucleotide-sensitive proteasome-interacting proteins by mass spectrometric analysis of affinity-purified proteasomes. *Molecular biology of the cell* **11:** 3425-3439

Wang K, Sturt-Gillespie B, Hittle JC, Macdonald D, Chan GK, Yen TJ, Liu ST (2014) Thyroid hormone receptor interacting protein 13 (TRIP13) AAA-ATPase is a novel mitotic checkpoint-silencing protein. *The Journal of biological chemistry* **289:** 23928-23937

Wojtasz L, Cloutier JM, Baumann M, Daniel K, Varga J, Fu J, Anastassiadis K, Stewart AF, Remenyi A, Turner JM, Toth A (2012) Meiotic DNA double-strand breaks and chromosome asynapsis in mice are monitored by distinct HORMAD2-independent and -dependent mechanisms. *Genes & development* **26:** 958-973

Wojtasz L, Daniel K, Roig I, Bolcun-Filas E, Xu H, Boonsanay V, Eckmann CR, Cooke HJ, Jasin M, Keeney S, McKay MJ, Toth A (2009) Mouse HORMAD1 and HORMAD2, two conserved meiotic chromosomal proteins, are depleted from synapsed chromosome axes with the help of TRIP13 AAA-ATPase. *PLoS genetics* **5:** e1000702

Xu H, Beasley MD, Warren WD, van der Horst GT, McKay MJ (2005) Absence of mouse REC8 cohesin promotes synapsis of sister chromatids in meiosis. *Developmental cell* **8:** 949-961

Yost S, de Wolf B, Hanks S, Zachariou A, Marcozzi C, Clarke M, de Voer R, Etemad B, Uijttewaal E, Ramsay E, Wylie H, Elliott A, Picton S, Smith A, Smithson S, Seal S, Ruark E, Houge G, Pines J, Kops G, Rahman N (2017) Biallelic TRIP13 mutations predispose to Wilms tumor and chromosome missegregation. *Nature genetics* **49:** 1148-1151

Yu G, Wang LG, Han Y, He QY (2012) clusterProfiler: an R package for comparing biological themes among gene clusters. *Omics : a journal of integrative biology* **16:** 284-287

Zickler D, Kleckner N (2015) Recombination, Pairing, and Synapsis of Homologs during Meiosis. *Cold Spring Harbor perspectives in biology* **7**

Agarwal A, Sharma R, Durairajanayagam D, Cui Z, Ayaz A, Gupta S, Willard B, Gopalan B, Sabanegh E (2015) Differential proteomic profiling of spermatozoal proteins of infertile men with unilateral or bilateral varicocele. *Urology* **85:** 580-588

Ahuja JS, Sandhu R, Mainpal R, Lawson C, Henley H, Hunt PA, Yanowitz JL, Borner GV (2017) Control of meiotic pairing and recombination by chromosomally tethered 26S proteasome. *Science* **355:** 408-411

Bannister LA, Reinholdt LG, Munroe RJ, Schimenti JC (2004) Positional cloning and characterization of mouse mei8, a disrupted allelle of the meiotic cohesin Rec8. *Genesis* **40:** 184-194

Barral S, Morozumi Y, Tanaka H, Montellier E, Govin J, de Dieuleveult M, Charbonnier G, Coute Y, Puthier D, Buchou T, Boussouar F, Urahama T, Fenaille F, Curtet S, Hery P, Fernandez-Nunez N, Shiota H, Gerard M, Rousseaux S, Kurumizaka H, Khochbin S (2017) Histone Variant H2A.L.2 Guides Transition Protein-Dependent Protamine Assembly in Male Germ Cells. *Molecular cell* **66:** 89-101 e108

Baudat F, Imai Y, de Massy B (2013) Meiotic recombination in mammals: localization and regulation. *Nature reviews Genetics* **14:** 794-806

Belle A, Tanay A, Bitincka L, Shamir R, O'Shea EK (2006) Quantification of protein half-lives in the budding yeast proteome. *Proceedings of the National Academy of Sciences of the United States of America* **103:** 13004-13009

Bolcun-Filas E, Hall E, Speed R, Taggart M, Grey C, de Massy B, Benavente R, Cooke HJ (2009) Mutation of the mouse Syce1 gene disrupts synapsis and suggests a link between synaptonemal complex structural components and DNA repair. *PLoS genetics* **5:** e1000393

Bolcun-Filas E, Rinaldi VD, White ME, Schimenti JC (2014) Reversal of female infertility by Chk2 ablation reveals the oocyte DNA damage checkpoint pathway. *Science* **343:** 533-536

Bousquet-Dubouch MP, Baudelet E, Guerin F, Matondo M, Uttenweiler-Joseph S, Burlet-Schiltz O, Monsarrat B (2009) Affinity purification strategy to capture human endogenous proteasome complexes diversity and to identify proteasome-interacting proteins. *Molecular & cellular proteomics : MCP* **8:** 1150-1164

Brouwer CA, Postma A, Hooimeijer HL, Smit AJ, Vonk JM, van Roon AM, van den Berg MP, Dolsma WV, Lefrandt JD, Bink-Boelkens MT, Zwart N, de Vries EG, Tissing WJ, Gietema JA (2013) Endothelial damage in long-term survivors of childhood cancer. *Journal of clinical oncology : official journal of the American Society of Clinical Oncology* **31:** 3906-3913

Bruggeman JW, Koster J, Lodder P, Repping S, Hamer G (2018) Massive expression of germ cell-specific genes is a hallmark of cancer and a potential target for novel treatment development. *Oncogene*

Caburet S, Arboleda VA, Llano E, Overbeek PA, Barbero JL, Oka K, Harrison W, Vaiman D, Ben-Neriah Z, Garcia-Tunon I, Fellous M, Pendas AM, Veitia RA, Vilain E (2014) Mutant cohesin in premature ovarian failure. *The New England journal of medicine* **370:** 943-949

Cascio P, Hilton C, Kisselev AF, Rock KL, Goldberg AL (2001) 26S proteasomes and immunoproteasomes produce mainly N-extended versions of an antigenic peptide. *The EMBO journal* **20:** 2357-2366

Collins GA, Goldberg AL (2017) The Logic of the 26S Proteasome. *Cell* **169:** 792-806

Consortium GT (2015) Human genomics. The Genotype-Tissue Expression (GTEx) pilot analysis: multitissue gene regulation in humans. *Science* **348:** 648-660

Cox J, Mann M (2008) MaxQuant enables high peptide identification rates, individualized p.p.b.-range mass accuracies and proteome-wide protein quantification. *Nature biotechnology* **26:** 1367-1372

da Cruz I, Rodriguez-Casuriaga R, Santinaque FF, Farias J, Curti G, Capoano CA, Folle GA, Benavente R, Sotelo-Silveira JR, Geisinger A (2016) Transcriptome analysis of highly purified mouse spermatogenic cell populations: gene expression signatures switch from meiotic-to postmeiotic-related processes at pachytene stage. *BMC genomics* **17:** 294

Dai J, Voloshin O, Potapova S, Camerini-Otero RD (2017) Meiotic Knockdown and Complementation Reveals Essential Role of RAD51 in Mouse Spermatogenesis. *Cell reports* **18:** 1383-1394

Daniel K, Lange J, Hached K, Fu J, Anastassiadis K, Roig I, Cooke HJ, Stewart AF, Wassmann K, Jasin M, Keeney S, Toth A (2011) Meiotic homologue alignment and its quality surveillance are controlled by mouse HORMAD1. *Nature cell biology* **13:** 599-610

Davies OR, Maman JD, Pellegrini L (2012) Structural analysis of the human SYCE2-TEX12 complex provides molecular insights into synaptonemal complex assembly. *Open biology* **2:** 120099

de Vries FA, de Boer E, van den Bosch M, Baarends WM, Ooms M, Yuan L, Liu JG, van Zeeland AA, Heyting C, Pastink A (2005) Mouse Sycp1 functions in synaptonemal complex assembly, meiotic recombination, and XY body formation. *Genes & development* **19:** 1376-1389

Ding Y, Kaido M, Llano E, Pendas AM, Kitajima TS (2018) The Post-anaphase SUMO Pathway Ensures the Maintenance of Centromeric Cohesion through Meiosis I-II Transition in Mammalian Oocytes. *Current biology : CB* **28:** 1661-1669 e1664

Finley D (2009) Recognition and processing of ubiquitin-protein conjugates by the proteasome. *Annual review of biochemistry* **78:** 477-513

Glotzer M, Murray AW, Kirschner MW (1991) Cyclin is degraded by the ubiquitin pathway. *Nature* **349:** 132-138

Gomes AV, Young GW, Wang Y, Zong C, Eghbali M, Drews O, Lu H, Stefani E, Ping P (2009) Contrasting proteome biology and functional heterogeneity of the 20 S proteasome complexes in mammalian tissues. *Molecular & cellular proteomics : MCP* **8:** 302-315

Gomez HL, Felipe-Medina N, Sanchez-Martin M, Davies OR, Ramos I, Garcia-Tunon I, de Rooij DG, Dereli I, Toth A, Barbero JL, Benavente R, Llano E, Pendas AM (2016) C14ORF39/SIX6OS1 is a constituent of the synaptonemal complex and is essential for mouse fertility. *Nature communications* **7:** 13298

Griffin TA, Nandi D, Cruz M, Fehling HJ, Kaer LV, Monaco JJ, Colbert RA (1998) Immunoproteasome assembly: cooperative incorporation of interferon gamma (IFN-gamma)-inducible subunits. *The Journal of experimental medicine* **187:** 97-104

Guo X, Wang X, Wang Z, Banerjee S, Yang J, Huang L, Dixon JE (2016) Site-specific proteasome phosphorylation controls cell proliferation and tumorigenesis. *Nature cell biology* **18:** 202-212

Hellmuth S, Pohlmann C, Brown A, Bottger F, Sprinzl M, Stemmann O (2015) Positive and negative regulation of vertebrate separase by Cdk1-cyclin B1 may explain why securin is dispensable. *The Journal of biological chemistry* **290:** 8002-8010

Hlady RA, Novakova S, Opavska J, Klinkebiel D, Peters SL, Bies J, Hannah J, Iqbal J, Anderson KM, Siebler HM, Smith LM, Greiner TC, Bastola D, Joshi S, Lockridge O, Simpson MA, Felsher DW, Wagner KU, Chan WC, Christman JK, Opavsky R (2012) Loss of Dnmt3b function upregulates the tumor modifier Ment and accelerates mouse lymphomagenesis. *The Journal of clinical investigation* **122:** 163-177

Huang L, Haratake K, Miyahara H, Chiba T (2016) Proteasome activators, PA28gamma and PA200, play indispensable roles in male fertility. *Scientific reports* **6:** 23171

Inobe T, Matouschek A (2014) Paradigms of protein degradation by the proteasome. *Current opinion in structural biology* **24:** 156-164

Jiang H, Gao Q, Zheng W, Yin S, Wang L, Zhong L, Ali A, Khan T, Hao Q, Fang H, Sun X, Xu P, Pandita TK, Jiang X, Shi Q (2018) MOF influences meiotic expansion of H2AX phosphorylation and spermatogenesis in mice. *PLoS genetics* **14:** e1007300

Khor B, Bredemeyer AL, Huang CY, Turnbull IR, Evans R, Maggi LB, Jr., White JM, Walker LM, Carnes K, Hess RA, Sleckman BP (2006) Proteasome activator PA200 is required for normal spermatogenesis. *Molecular and cellular biology* **26:** 2999-3007

Kim J, Ishiguro K, Nambu A, Akiyoshi B, Yokobayashi S, Kagami A, Ishiguro T, Pendas AM, Takeda N, Sakakibara Y, Kitajima TS, Tanno Y, Sakuno T, Watanabe Y (2015) Meikin is a conserved regulator of meiosis-I-specific kinetochore function. *Nature* **517:** 466-471

Kisselev AF, Akopian TN, Castillo V, Goldberg AL (1999) Proteasome active sites allosterically regulate each other, suggesting a cyclical bite-chew mechanism for protein breakdown. *Molecular cell* **4:** 395-402

Llano E, Gomez HL, Garcia-Tunon I, Sanchez-Martin M, Caburet S, Barbero JL, Schimenti JC, Veitia RA, Pendas AM (2014) STAG3 is a strong candidate gene for male infertility. *Human molecular genetics* **23:** 3421-3431

Marangos P, Carroll J (2008) Securin regulates entry into M-phase by modulating the stability of cyclin B. *Nature cell biology* **10:** 445-451

Meyer HJ, Rape M (2014) Enhanced protein degradation by branched ubiquitin chains. *Cell* **157:** 910-921

Mikolcevic P, Isoda M, Shibuya H, del Barco Barrantes I, Igea A, Suja JA, Shackleton S, Watanabe Y, Nebreda AR (2016) Essential role of the Cdk2 activator RingoA in meiotic telomere tethering to the nuclear envelope. *Nature communications* **7:** 11084

Mimitou EP, Symington LS (2009) Nucleases and helicases take center stage in homologous recombination. *Trends in biochemical sciences* **34:** 264-272

Moens PB, Marcon E, Shore JS, Kochakpour N, Spyropoulos B (2007) Initiation and resolution of interhomolog connections: crossover and non-crossover sites along mouse synaptonemal complexes. *Journal of cell science* **120:** 1017-1027

Murata S, Yashiroda H, Tanaka K (2009) Molecular mechanisms of proteasome assembly. *Nature reviews Molecular cell biology* **10:** 104-115

Nelson CR, Hwang T, Chen PH, Bhalla N (2015) TRIP13PCH-2 promotes Mad2 localization to unattached kinetochores in the spindle checkpoint response. *The Journal of cell biology* **211:** 503-516

Pivot-Pajot C, Caron C, Govin J, Vion A, Rousseaux S, Khochbin S (2003) Acetylation-dependent chromatin reorganization by BRDT, a testis-specific bromodomain-containing protein. *Molecular and cellular biology* **23:** 5354-5365

Planello AC, Ji J, Sharma V, Singhania R, Mbabaali F, Muller F, Alfaro JA, Bock C, De Carvalho DD, Batada NN (2014) Aberrant DNA methylation reprogramming during induced pluripotent stem cell generation is dependent on the choice of reprogramming factors. *Cell regeneration* **3:** 4

Qian MX, Pang Y, Liu CH, Haratake K, Du BY, Ji DY, Wang GF, Zhu QQ, Song W, Yu Y, Zhang XX, Huang HT, Miao S, Chen LB, Zhang ZH, Liang YN, Liu S, Cha H, Yang D, Zhai Y, Komatsu T, Tsuruta F, Li H, Cao C, Li W, Li GH, Cheng Y, Chiba T, Wang L, Goldberg AL, Shen Y, Qiu XB (2013) Acetylation-mediated proteasomal degradation of core histones during DNA repair and spermatogenesis. *Cell* **153:** 1012-1024

Rao HB, Qiao H, Bhatt SK, Bailey LR, Tran HD, Bourne SL, Qiu W, Deshpande A, Sharma AN, Beebout CJ, Pezza RJ, Hunter N (2017) A SUMO-ubiquitin relay recruits proteasomes to chromosome axes to regulate meiotic recombination. *Science* **355:** 403-407

Rathke C, Baarends WM, Awe S, Renkawitz-Pohl R (2014) Chromatin dynamics during spermiogenesis. *Biochimica et biophysica acta* **1839:** 155-168

Rattani A, Vinod PK, Godwin J, Tachibana-Konwalski K, Wolna M, Malumbres M, Novak B, Nasmyth K (2014) Dependency of the spindle assembly checkpoint on Cdk1 renders the anaphase transition irreversible. *Current biology : CB* **24:** 630-637

Rogakou EP, Pilch DR, Orr AH, Ivanova VS, Bonner WM (1998) DNA double-stranded breaks induce histone H2AX phosphorylation on serine 139. *The Journal of biological chemistry* **273:** 5858-5868

Roig I, Dowdle JA, Toth A, de Rooij DG, Jasin M, Keeney S (2010) Mouse TRIP13/PCH2 is required for recombination and normal higher-order chromosome structure during meiosis. *PLoS genetics* **6**

Rouillard AD, Gundersen GW, Fernandez NF, Wang Z, Monteiro CD, McDermott MG, Ma'ayan A (2016) The harmonizome: a collection of processed datasets gathered to serve and mine knowledge about genes and proteins. *Database : the journal of biological databases and curation* **2016**

Sanchez-Lanzas R, Castano JG (2014) Proteins directly interacting with mammalian 20S proteasomal subunits and ubiquitin-independent proteasomal degradation. *Biomolecules* **4:** 1140-1154

Schmidt M, Haas W, Crosas B, Santamaria PG, Gygi SP, Walz T, Finley D (2005) The HEAT repeat protein Blm10 regulates the yeast proteasome by capping the core particle. *Nature structural & molecular biology* **12:** 294-303

Shang E, Nickerson HD, Wen D, Wang X, Wolgemuth DJ (2007) The first bromodomain of Brdt, a testis-specific member of the BET sub-family of double-bromodomain-containing proteins, is essential for male germ cell differentiation. *Development* **134:** 3507-3515

Shinohara M, Oh SD, Hunter N, Shinohara A (2008) Crossover assurance and crossover interference are distinctly regulated by the ZMM proteins during yeast meiosis. *Nature genetics* **40:** 299-309

Singh P, Schimenti JC, Bolcun-Filas E (2015) A mouse geneticist's practical guide to CRISPR applications. *Genetics* **199:** 1-15

Uechi H, Hamazaki J, Murata S (2014) Characterization of the testis-specific proteasome subunit alpha4s in mammals. *The Journal of biological chemistry* **289:** 12365-12374

Verma R, Chen S, Feldman R, Schieltz D, Yates J, Dohmen J, Deshaies RJ (2000) Proteasomal proteomics: identification of nucleotide-sensitive proteasome-interacting proteins by mass spectrometric analysis of affinity-purified proteasomes. *Molecular biology of the cell* **11:** 3425-3439

Wang K, Sturt-Gillespie B, Hittle JC, Macdonald D, Chan GK, Yen TJ, Liu ST (2014) Thyroid hormone receptor interacting protein 13 (TRIP13) AAA-ATPase is a novel mitotic checkpoint-silencing protein. *The Journal of biological chemistry* **289:** 23928-23937

Wojtasz L, Cloutier JM, Baumann M, Daniel K, Varga J, Fu J, Anastassiadis K, Stewart AF, Remenyi A, Turner JM, Toth A (2012) Meiotic DNA double-strand breaks and chromosome asynapsis in mice are monitored by distinct HORMAD2-independent and -dependent mechanisms. *Genes & development* **26:** 958-973

Wojtasz L, Daniel K, Roig I, Bolcun-Filas E, Xu H, Boonsanay V, Eckmann CR, Cooke HJ, Jasin M, Keeney S, McKay MJ, Toth A (2009) Mouse HORMAD1 and HORMAD2, two conserved meiotic chromosomal proteins, are depleted from synapsed chromosome axes with the help of TRIP13 AAA-ATPase. *PLoS genetics* **5:** e1000702

Xu H, Beasley MD, Warren WD, van der Horst GT, McKay MJ (2005) Absence of mouse REC8 cohesin promotes synapsis of sister chromatids in meiosis. *Developmental cell* **8:** 949-961

Yost S, de Wolf B, Hanks S, Zachariou A, Marcozzi C, Clarke M, de Voer R, Etemad B, Uijttewaal E, Ramsay E, Wylie H, Elliott A, Picton S, Smith A, Smithson S, Seal S, Ruark E, Houge G, Pines J, Kops

G, Rahman N (2017) Biallelic TRIP13 mutations predispose to Wilms tumor and chromosome missegregation. *Nature genetics* **49:** 1148-1151

Yu G, Wang LG, Han Y, He QY (2012) clusterProfiler: an R package for comparing biological themes among gene clusters. *Omics : a journal of integrative biology* **16:** 284-287

Zickler D, Kleckner N (2015) Recombination, Pairing, and Synapsis of Homologs during Meiosis. *Cold Spring Harbor perspectives in biology* **7**

Legends to figures

Figure 1. Transcriptional analysis and distribution of PSMA8 in mouse. (A) Relative transcription of *Psma8* mRNA by quantitative reverse transcription PCR (RT-qPCR) in mouse tissues. *β-actin* transcription was used to normalize the expression (mean ± s.d., three replicates). (B) Western blot analysis of protein extracts from wild type testis (from P8 to adult) and cell lines (TM3, TM4 and GC1) with a specific antibody against the C-term (α4S) and whole recombinant PSMA8 protein (PSMA8-R2). α-Tubulin was used as loading control. The corresponding bands to PSMA8 and PSMA7 are indicated in the right of the panel. Note that from P16 to adult the intensity of both PSMA8 and PSMA7 bands impedes its independent observation. (C) Double labelling of endogenous PSMA8 (green) and SYCP3 (red) in mouse spermatocytes. DNA was stained with DAPI (blue). During pachytene, PSMA8 is located at the synapsed autosomal LEs and at the PAR of the sex XY bivalent. (D) Double immunolabelling of spermatocytes spread preparations with PSMA8 (green) and SYCP1 (red), showing that PSMA8 localizes to the synapsed LEs but do not perfectly co-localize with SYCP1. PAR of the sex XY bivalent is indicated with an arrow. (E) Immuno-localization of PSMA8 in mouse testis after *in vivo* electroporation of a plasmid encoding a protein fusion of PSMA8 with GFP (GFP-PSMA8). PSMA8 was detected with anti-GFP antibody (green) and endogenous SYCP3 was detected using mouse anti-SYCP3 (red). DNA was stained with DAPI (blue). Bar in panels, 10 μm.

Figure 2. PSMA8 localization is dependent on synapsis. Double labelling of PSMA8 (green) and SYCP3 (red) in *Rec8*$^{-/-}$ and *Six6os1*$^{-/-}$. PSMA8 is detected in the pseudosynapsed AEs of the meiotic *Rec8* cohesin mutant but is absent from unsynapsed AEs in *Six6os1*$^{-/-}$ spermatocytes. Bar in panels, 10 μm.

Figure 3. Generation and genetic characterization of *Psma8* deficient mice. (A) Diagrammatic representation of the mouse *Psma8* locus (WT) and the genome editing strategy showing the sgRNAs located on exon 1 and intron 1 (see methods), the corresponding coding exons (light grey) and non-coding exons (open boxes). Thin (non-

coding) and thick (coding sequences) lines under exons represent the expected transcript derived from wild-type (black) and *Psma8* edited allele (blue). ATG, initiation codon; TGA, stop codon. The nucleotide sequence of the 56 base pair deletion derived from PCR amplification of DNA from the *Psma8* $^{edited/edited}$ is indicated (Δ). Primers (F and R) are represented by arrows. (B) PCR analysis of genomic DNA from three littermate progeny of *Psma8*$^{+/-}$ heterozygote crosses. The PCR amplification with primers F and R revealed 222 and 166 bp fragments for wild-type and disrupted alleles respectively. Wild-type (WT, +/+), heterozygous (Het, +/-), and homozygous knock-out (KO, -/-) animals. (C) Western blot analysis of protein extracts from wild type testis (P22 and adult), KO testis (P16, P22 and adult) with a specific antibody against the C-term (α4S) and whole recombinant PSMA8 protein (PSMA8-R2). α-Tubulin was used as loading control. The corresponding bands to PSMA8 and PSMA7 are indicated in the right of the panel. Note that at the P22 and in adult stages the intensity of both bands abolishes its independent observation. (D) Double immunofluorescence of spermatocytes at pachytene stage obtained from *Psma8*$^{+/+}$ and *Psma8*$^{-/-}$ mice using SYCP3 (red) and a rabbit polyclonal antibody against PSMA8 (green). Green labelling in Psma8$^{-/-}$ spermatocytes (49% of the wild type) represents cross-reactivity of the antiserum with PSMA7. Plot under the image panel represents the quantification of intensity from *Psma8*$^{+/+}$ and *Psma8*$^{-/-}$ spermatocytes. Welch´s *t*-test analysis: * $p<0.01$; ** $p<0.001$; *** $p<0.0001$. Bar in panels, 10 μm.

Figure 4. PSMA8 deficiency leads to azoospermia. (A) Genetic ablation of *Psma8* leads to a reduction of the testis size (n=6, WT and KO; Welch´s *t*-test analysis: $p<0.0001$), and (B) a complete arrest of spermatogenesis in early round spermatid as shown in PAS and haematoxylin stained testis sections. Massive apoptosis of spermatocytes is indicated (asterisks). The spermatogenic arrest leads to empty epididymides and azoospermia. Bar in upper panels, 100 μm and in lower panels, 5 μm. (**St**) Seminiferous tubules. (**Ep**) Epididymides. (C) Low magnification view of a representative squash preparation of seminiferous tubules showing the accumulation of metaphases I and metaphase II in knock-out *Psma8* in comparison with a representative wild-type view (WT, left). The identity of

metaphases I (asterisks)/metaphases II was confirmed by the immunolabelling of SYCP3. Chromosomes were counterstained with DAPI (blue). Plot onto the image panel represent the quantification of metaphase I and II (normal and apoptotic) from *Psma8*$^{+/+}$ and *Psma8*$^{-/-}$ tubules. Welch´s *t*-test analysis: * p<0.01; ** p<0.001; *** p<0.0001. (D) FACs analysis of cells from whole seminiferous tubules from wild type and *Psma8*$^{-/-}$ showing in both genotypes (N=2) the presence of the tetraploid, diploid and haploid compartment as a result of the early spermatid arrest.

Figure 5. PSMA8 is needed for the expression/assembly of the activator subunit pa200. (A) Western blot analysis of protein extracts from WT and KO testis. A band of the expected molecular weight of pa200 was obtained in the WT but was completely absent in the KO. α-tubulin was used as loading control. (B) Double immunolabelling of pa200 and SYCP3 in chromosome spreads. pa200 is detected at the chromosome axes of the autosomal and XY bivalents during pachytene in wild type spermatocytes in contrast to the absence of labelling in *Psma8*$^{-/-}$ spermatocytes. Nuclear DNA was counterstained with DAPI. Bar in panels, 10 μm.

Figure 6. Aberrant metaphase I /II and spermatids in *Psma8*-deficient mice. (A) Double immunolabelling of Caspase3 (green) and SYCP3 (red) showing normal metaphase I cells and apoptotic metaphase I in chromosomes spreads from seminiferous tubules from *Psma8*$^{+/+}$ and *Psma8*$^{-/-}$ animals, respectively. Chromatin was counterstained with DAPI. Apoptotic cells were pseudocolored in green. (B) Double labelling of TUNEL (green) and SYCP3 (red) was directly performed onto chromosome spreads from WT and KO. *Psma8*$^{+/+}$ metaphase I showing absence of TUNEL labelling and positive SYCP3 labelling at the centromeres. *Psma8*$^{-/-}$ metaphase I cells showing TUNEL positive staining and SYCP3 positive and negative labelling (upper and mid panel). *Psma8*$^{-/-}$ anaphase I cell showing TUNEL positive staining and SYCP3 positive and negative labelling. (C) Double immunolabelling of SYCP3

(green) with ACA (red) in wild-type and *Psma8*$^{-/-}$ spermatocytes at metaphase II. (D) Immunolabeling of ACA (red) and DAPI staining of squashed tubules from *Psma8*$^{+/+}$ and *Psma8*$^{-/-}$ showing unambiguously the presence of aberrant spermatids (ACA and heterochromatin distribution) with atypical chromatin and nuclear shape. Bar in panels, 10 μm.

Figure 7. DSB repair is not affected in the absence of PSMA8. (A) Double immunolabelling of γ-H2AX (green) with SYCP3 (red). DSBs are generated at leptotene (see Fig EV5) and at pachytene stage the γ-H2AX labelling disappears from the autosomes and remains only at the sex body of the spermatocytes in both *Psma8*$^{+/+}$ and *Psma8*$^{-/-}$ (B) Double immunolabelling of SYCP3 (red) and RAD51 (green). RAD51 foci associated to the AEs completely dissociates at pachytene with the exception of the sex body. (C) Double immunolabelling of SYCP3 (red) with MLH1 (green). MLH1 foci are present along each autosomal SC in wild-type and *Psma8*$^{-/-}$ pachynema meiocytes in a similar way. Plot under the image panel represent the quantification of number of foci from *Psma8*$^{+/+}$ and *Psma8*$^{-/-}$ spermatocytes. Welch´s *t*-test analysis: * $p<0.01$; ** $p<0.001$; *** $p<0.0001$. Bar in panels, 10 μm.

Figure 8. PSMA8 deficiency provokes an slight increase of acetylated histones at prophase I. (A) Double immunolabelling of H2AacK5 (green), (B) H3ac and (C) H4ac with SYCP3 (red) in wild-type and *Psma8*$^{-/-}$ diplonemas. (D) Double immunolabelling of H4ac (green) with SYCP3 (red) in wild-type and *Psma8*$^{-/-}$ metaphase I cells showing a qualitative increase of labelling in the mutant metaphase I. Plots right to each panel represent the quantification of the fluorescence intensity from *Psma8*$^{+/+}$ and *Psma8*$^{-/-}$ spermatocytes at early pachytene (EP), mid pachytene (MP), late Pachytene (LP), early diplotene (ED) and late diplotene (LD) corresponding to the immunolabeling of EV6-8. Welch´s *t*-test analysis: * $p<0.01$; ** $p<0.001$; *** $p<0.0001$. Bar in panels, 10 μm.

Figure 9. **Proteasome activity and global pattern of ubiquitination, sumoylation and acetylation in Psma8-deficient testis**. (A) Proteasome activity of *Psma8* deficient testis**.** 100 µg of protein from whole testis extracts of *Psma8*$^{+/+}$and *Psma8*$^{-/-}$ mice were inoculated into 96-well plate and the proteasome peptidases activities were measured. The activities relative to WT are shown. Bars, represent Standard Deviation (SD). (B) Double immunolabelling of SYCP3 (red) and Ubiquitin, SUMO1 and SUMO2/3 (green) in mouse spermatocytes in pachytene. Chromatin was stained with DAPI. (C) Western blot analysis of protein extracts from adult wild type and KO testis with a specific antibody against Ubiquitin (Ubiq) and the Ac-Lysine (Ac-Lys). β-actin was used as loading control. Welch´s *t*-test analysis: * $p<0.01$; ** $p<0.001$; *** $p<0.0001$. Bar in panels, 10 µm.

Figure 10. SYCP1 interacts with PSMA8 and is accumulated in metaphase I cells. (A) HEK293T cells were transfected with Flag-PSMA8 and GFP-SYCP1. Protein complexes were immunoprecipitated overnight with either an anti-Flag or anti-EGFP or IgGs (negative control), and were analysed by immunoblotting with the indicated antibody. PSMA8 co-immunoprecipitates (co-IP) with SYCP1. (B) Double immunolabelling of endogenous SYCP1 (green) and SYCP3 (red) in mouse spermatocytes at metaphase I. Chromatin was stained with DAPI (blue). Bar in panels, 10 µm.

Figure 11. PSMA8 deficiency provokes an accumulation of CDK1 in spermatocytes. (A) HEK293T cells were transfected with Flag-PSMA8 and GFP-CDK1. Protein complexes were immunoprecipitated overnight with either an anti-Flag or anti-EGFP or IgGs (negative control), and were analysed by immunoblotting with the indicated antibody. PSMA8 co-immunoprecipitates (co-IP) with CDK1 (as well as reciprocally). (B) Double labelling of endogenous CDK1 (green) and SYCP3 (red) in mouse spermatocytes at metaphase I. Chromatin was stained with DAPI (blue). During metaphase I, CDK1 labels in a slight and disperse way the chromosomes and in a more intensely fashion the centromeres of bivalents. This labelling pattern is enhanced in a normal *Psma8*-deficient metaphase I and greatly enhanced in an aberrant metaphase-like I which shows the accumulation of CDK1 inside the spermatocyte. (C) Double immunolabelling of endogenous CDK2 (green) and SYCP3 (red)

in WT and KO mouse spermatocytes in pachytene (upper panel) and metaphase I (lower panel) showing similar labelling at the telomeres and centromeres, respectively (Mikolcevic et al, 2016). (D) Western blot analysis of testis extracts from WT and KO mice with a specific antibody against CDK1. β-actin was used as a loading control. (E) Double labelling of endogenous CDK1-Tyr15phosphorylated (green) and SYCP3 (red) in mouse spermatocytes at metaphase I showing similar expression levels in *Psma8*$^{+/+}$ and *Psma8*$^{-/-}$. Chromatin was stained with DAPI (blue). (F) Double immunofluorescence of PTTG1 (green) and SYCP3 (red) metaphase I and western blot analysis of testis extracts against PTTG1 from *Psma8*$^{-/-}$ and *Psma8*$^{+/+}$ showing similar expression levels of PTTG1. Bar in panels, 10 μm.

Figure 12. PSMA8 and its interactions with other proteins of the SC. (A) PSMA8 co-IP with SYCE3 and SIX6OS1. HEK293T cells were transfected with plasmids encoding Flag-SIX6OS1, GFP-SYCE3 and Flag-PSMA8. Protein complexes were immunoprecipitated overnight with either an anti-Flag or anti-EGFP or IgGs (negative control), and were analysed by immunoblotting with the indicated antibody. (B) Double immunofluorescence of transfected HEK293T cells with plasmids encoding Flag-PSMA8 alone or together with plasmid encoding SYCP3-HA and immuno-detected with antibodies against PSMA8 (green) or SYCP3 (red). Transfected PSMA8 alone is delocalized and occupies the whole cell whereas when co-transfected with SYCP3-HA is recruited to form polycomplexes. (C) SYCP3 is accumulated *in vivo* in *Psma8*$^{-/-}$ metaphase I and metaphase II. Double immunolabelling of squashed tubules with SYCP3 (green) and ACA (red) in wild-type and *Psma8*$^{-/-}$ spermatocytes at metaphase I and II. *Psma8*$^{-/-}$ metaphases I show labelling for SYCP3 in aggregates (absent in the WT) in addition to its typical labelling at the centromeres. Metaphases II from *Psma8*$^{-/-}$ show labelling for SYCP3 around the kinetochores whereas wild type metaphases II never show any SYCP3 labelling. Bar in panels, 10 μm.

Figure 13. TRIP13 levels are increased in Psma8-deficient spermatocytes. (A) TRIP13 (green) labels the telomeres at pachytene and the intensity of the labelling decreases through

desynapsis at diakinesis and diplotene. This labelling is enhanced during prophase I in the *Psma8* mutants but not its main labelling pattern. At metaphase I a faint labelling of sister kinetochores is observed in the *Psma8*$^{-/-}$ spermatocytes that is absent in the wild type. Plot under the panel represents the quantification of the fluorescence intensity from *Psma8*$^{+/+}$ and *Psma8*$^{-/-}$ spermatocytes at pachytene and late diplotene. (B) HEK293T cells were transfected with a plasmid encoding TRIP13-GFP and PSMA8-Flag. Protein complexes were immunoprecipitated overnight with either an anti-Flag or anti-EGFP or IgGs (negative control), and were analysed by immunoblotting with the indicated antibody. Bar in panels, 10 μm.

A

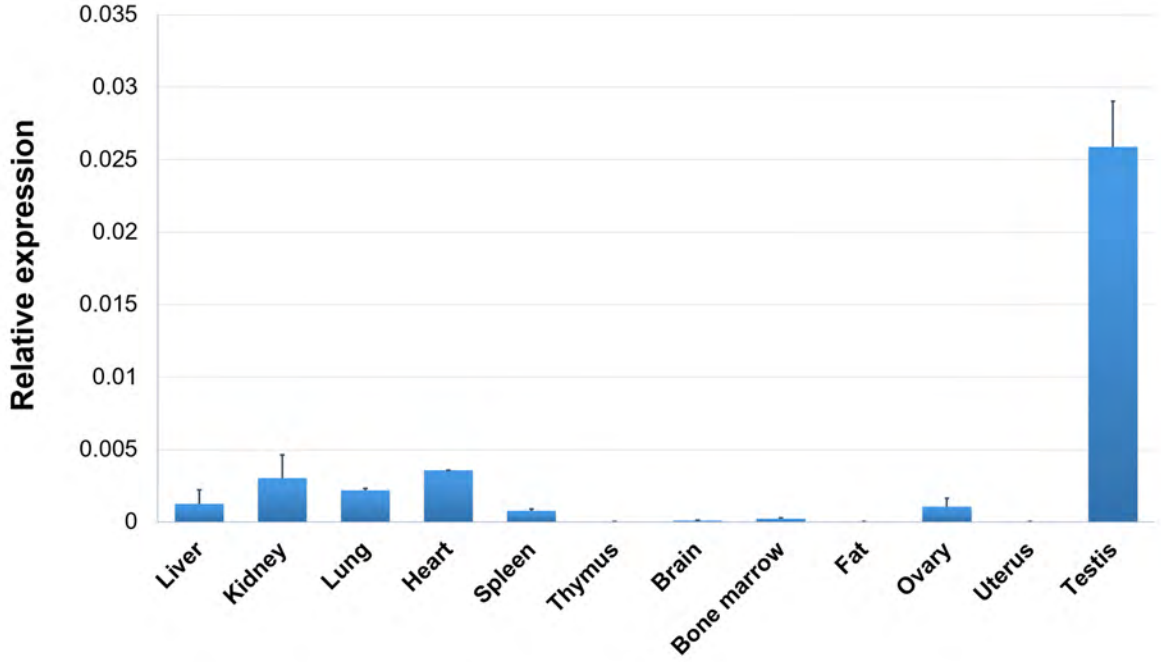

B

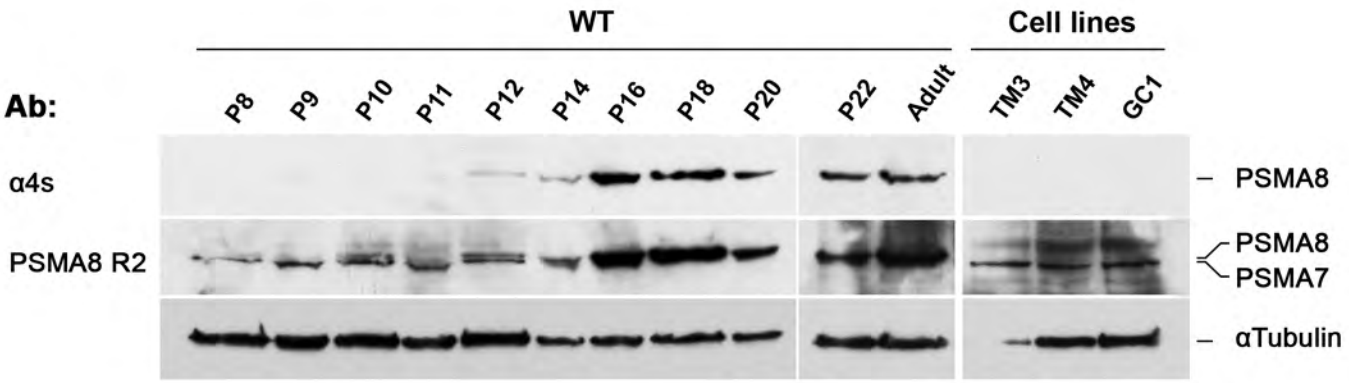

C

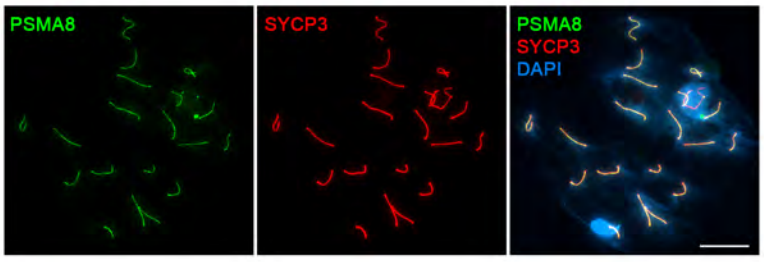

D

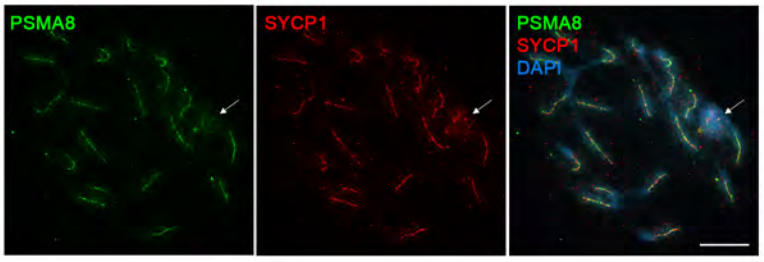

E

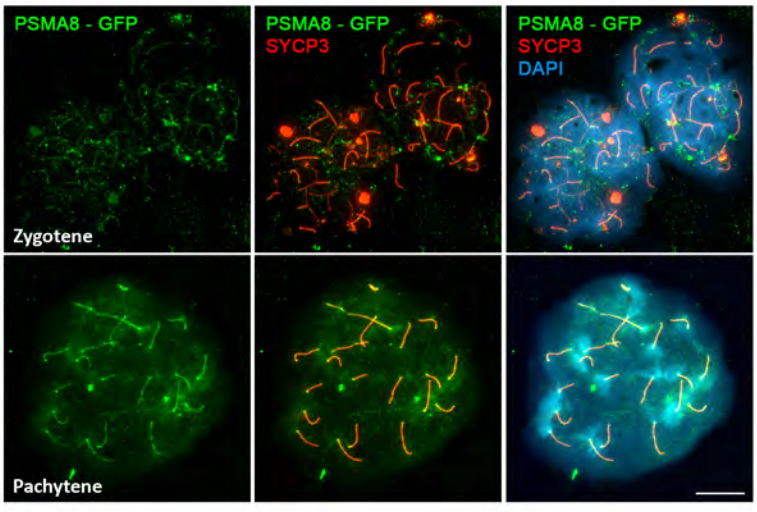

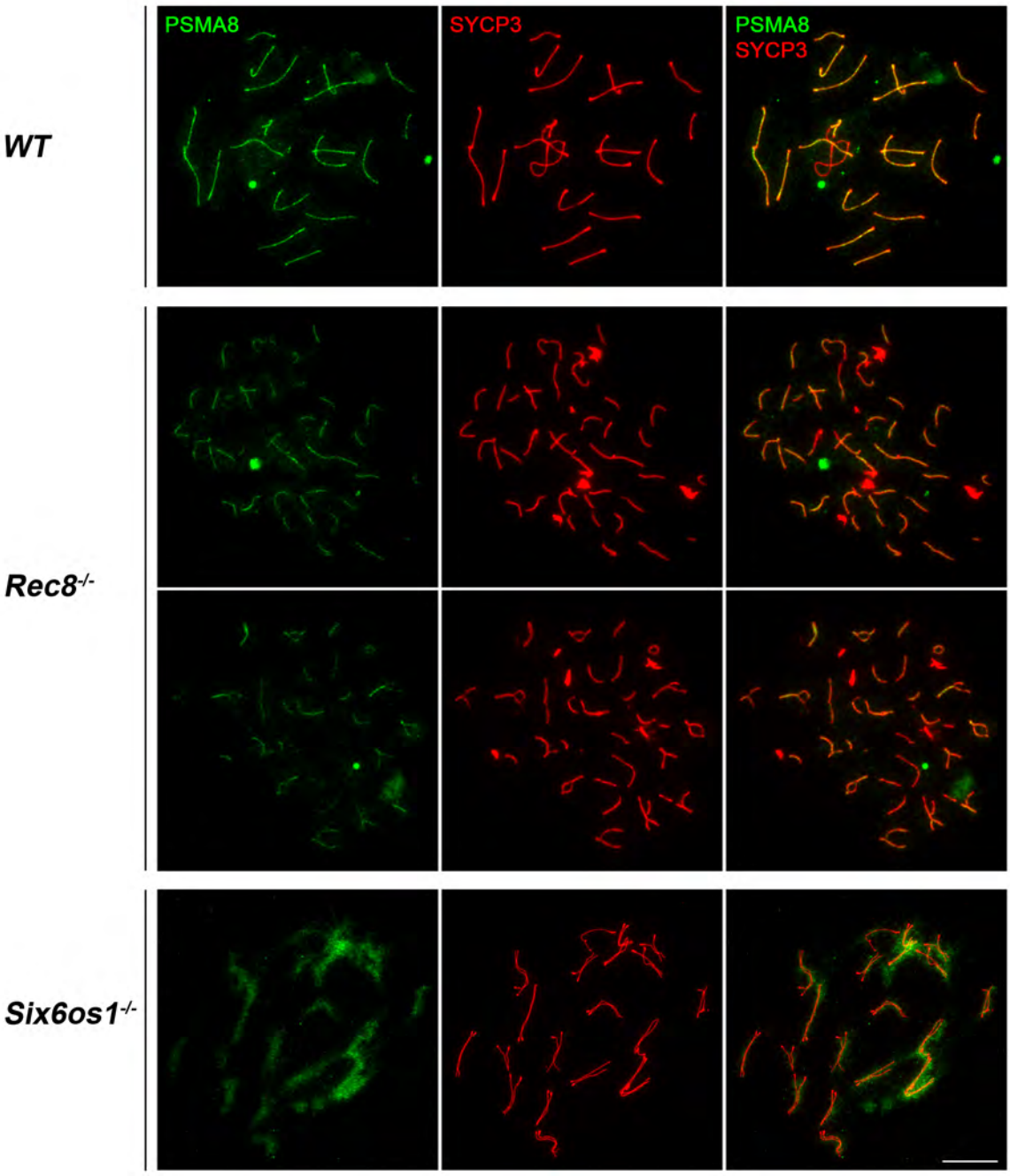

A

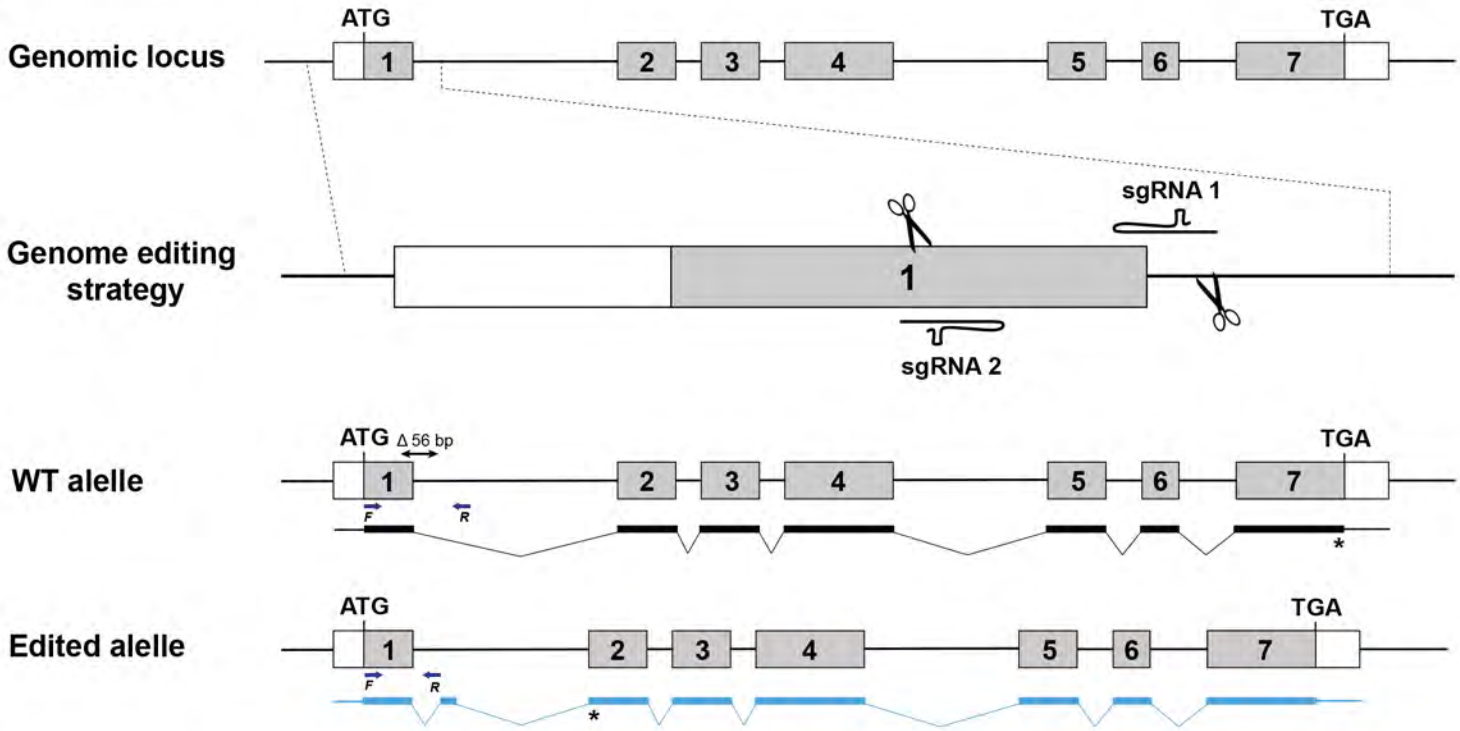

B

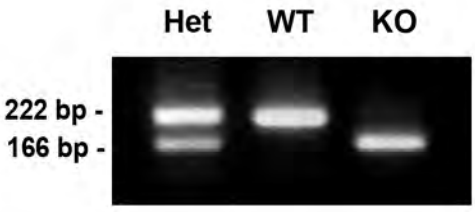

C

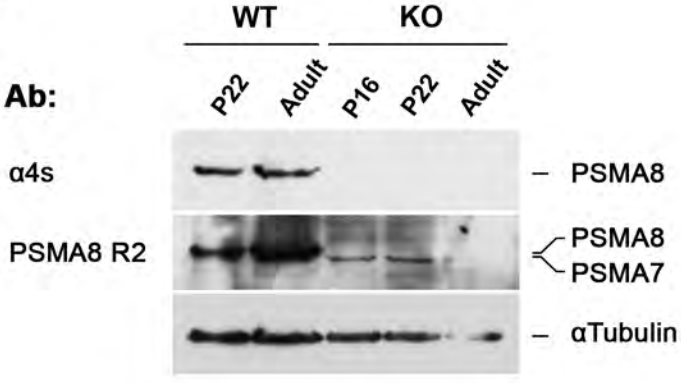

D

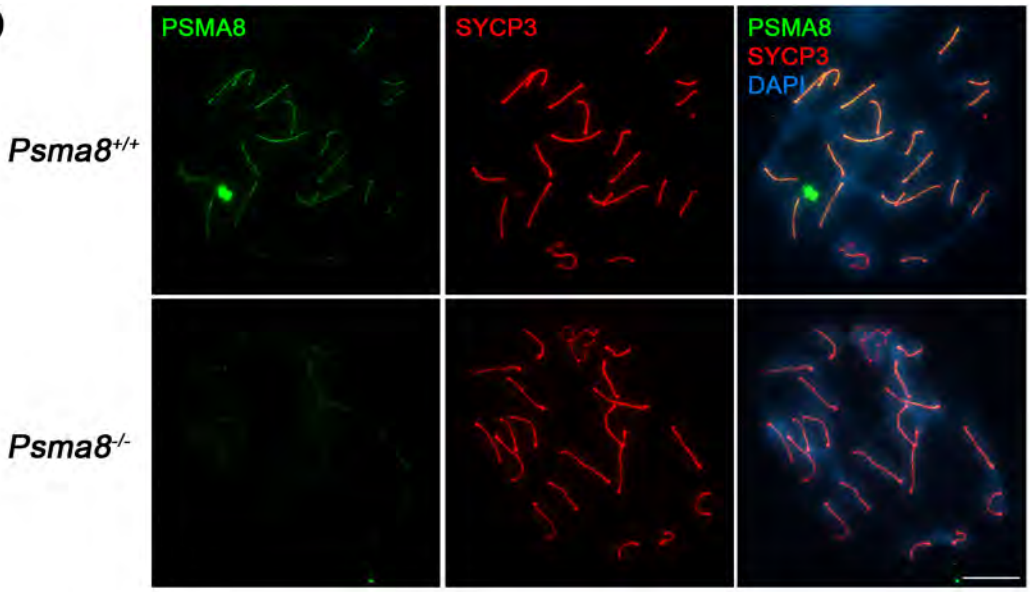

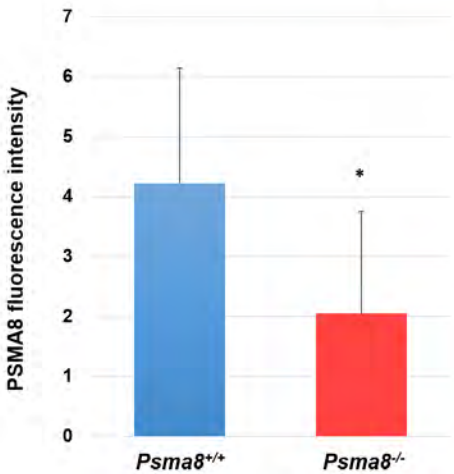

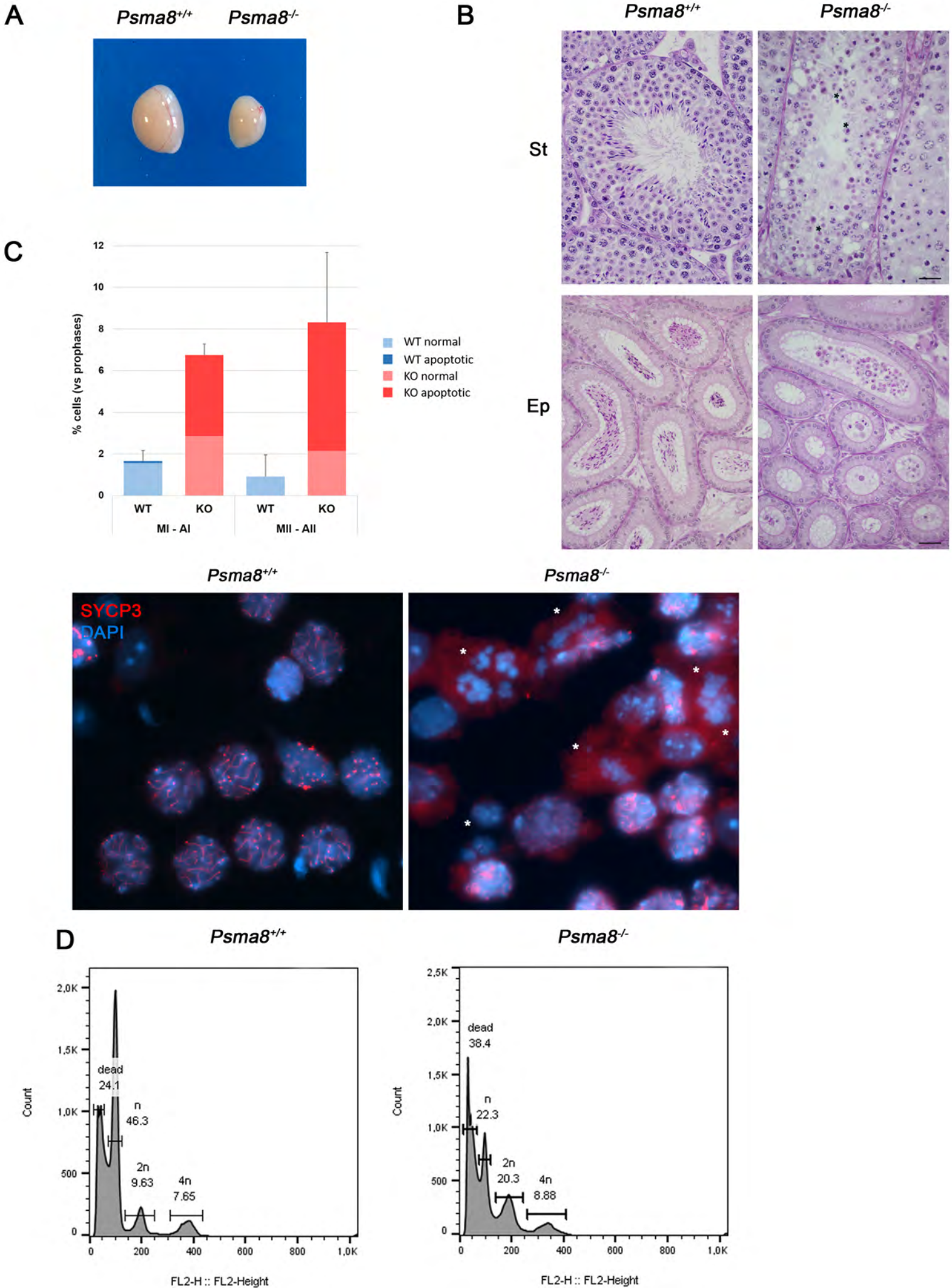

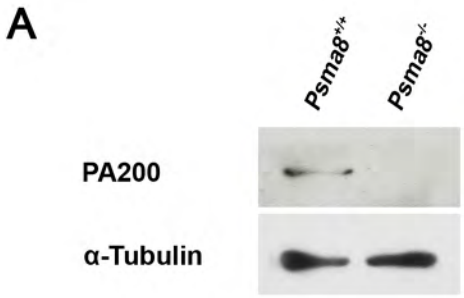

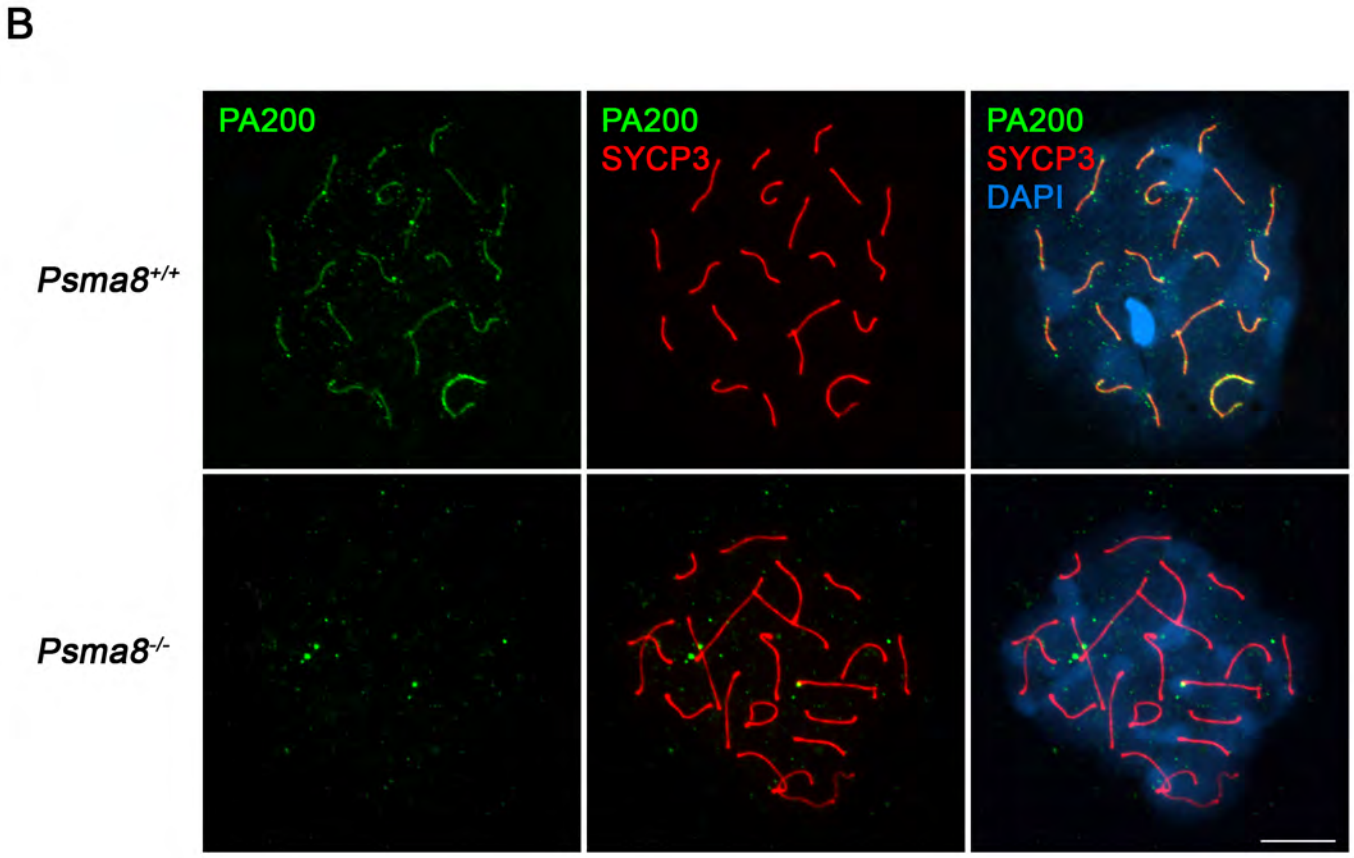

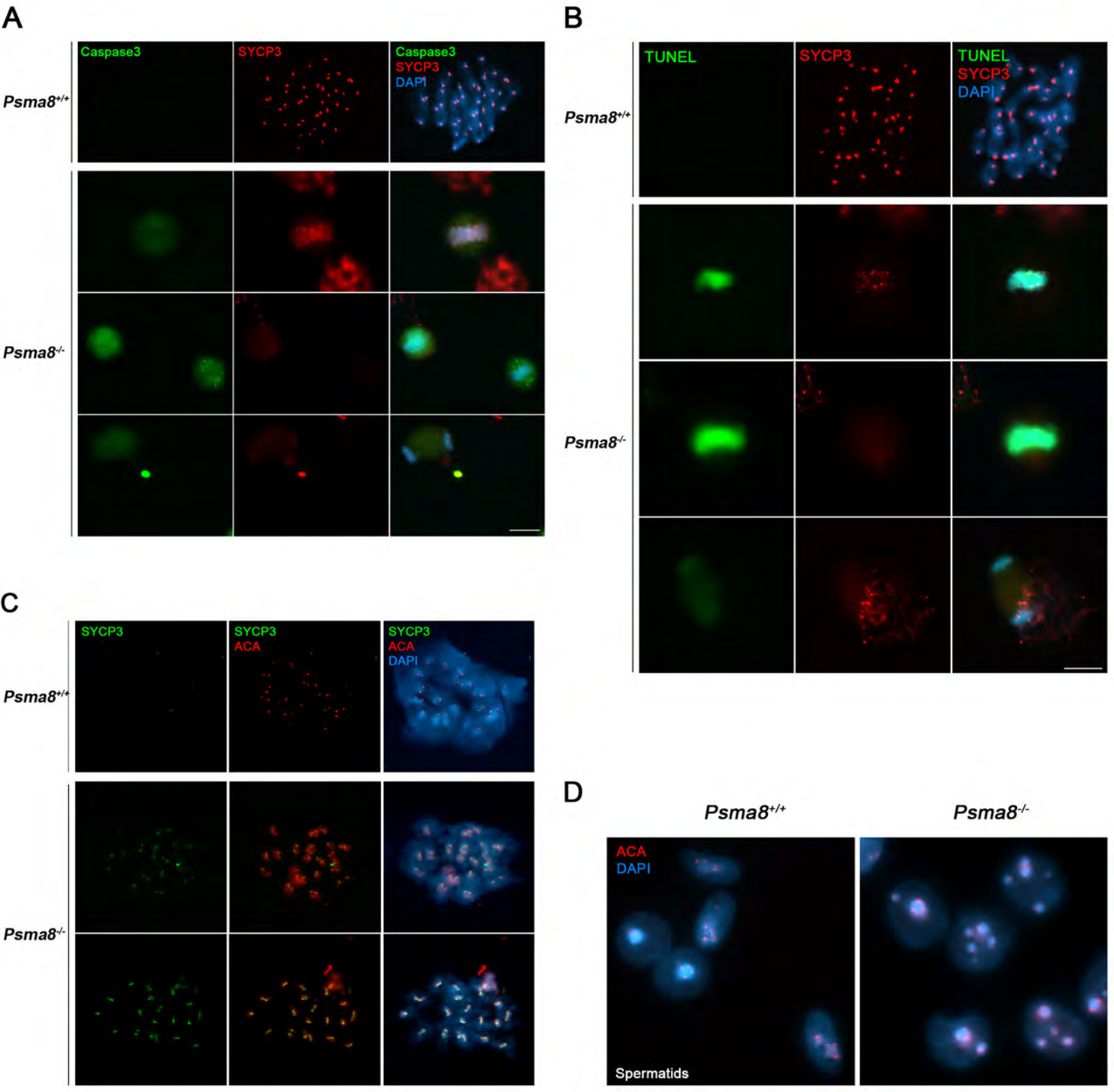

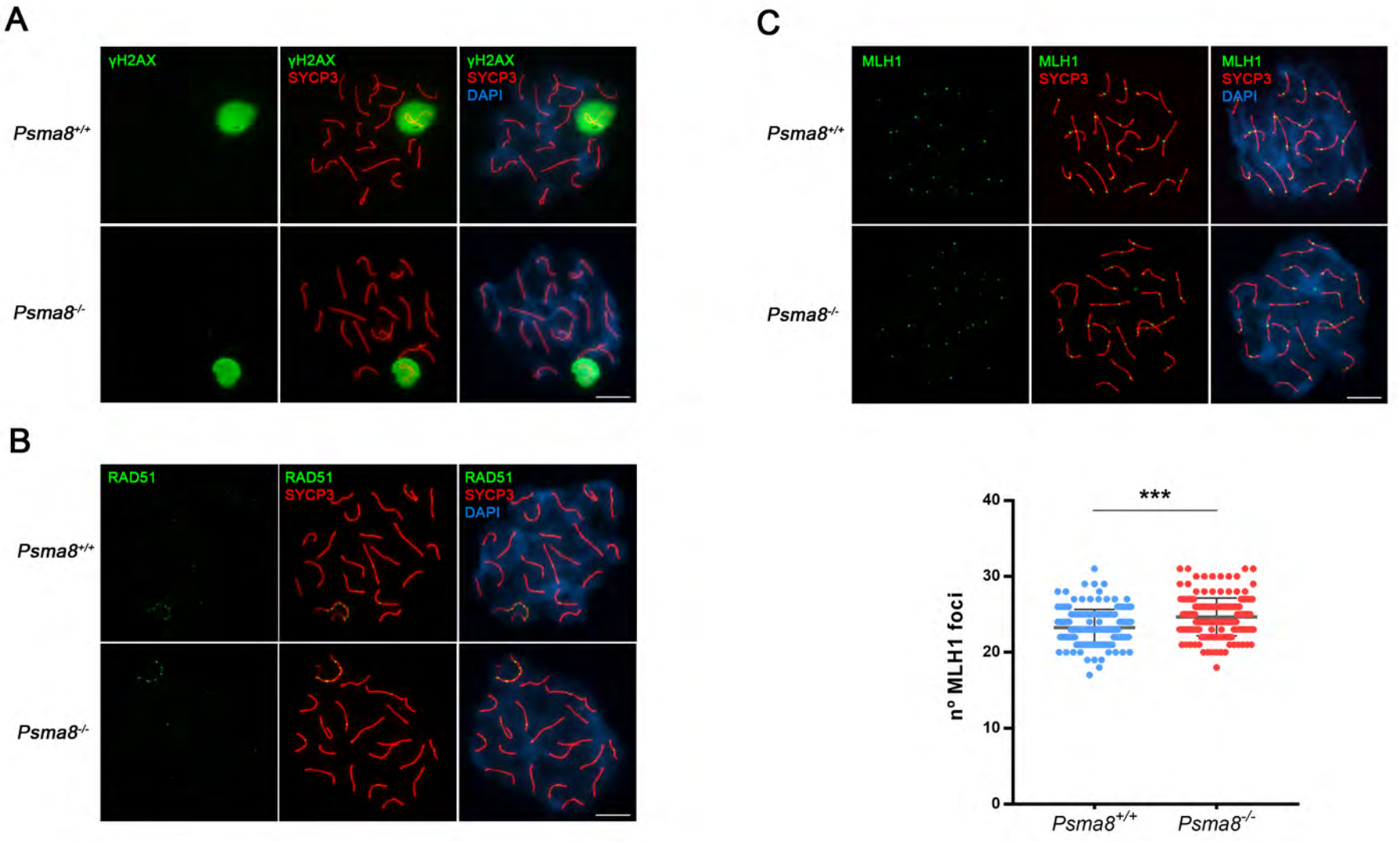
A
γH2AX
γH2AX
SYCP3
γH2AX
SYCP3
DAPI
Psma8+/+
Psma8-/-
B
RAD51
RAD51
SYCP3
RAD51
SYCP3
DAPI
Psma8+/+
Psma8-/-
C
MLH1
MLH1
SYCP3
MLH1
SYCP3
DAPI
Psma8+/+
Psma8-/-
***
nº MLH1 foci
40
30
20
10
0
Psma8+/+
Psma8-/-

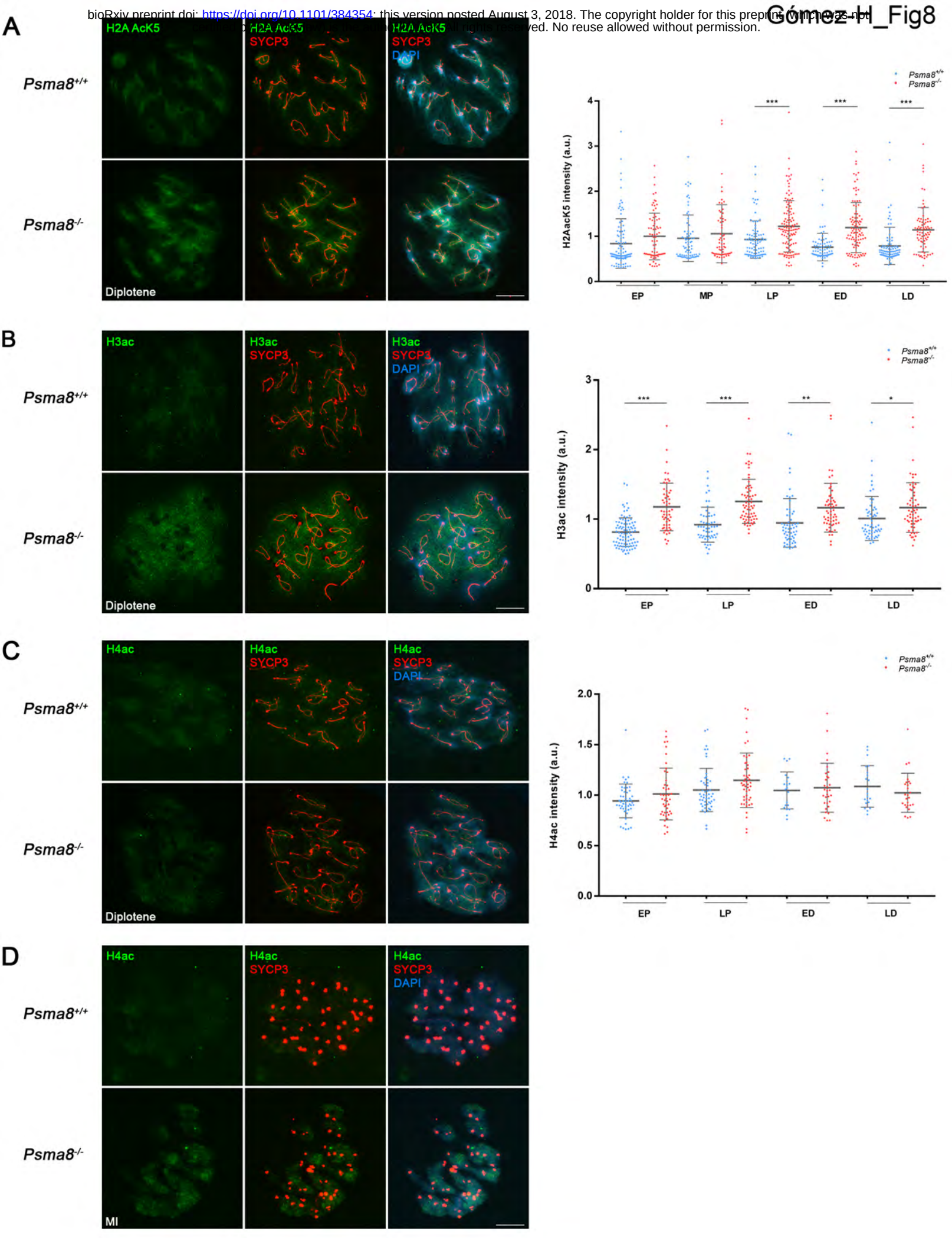

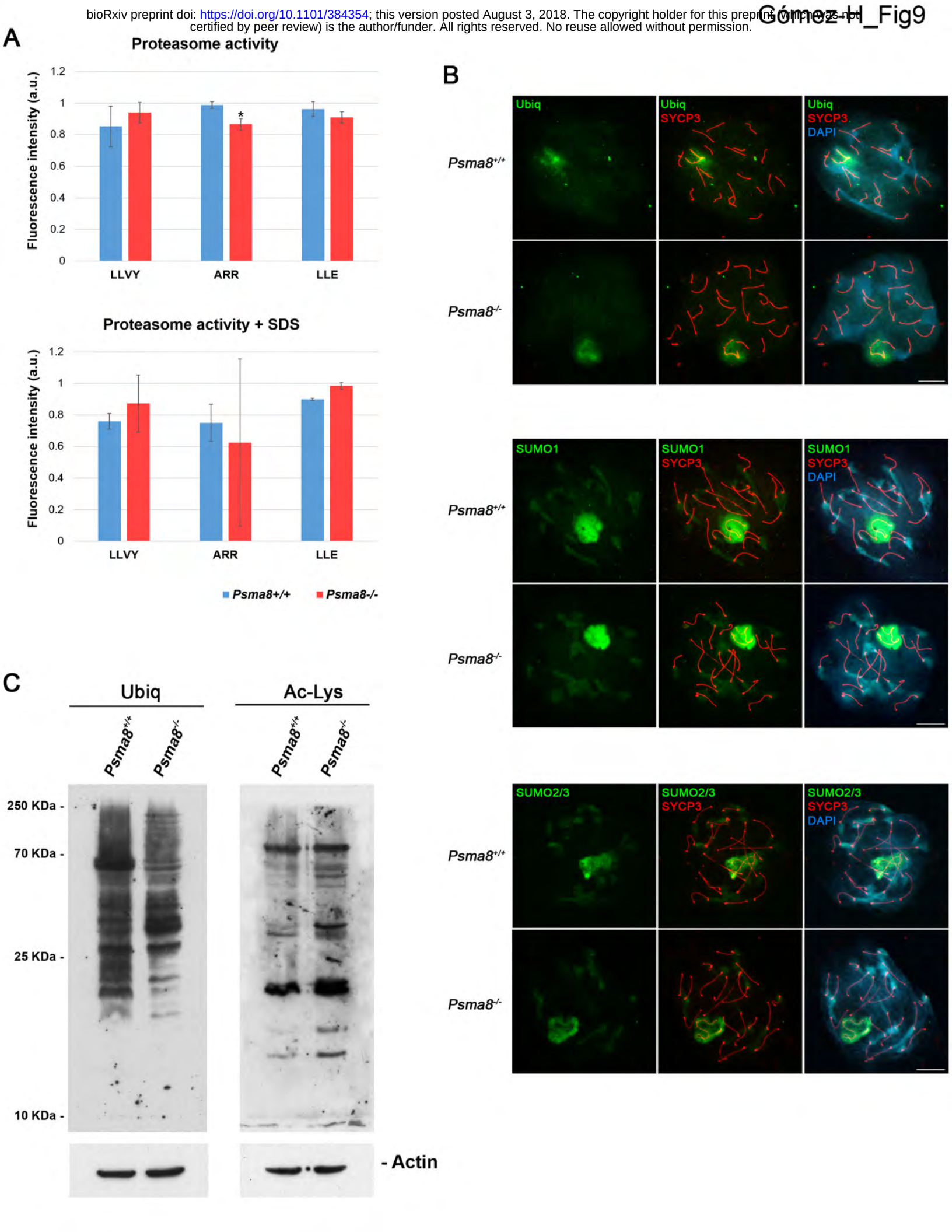

A

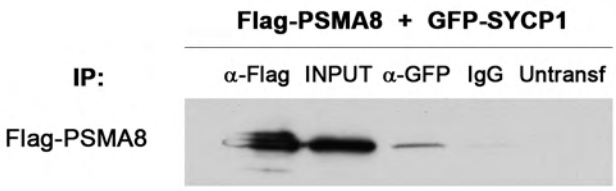

B

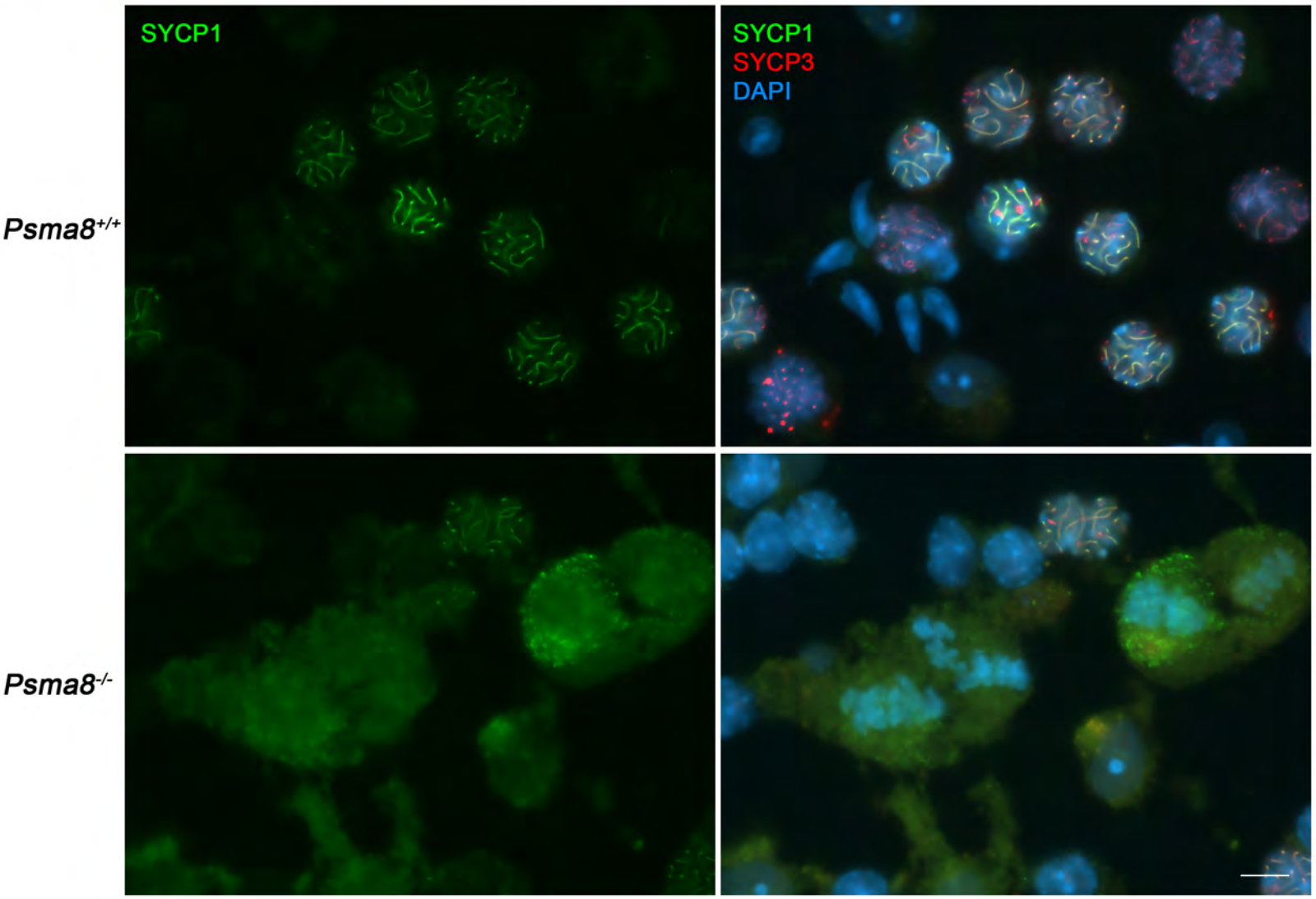

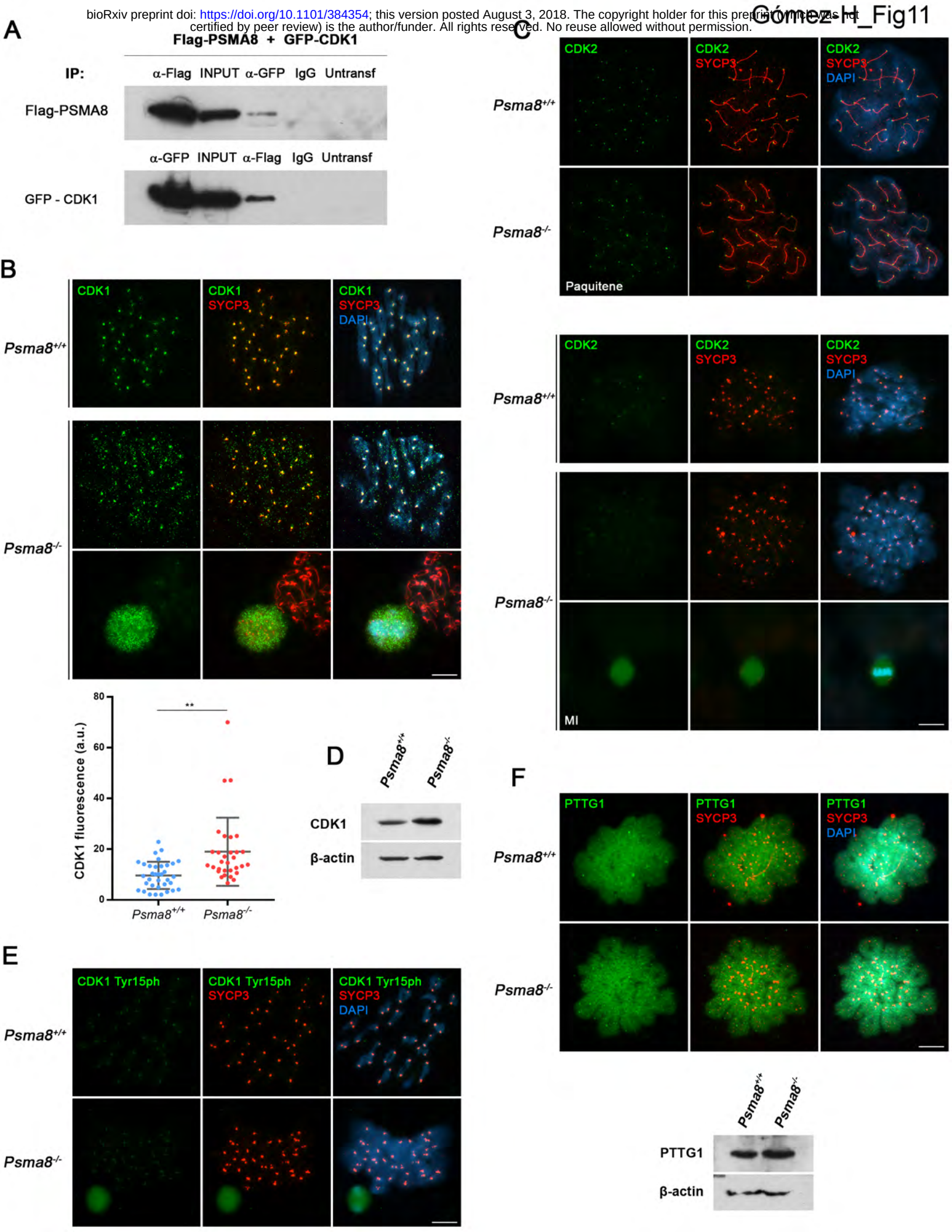

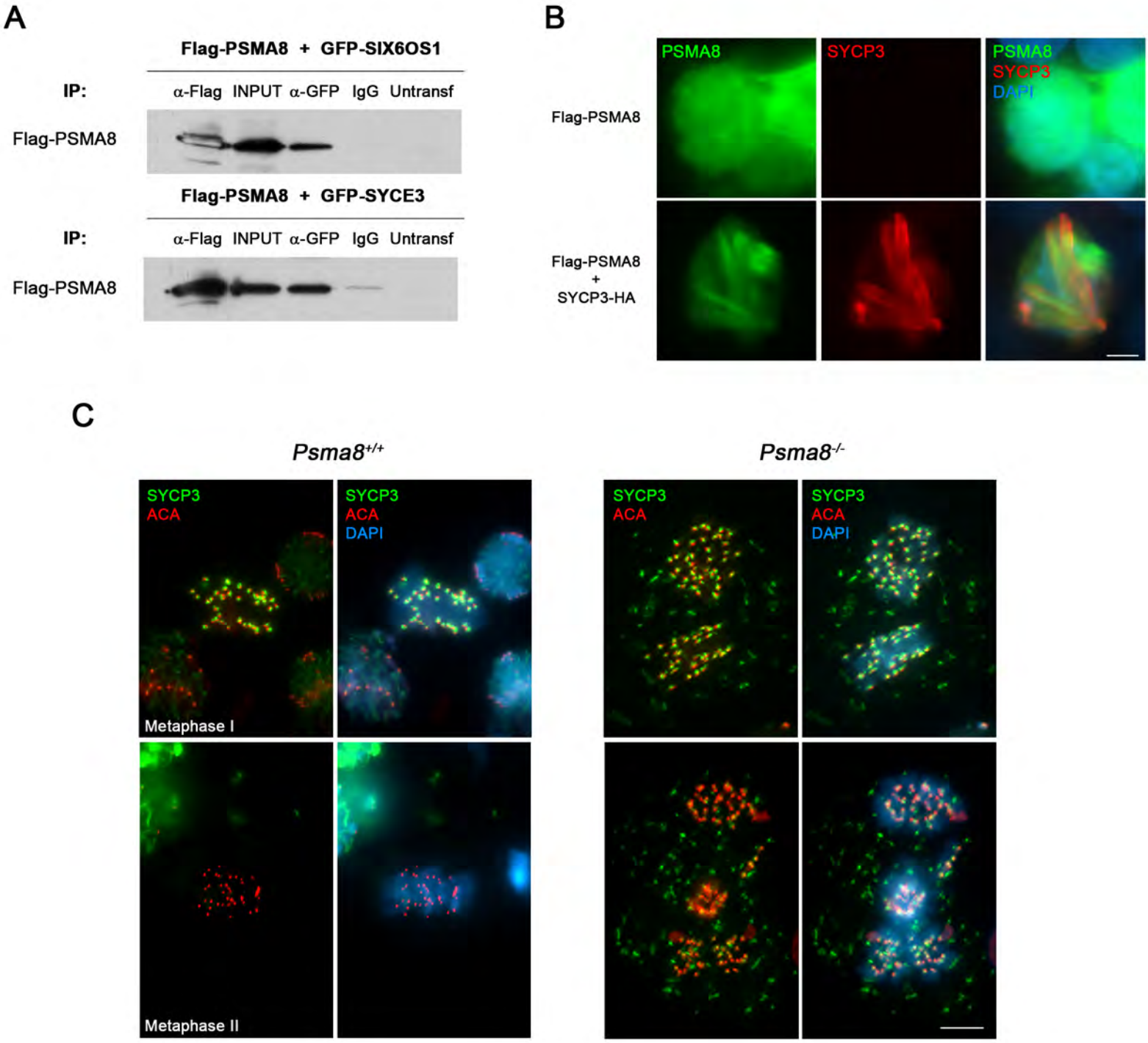

A

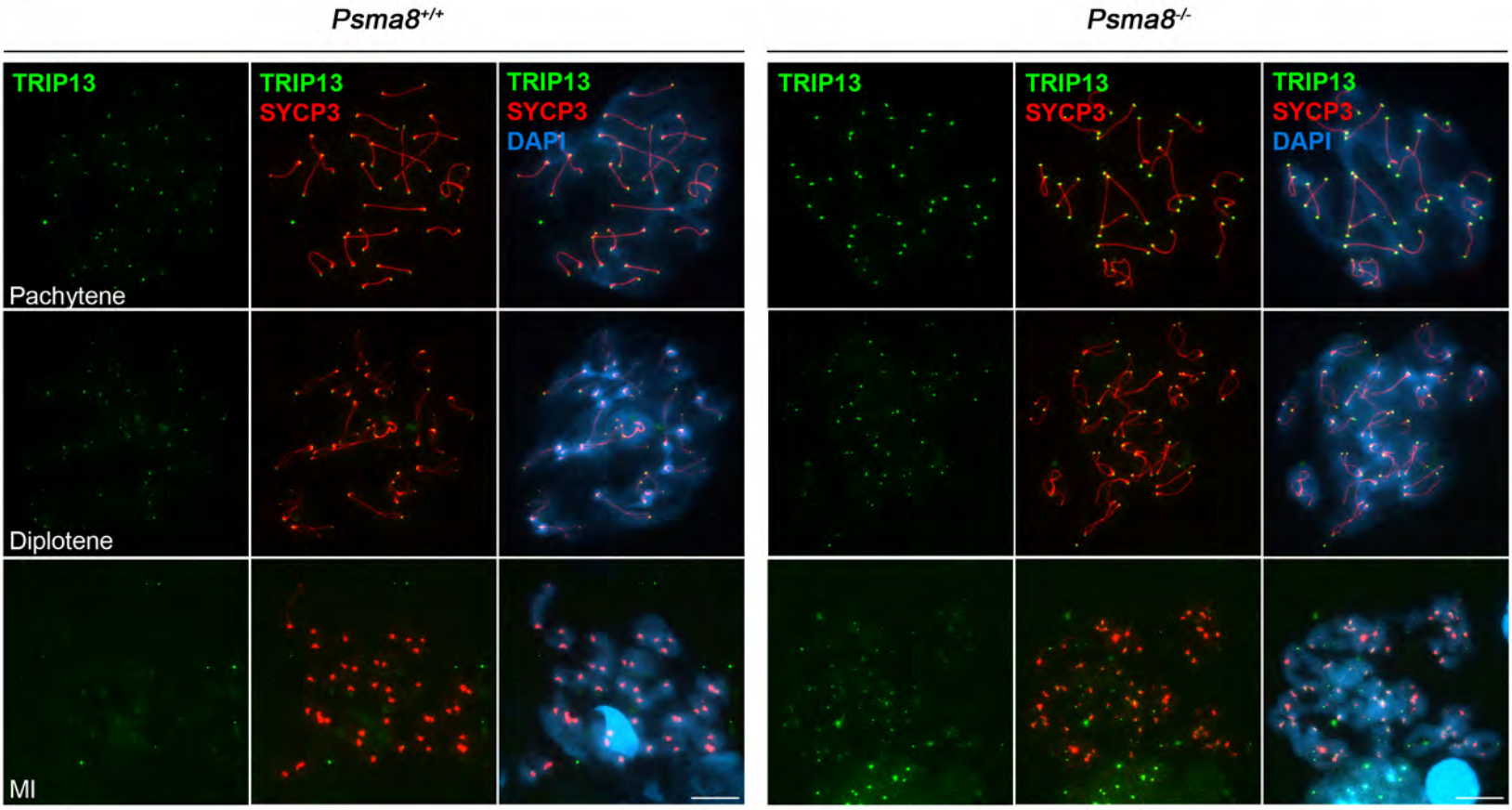

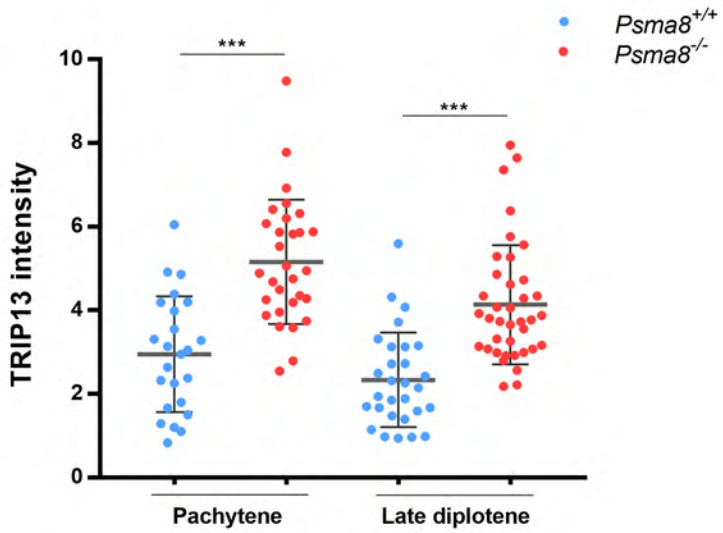

B

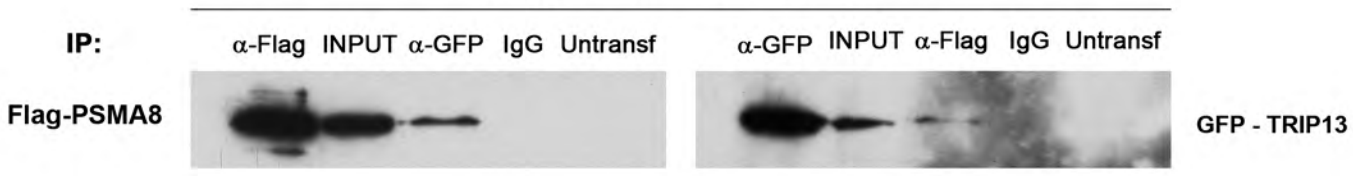

Figures EV1. Validation of the antibodies raised against PSMA8. (A) HEK293T cells were transfected with a plasmid encoding PSMA8-GFP, PSMA7-GFP or GFP and the whole extracts were analyzed by western blot using rabbit α-PSMA8-Cterm (left panel, 4S), rabbit α-PSMA8 (central panel, R2) and α-GFP (right panel, GFP). Immunodetection of α-tubulin was used as loading control. The corresponding band of 60 kDa representing PSMA8-GFP was obtained only with the α-α4S. Both bands of 60 kDa representing PSMA8-GFP and PSMA7-GFP were detected with the rabbit α-Psma8 R2. The bands of 60 kDa (PSMA7 and PSMA8) and 30 kDa (GFP) were all detected with the goat α- GFP (arrowheads) validating the experiments. (B) Immunofluorescence of HEK293T cells transfected with plasmids encoding PSMA8-GFP, PSMA7-GFP or GFP. Both PSMA8 and PSMA7 were detected with rabbit α-PSMA8-R2 (red) and GFP by direct fluorescence signal (green). Green and red signals co-localize in the cytoplasm of the transfected HEK293T cells. The experiments were reproduced three times. Bars represent 10 μm.

Figure EV2. **Localization of PSMA8 in mouse spermatocytes.** (A) Double labelling of endogenous PSMA8 (green) and SYCP3 (red) in mouse spermatocytes. DNA was stained with DAPI (blue). From the leptotene to zygotene stage, PSMA8 is detected at the synapsed autosomal LEs. At pachytene, PSMA8 is located at the totally synapsed axes and at the PAR of the sex XY bivalent. In diplotene, PSMA8 localizes at the still synapsed LEs and disappears at diakinesis. Bars represent 10 μm.

Figure EV3. *Psma8*$^{-/-}$ arrested spermatids do not express the transition proteins TNP1, TNP2, H2AL2. Immunolabelling of TNP1 (A), TNP2 (B) and H2AL2 (C) (green) show positive staining in round and elongatid spermatids from wild type mice but lack of staining in *Psma8*$^{-/-}$ mice. Chromatin was stained with DAPI. Bars represent 10 μm.

Figure EV4. Normal synapsis and desynapsis in spermatocytes lacking PSMA8. Double immunolabeling of SYCP3 (red) and SYCP1 (green) showing normal synapsis and desynapsis from early pachytene to late diplotene. DNA was stained with DAPI. Bars represent 10 μm.

Figure EV5. DSBs are generated and repaired in spermatocytes lacking PSMA8. (A) Double immunolabelling of γ-H2AX (green) with SYCP3 (red) in wild-type and *Psma8*$^{-/-}$ spermatocytes from leptotene to diplotene (upper pannel). In WT and KO leptonemas, γ-H2AX labels intensely the chromatin. After repair at pachytene, γ-H2AX labelling remains only in the chromatin of the unsynapsed sex body. Late round spermatids (LR) but not early round spermatid (ER) from wild type mice show positive staining for γ-H2AX but these highly differentiated cells are lacking in the *Psma8*$^{-/-}$ tubules which are arrested at early round spermatids without γ-H2AX staining (bottom panel). (B) Double immunolabelling of SYCP3 (red) and RAD51 (green). RAD51 foci associates to the AEs in leptonema spermatocytes of both genotypes (similar number of foci) and dissociate towards pachytene with a similar kinetics. Bars represent 10 μm. Plots under each image panel represent the quantification of intensity or number of foci from *Psma8*$^{+/+}$ and *Psma8*$^{-/-}$ spermatocytes. Welch´s *t*-test analysis: * $p<0.01$; ** $p<0.001$; *** $p<0.0001$. (Table EV4).

Figure EV6. PSMA8 deficiency provokes an slight increase of H2AacK5 at prophase I. (A) Double immunolabelling of H2AacK5 (green) with SYCP3 (red) in wild-type (left panel) and *Psma8*$^{-/-}$ spermatocytes (right panel). In WT and KO spermatocytes chromatin start to be labelled at early pachytene around chromosomes axes. Plots from each panel representing the quantification of fluorescence intensity from *Psma8*$^{+/+}$ and *Psma8*$^{-/-}$ spermatocytes are in Fig 8A. Bars represent 10 μm.

Figure EV7. PSMA8 deficiency provokes an slight increase of H3ac at prophase I. (A) Double immunolabelling of H3ac (green) with SYCP3 (red) in wild-type (left panel) and *Psma8*$^{-/-}$ spermatocytes (right panel). Spermatocytes from *Psma8*$^{+/+}$ and *Psma8*$^{-/-}$ show labelling for H3ac at early pachytene in a very diffuse manner surrounding chromosomes axes. Plots from each panel representing the quantification of fluorescence intensity from *Psma8*$^{+/+}$ and *Psma8*$^{-/-}$ spermatocytes are in Fig 8B. Bars represent 10 μm.

Figure EV8. PSMA8 deficiency provokes an slight increase of H4ac at prophase I and in round spermatids. (A) Double immunolabelling of H4ac (green) with SYCP3 (red) in wild-type and *Psma8*$^{-/-}$ spermatocytes. Spermatocytes from *Psma8*$^{+/+}$ and *Psma8*$^{-/-}$ show labelling for H4ac in a very diffuse manner surrounding chromosomes from

pachytene to metaphase I (right panel). In wild type metaphase I, H4ac labelling appears weakly painting the chromosomes and on some of the centromeres. However, *Psma8*-deficient cells show a more intense labelling specially at the centromeres. (Lower panel) Round spermatid from *Psma8*$^{-/-}$ accumulates H4ac labelling at the chromatin in comparison with the WT. Plots from each panel representing the quantification of fluorescence intensity from *Psma8*$^{+/+}$ and *Psma8*$^{-/-}$ spermatocytes are in Fig 8C. Bars represent 10 μm.

Figure EV9. PSMA8 deficiency does not affect global ubiquitination during prophase (A) Double immunolabelling of Ubiquitin (green) and SYCP3 (red) of spermatocytes at pachytene and diplotene stage from *Psma8*$^{+/+}$ and *Psma8*$^{-/-}$. Ubiqutin labelling decorates faintly the chromatin around chromosome and more intensely the sex body in a similar fashion in both genotypes. Bars represent 10 μm. Plot under the image panel represents the quantification of fluorescence intensity from wild-type and mutant meiocytes. Welch´s *t*-test analysis: * $p<0.01$; ** $p<0.001$; *** $p<0.0001$.

Figure EV10. PSMA8 deficiency does not affect global sumoylation during prophase I. (A) Double immunolabelling of SUMO1 (green) and SYCP3 (red) of spermatocytes at late pachytene and late diplotene stage from *Psma8*$^{+/+}$ and *Psma8*$^{-/-}$. SUMO1 labelling decorates the chromosome axes with very low intensity and the sex body intensely.
(B) Double immunolabelling of SUMO2/3 (green) and SYCP3 (red) of spermatocytes at late pachytene and late diplotene stage from *Psma8*$^{+/+}$ and *Psma8*$^{-/-}$. SUMO2/3 labelling is very similar to SUMO1. Bars represent 10 μm. Plots under each image panel represent the quantification of intensity from wild-type and mutant meiocytes. Welch´s *t*-test analysis: * $p<0.01$; ** $p<0.001$; *** $p<0.0001$.

Figure EV11. Lack of co-immunoprecipitation of PSMA8 with candidate interactors. (A) HEK293T cells were co-transfected with GFP-SYCE1, GFP-SYCE2, GFP-TEX12, GFP-TEX30, GFP-PIWIL1, and GFP-PIWIL2 and with Flag-PSMA8. Protein complexes were immunoprecipitated overnight with either an anti-Flag or anti-EGFP or IgGs (negative control) and were analysed by immunoblotting with the indicated antibody. PSMA8 does not co-immunoprecipitates (co-IP) with any of them.

Figure EV12. TRIP13 levels are increased in *Psma8*-deficient spermatocytes. (A) The results (using two independent antibodies) show a sharp labeling of the telomeres starting with low intensity at zygotene, increasing at pachytene and decreasing again through desynapsis at diplotene and diakinesis. The intensity of the TRIP13 (green) labelling is enhanced during prophase I in the *Psma8* mutants but not its labelling pattern. At metaphase I a faint labelling of sister kinetochores is observed in the *Psma8*-deficient spermatocytes that is absent in the wild type (faint stain over the centromeres). Bars represent 10 μm.

Figure EV13. HORMADS are not affected by the increased expresion of *Trip13* in the *Psma8*$^{-/-}$ spermatocytes. Double immunolabelling of HORMAD1 (A) and HORMAD2 (B) (green) with SYCP3 (red) in *Psma8*$^{+/+}$ and *Psma8*$^{-/-}$ spermatocytes at zygotene and pachytene stages. As synapsis progresses HORMAD1 and HORMAD2 are released from the AEs and maintained at the AE of the sex body similarly in the wild type and in the mutant spermatocytes. Bars represent 10 μm.

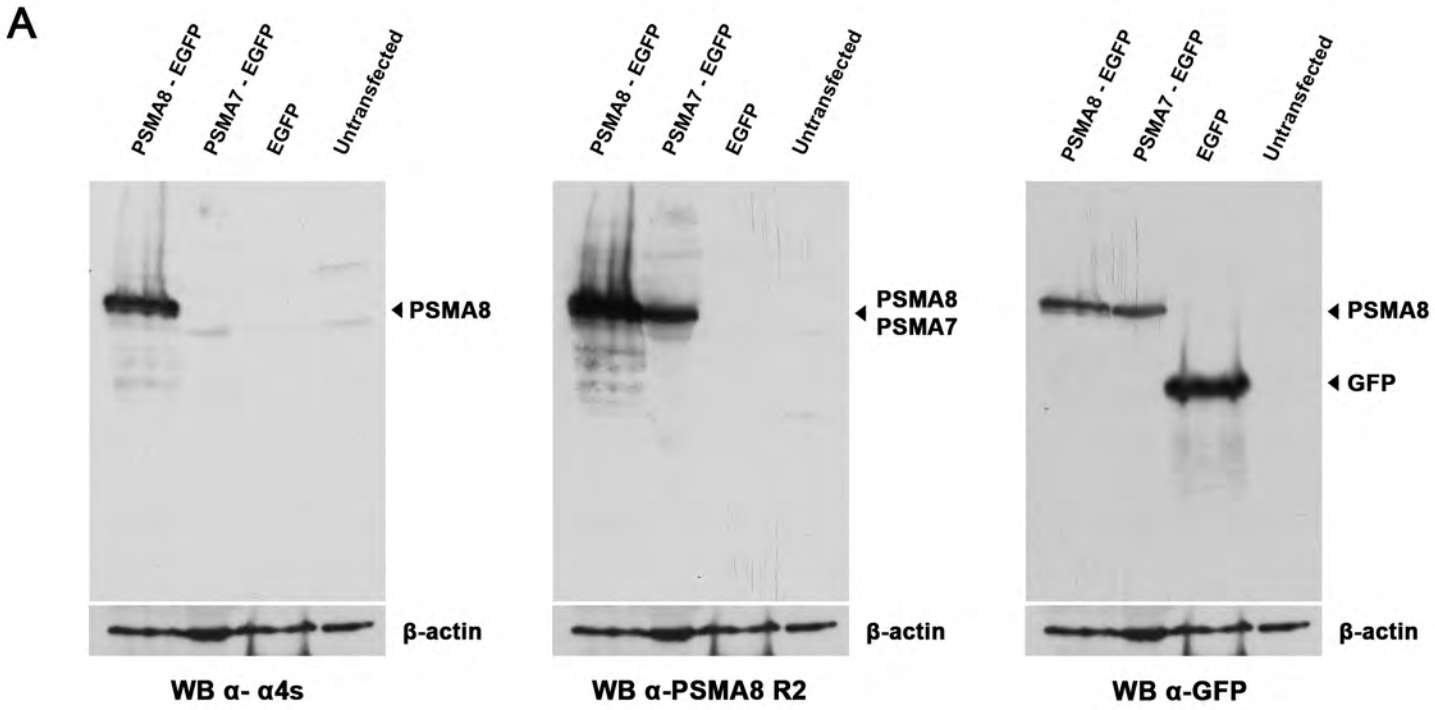

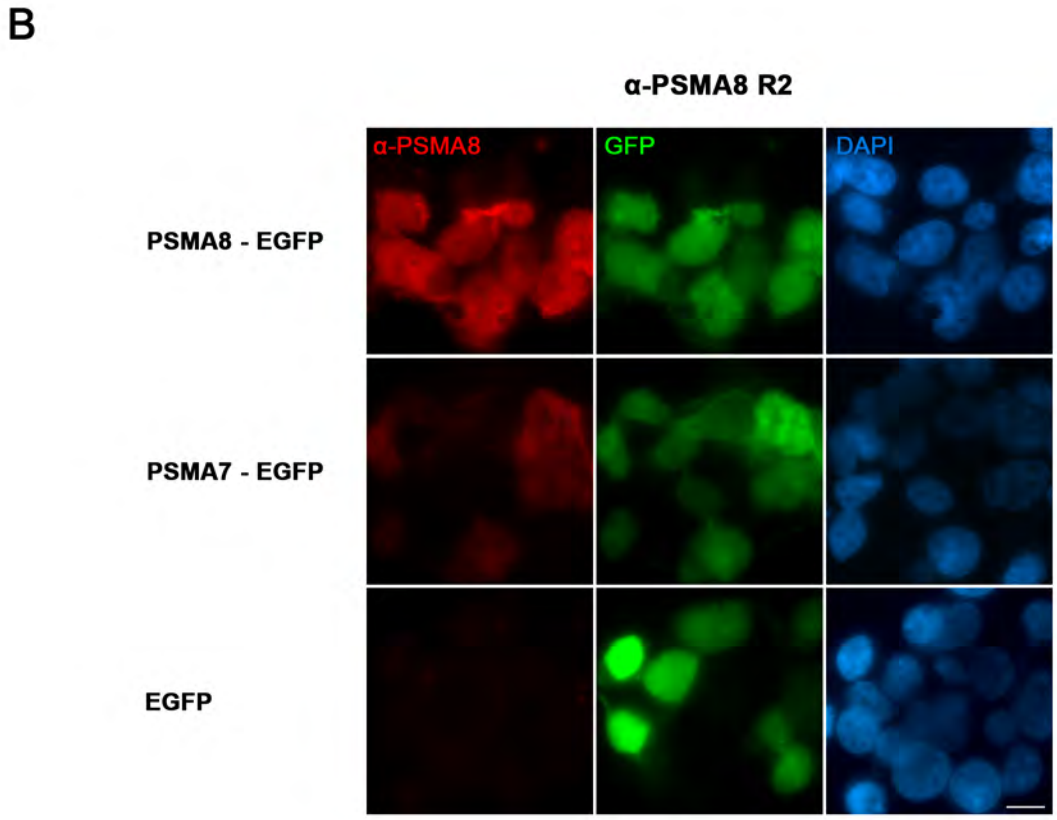

A

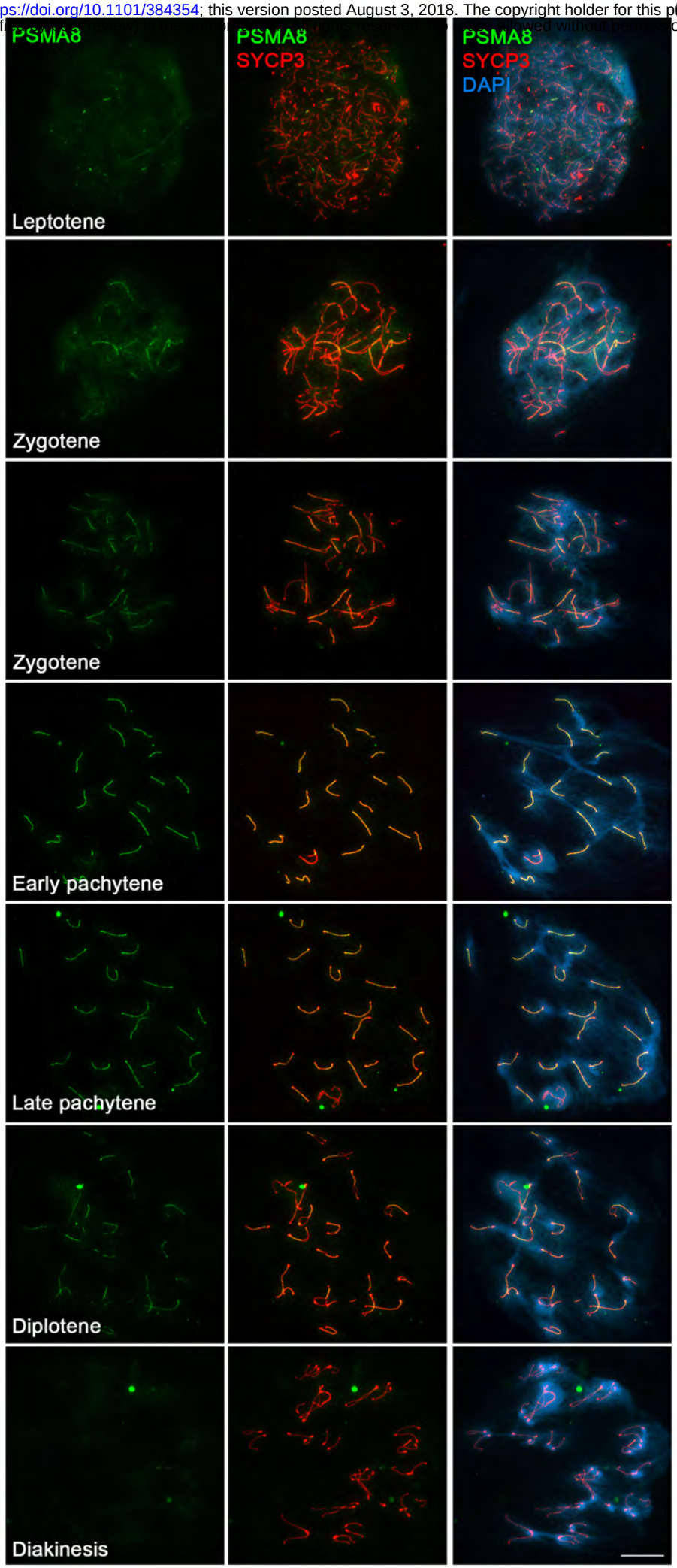

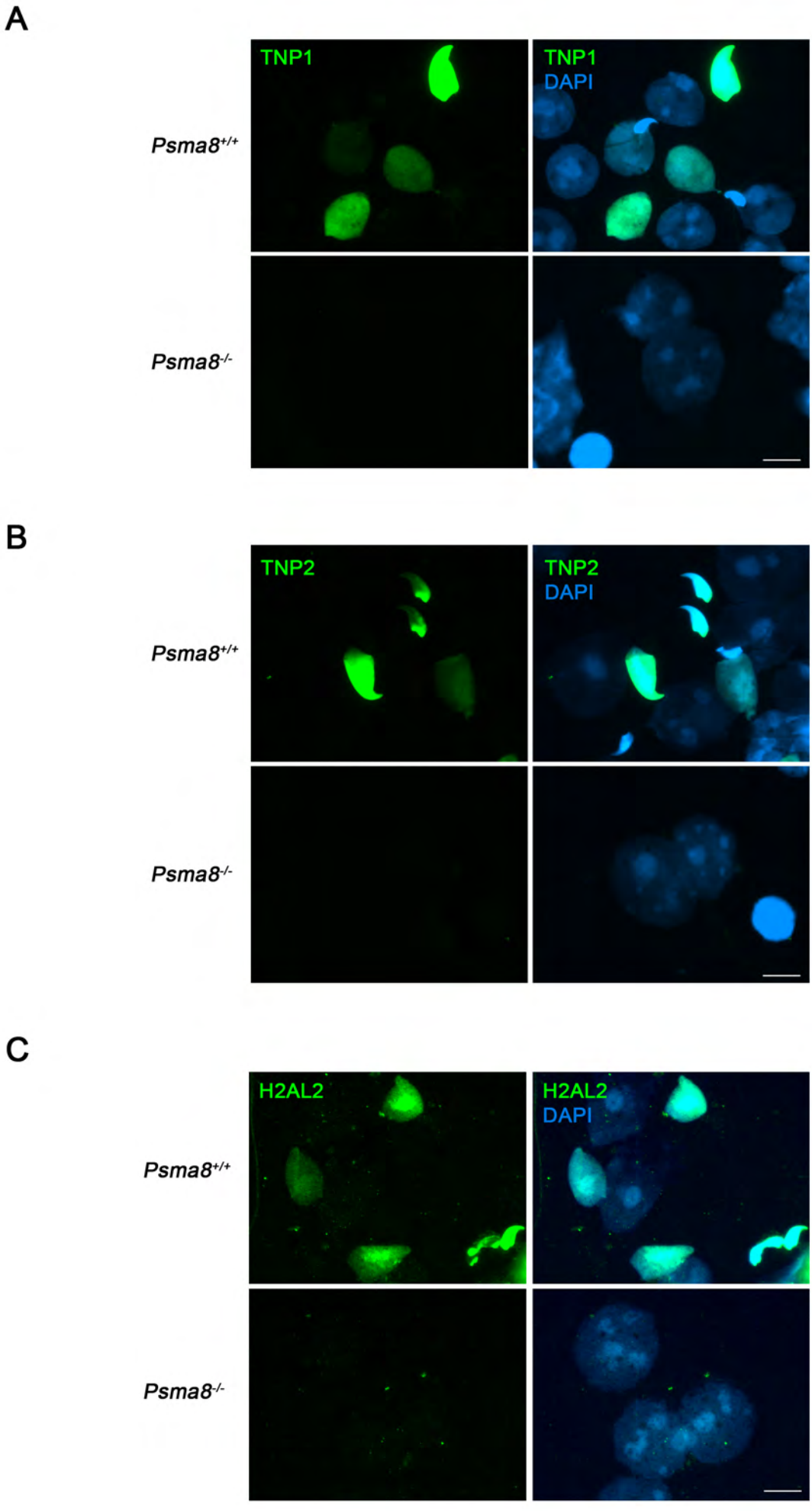

A

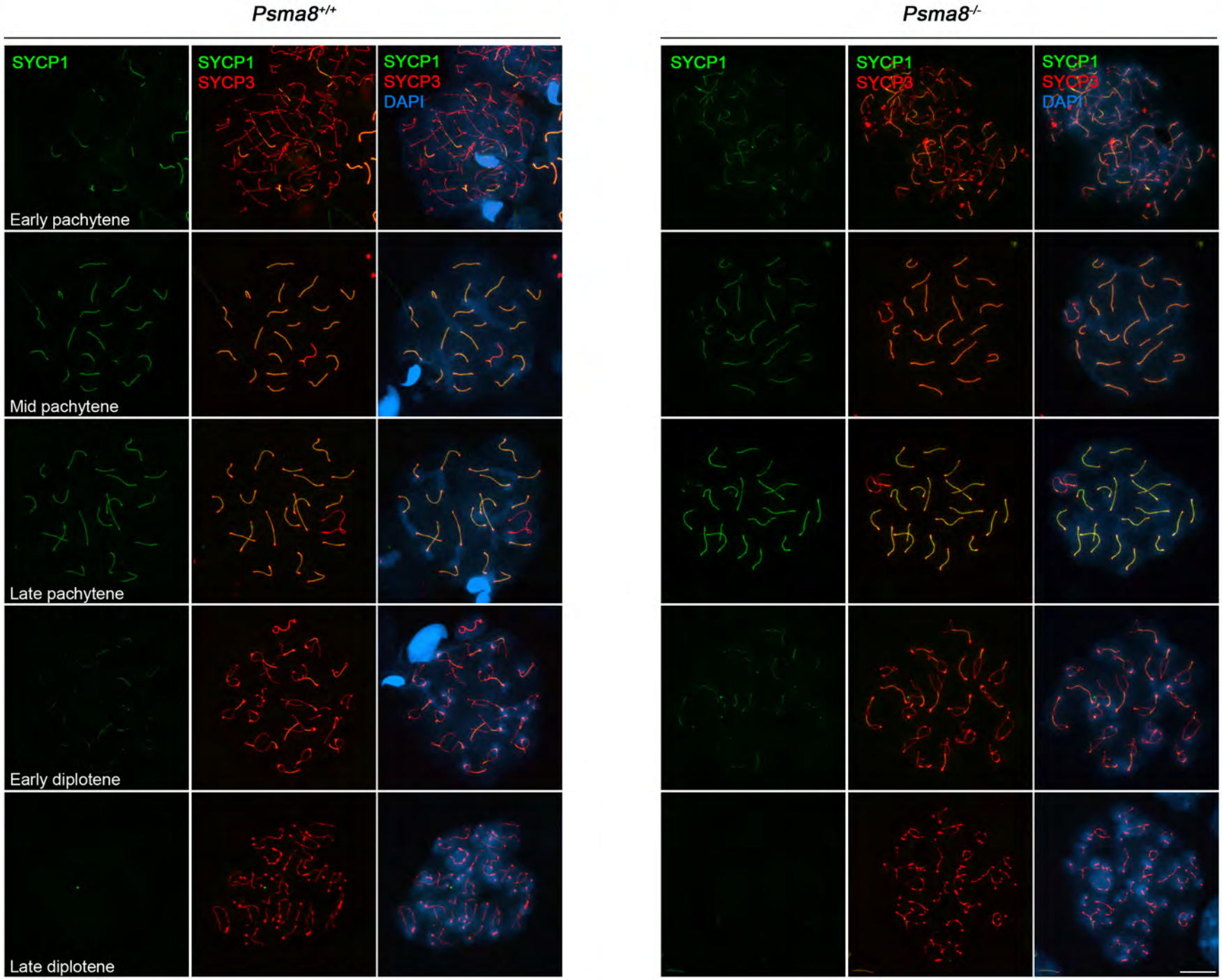
Psma8+/+
Psma8-/-
SYCP1
SYCP1
SYCP3
SYCP1
SYCP3
DAPI
Early pachytene
Mid pachytene
Late pachytene
Early diplotene
Late diplotene

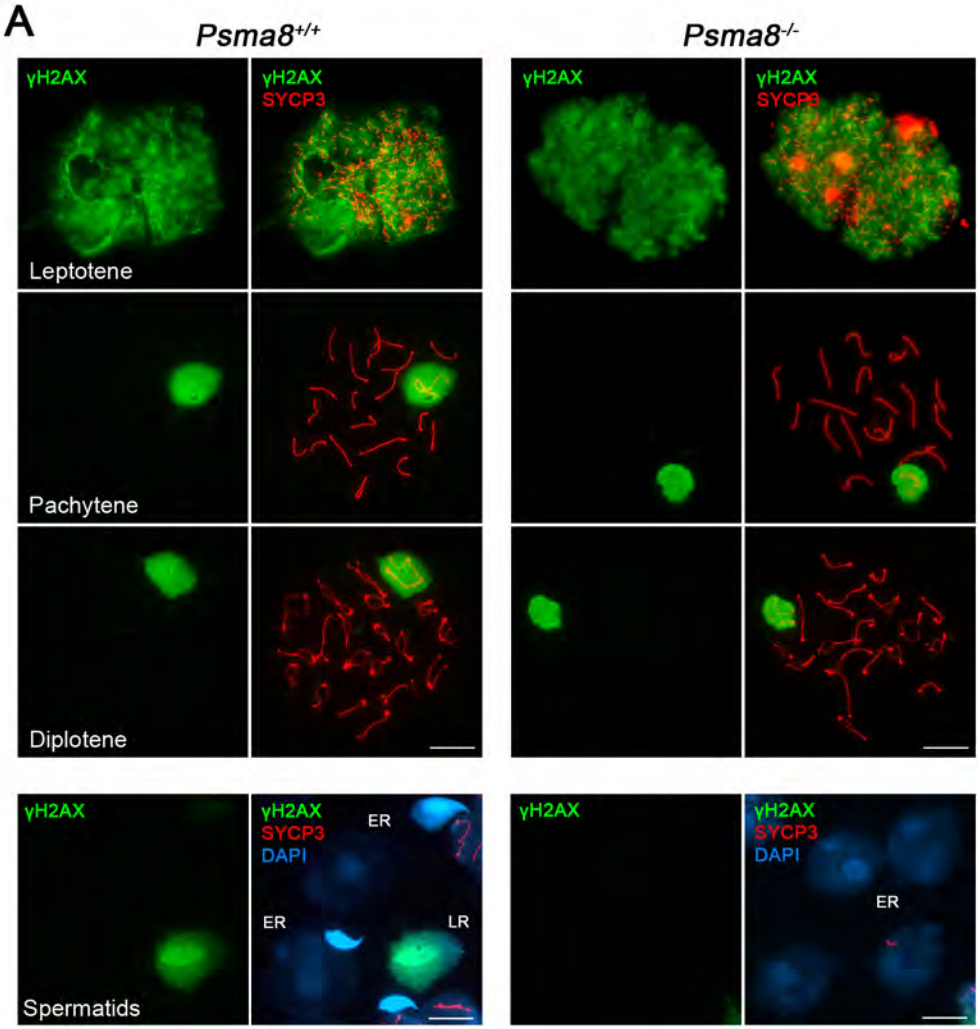
A
Psma8+/+
Psma8-/-
γH2AX
γH2AX SYCP3
Leptotene
Pachytene
Diplotene
γH2AX SYCP3 DAPI
ER
LR
Spermatids

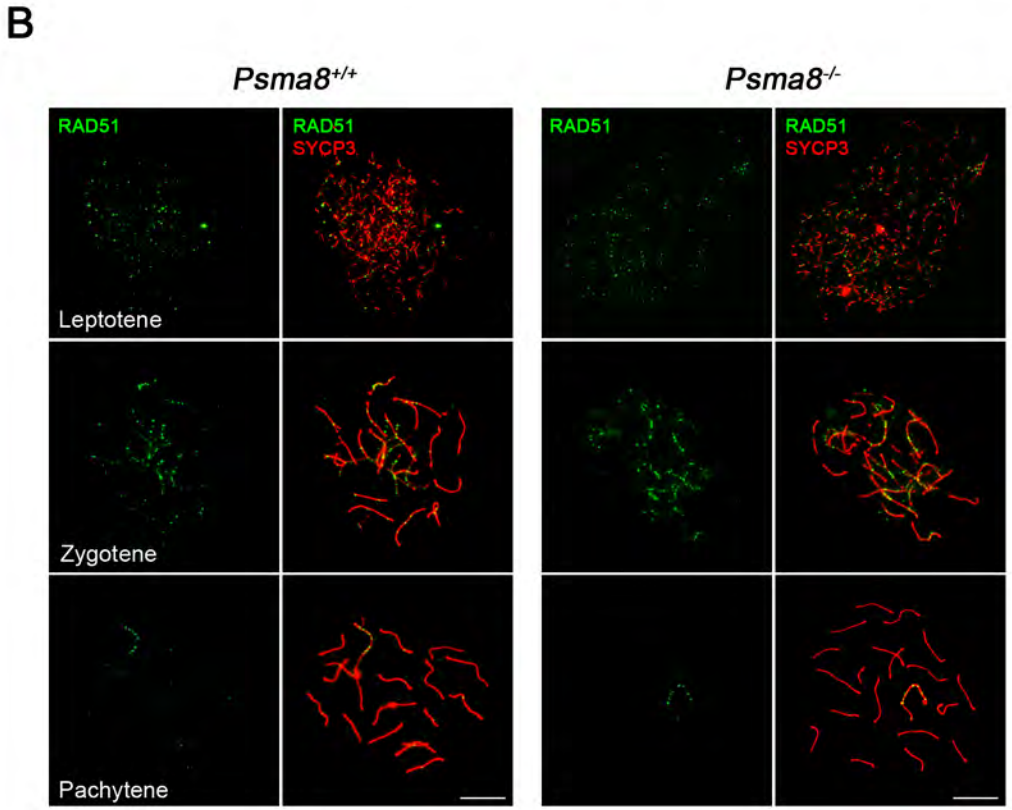
B
Psma8+/+
Psma8-/-
RAD51
RAD51 SYCP3
Leptotene
Zygotene
Pachytene

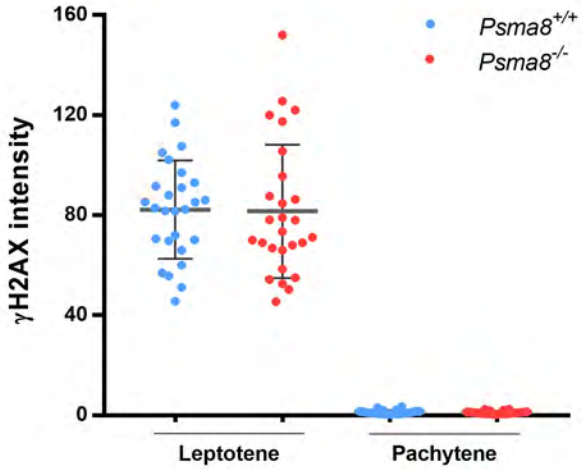
γH2AX intensity
160
120
80
40
0
Psma8+/+
Psma8-/-
Leptotene
Pachytene

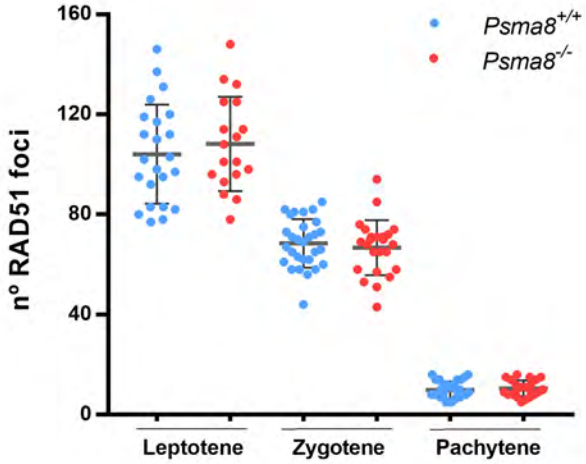
nº RAD51 foci
160
120
80
40
0
Psma8+/+
Psma8-/-
Leptotene
Zygotene
Pachytene

A

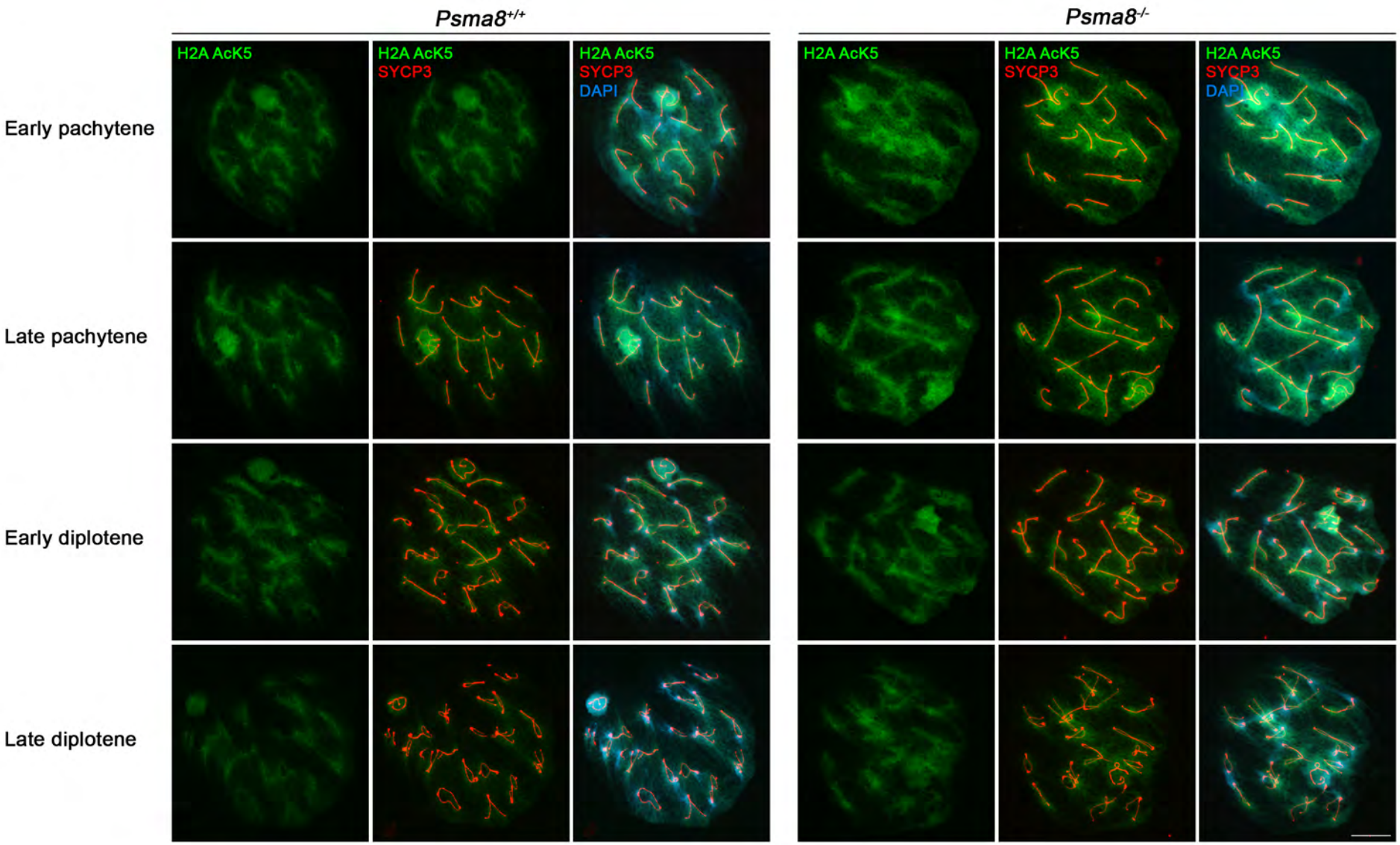
Psma8+/+
Psma8-/-
H2A AcK5
H2A AcK5
SYCP3
H2A AcK5
SYCP3
DAPI
Early pachytene
Late pachytene
Early diplotene
Late diplotene

A

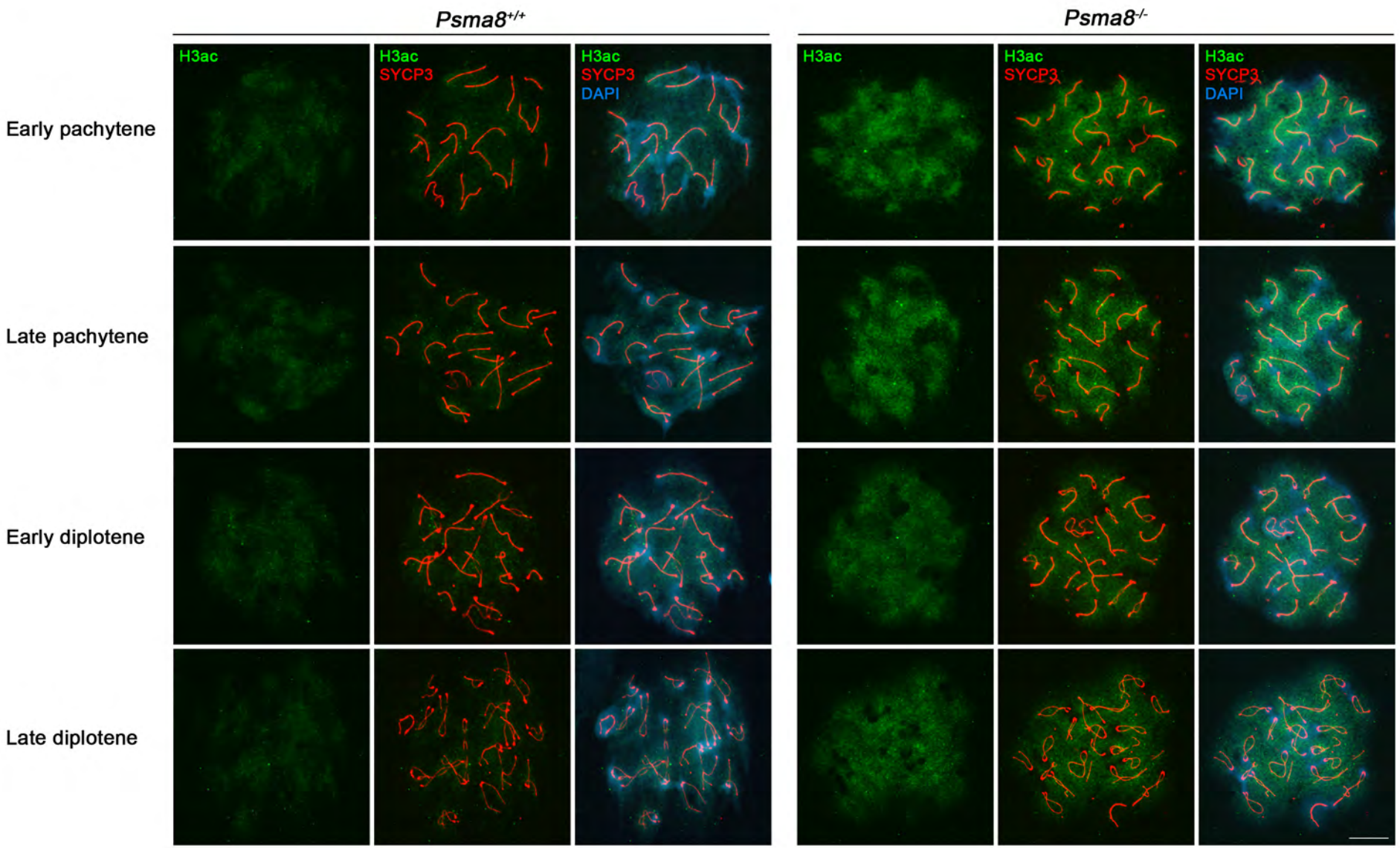
Psma8+/+
Psma8-/-
H3ac
H3ac
SYCP3
H3ac
SYCP3
DAPI
Early pachytene
Late pachytene
Early diplotene
Late diplotene

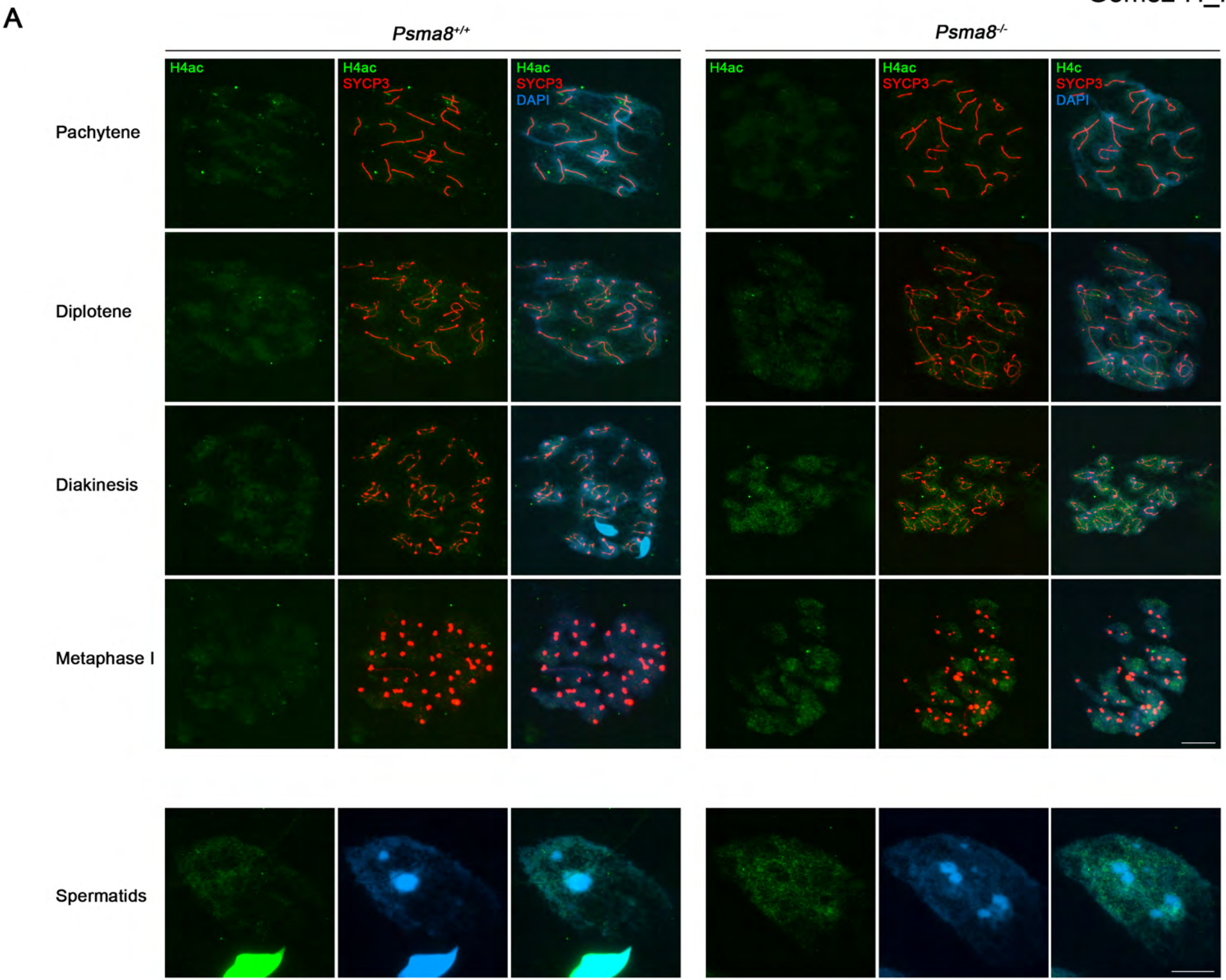
A
Psma8+/+
Psma8-/-
H4ac
H4ac
SYCP3
H4ac
SYCP3
DAPI
H4ac
H4ac
SYCP3
H4c
SYCP3
DAPI
Pachytene
Diplotene
Diakinesis
Metaphase I
Spermatids

A

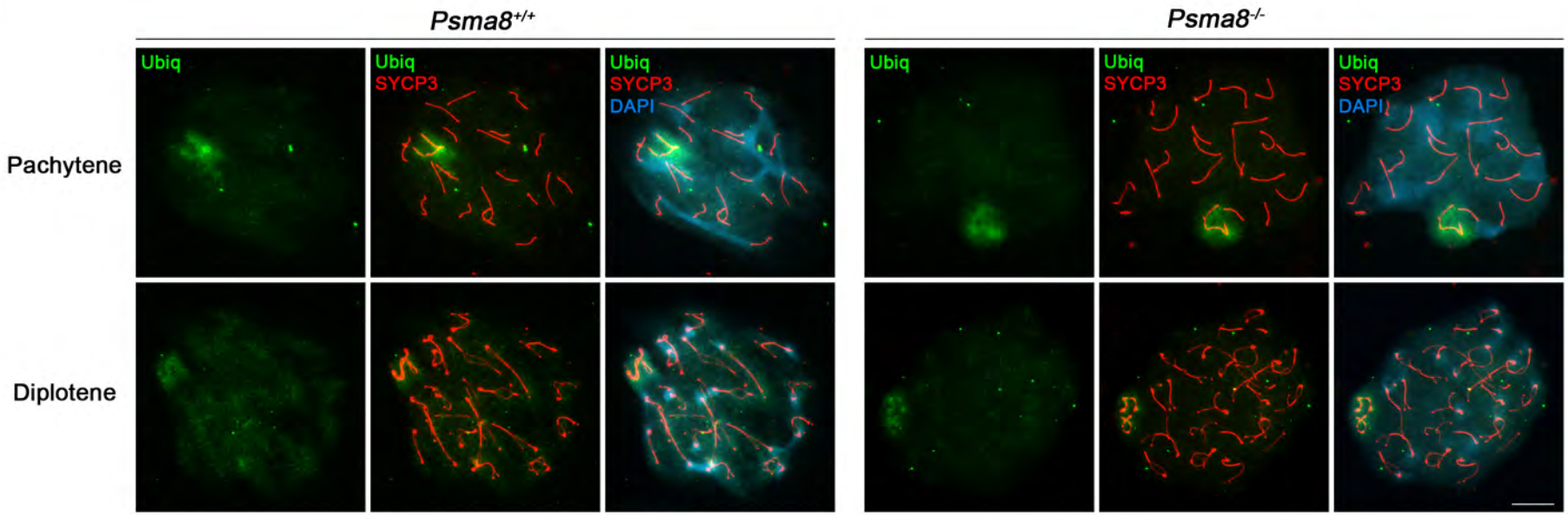
Psma8+/+
Psma8-/-
Pachytene
Diplotene
Ubiq
Ubiq
SYCP3
Ubiq
SYCP3
DAPI

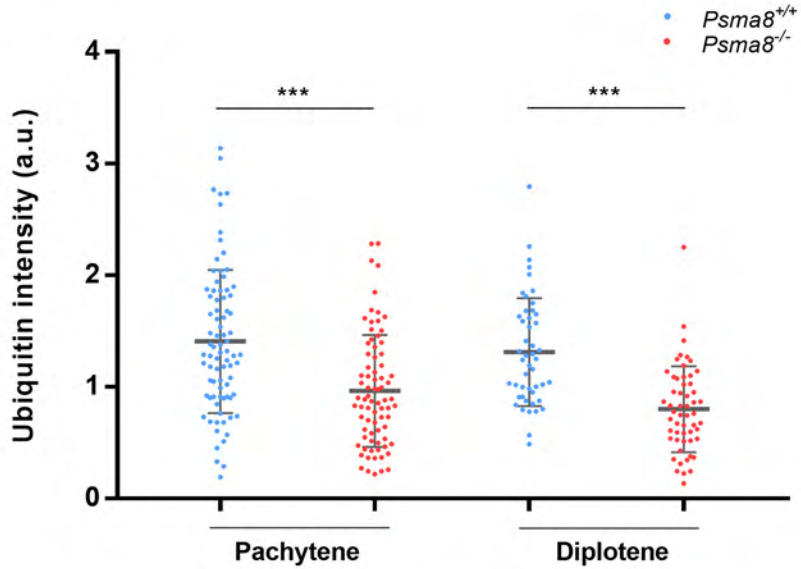
Psma8+/+
Psma8-/-
Ubiquitin intensity (a.u.)
0
1
2
3
4
***
***
Pachytene
Diplotene

A

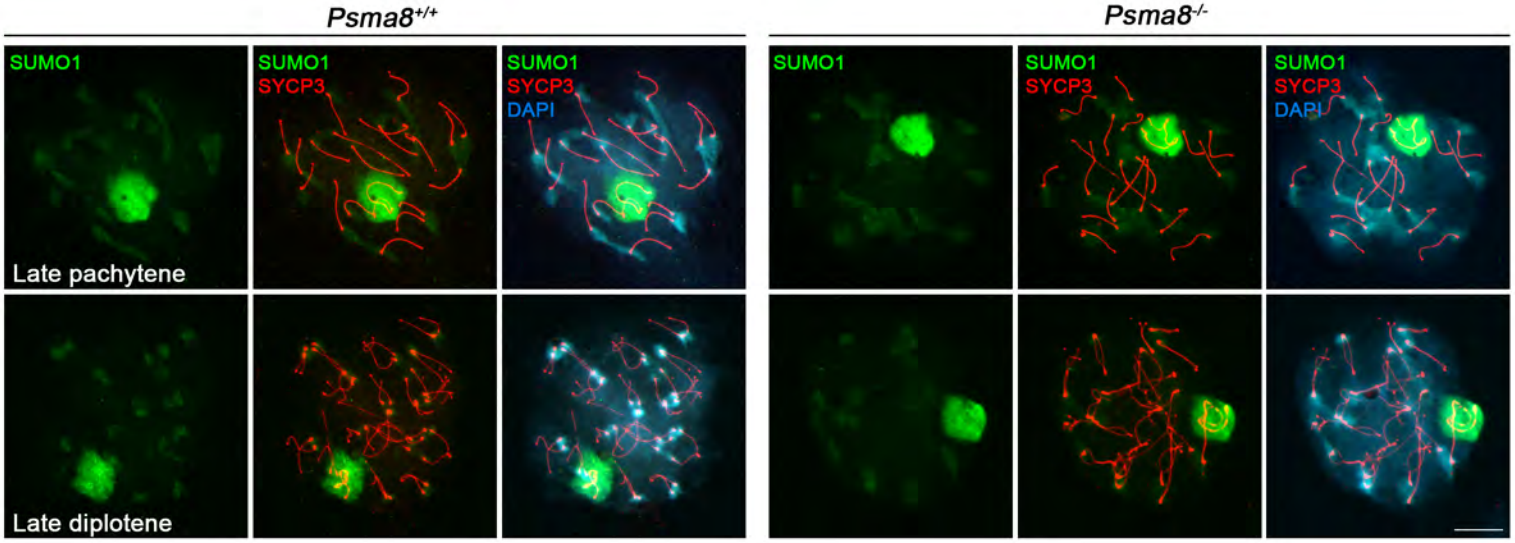

B

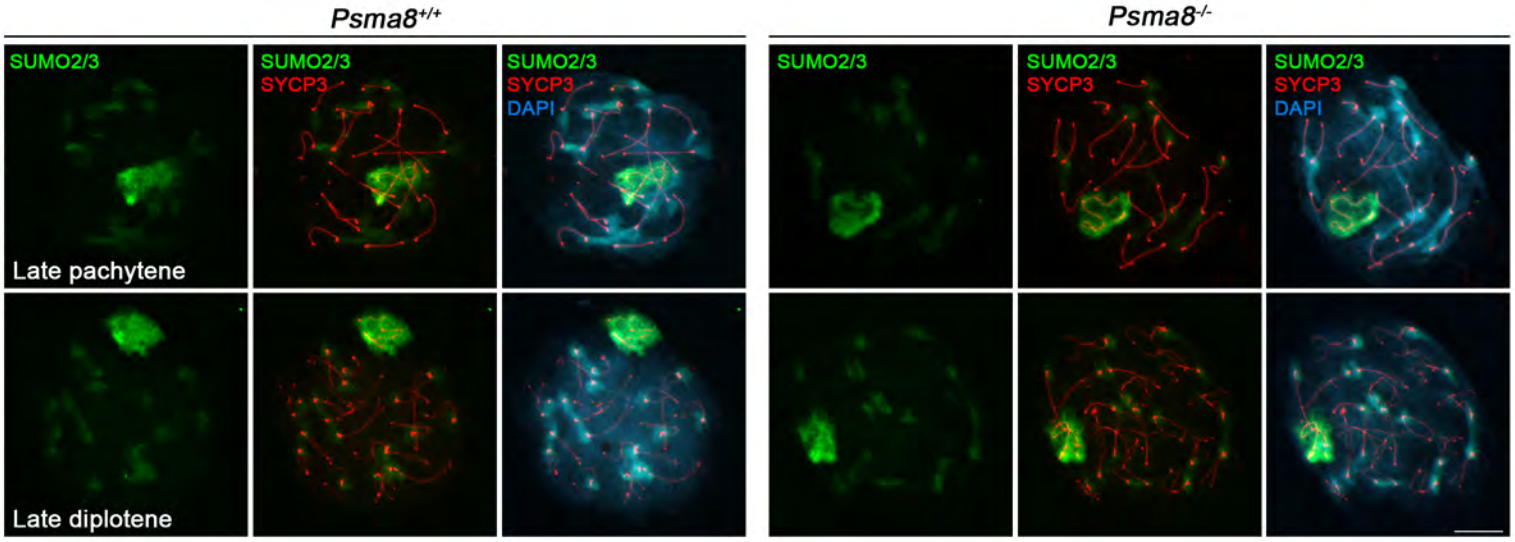

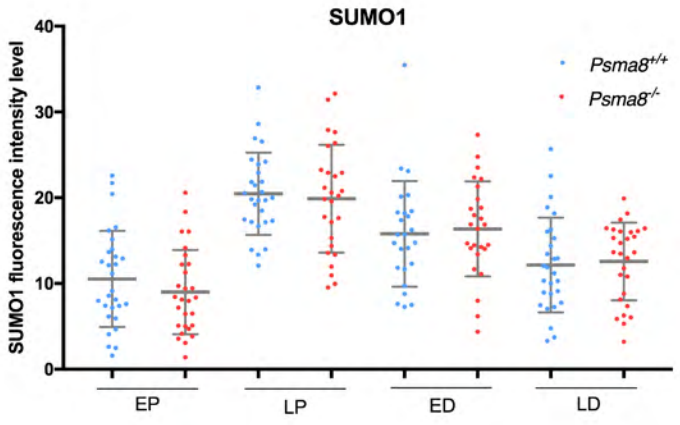

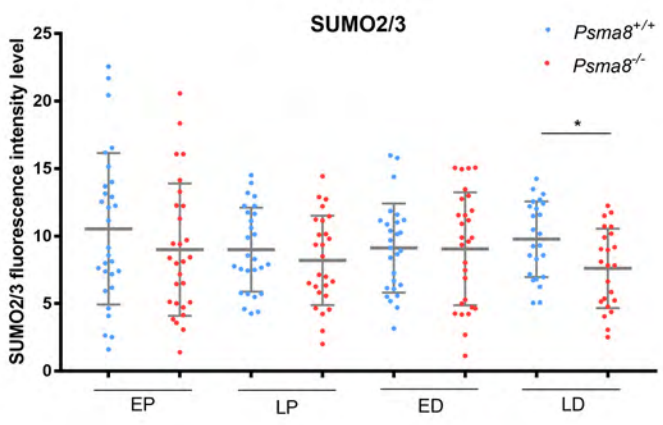

A

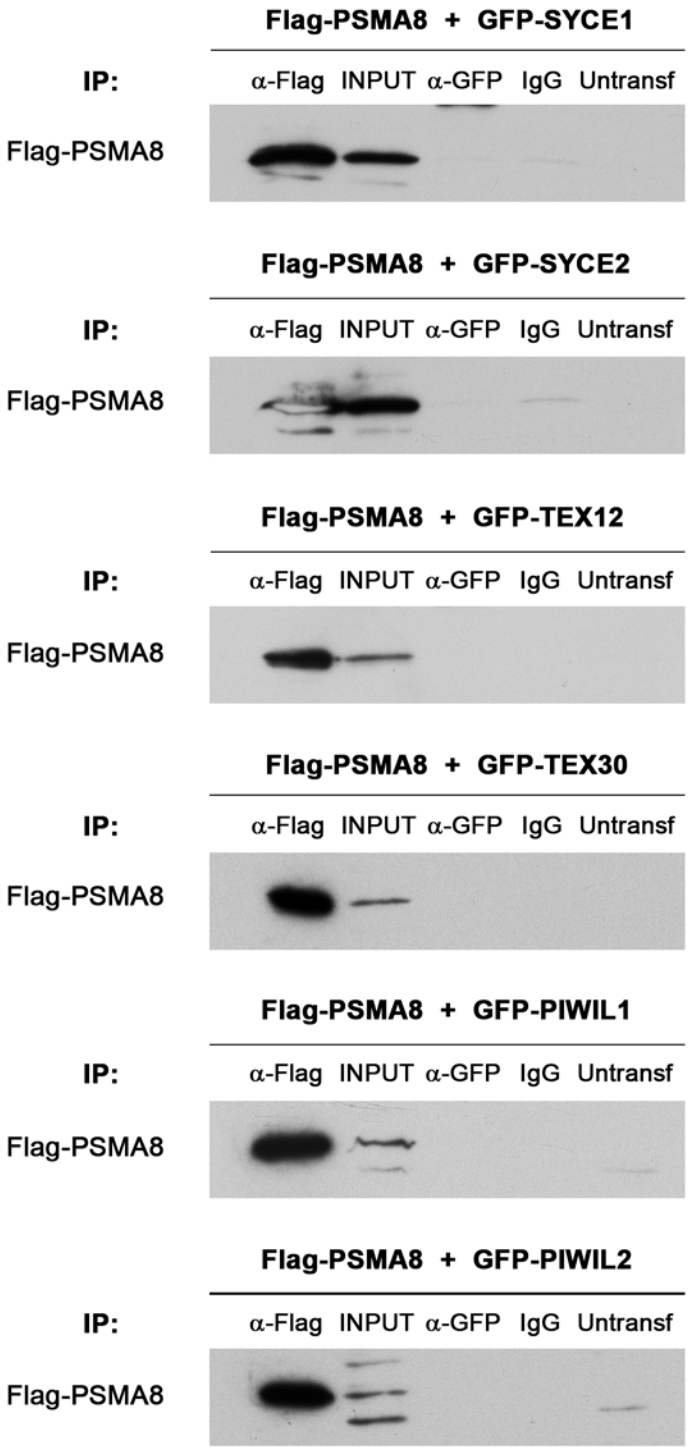

A

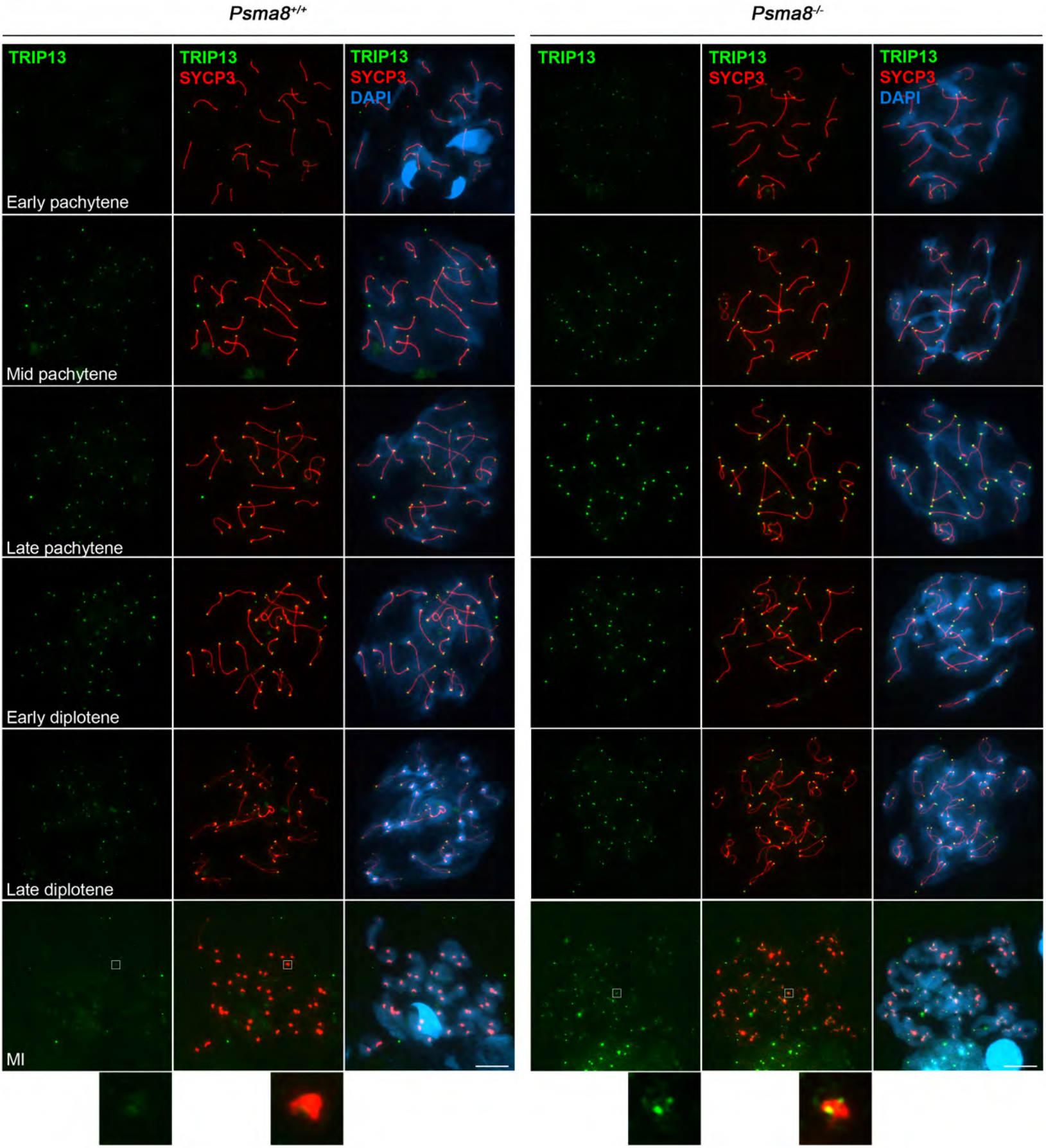

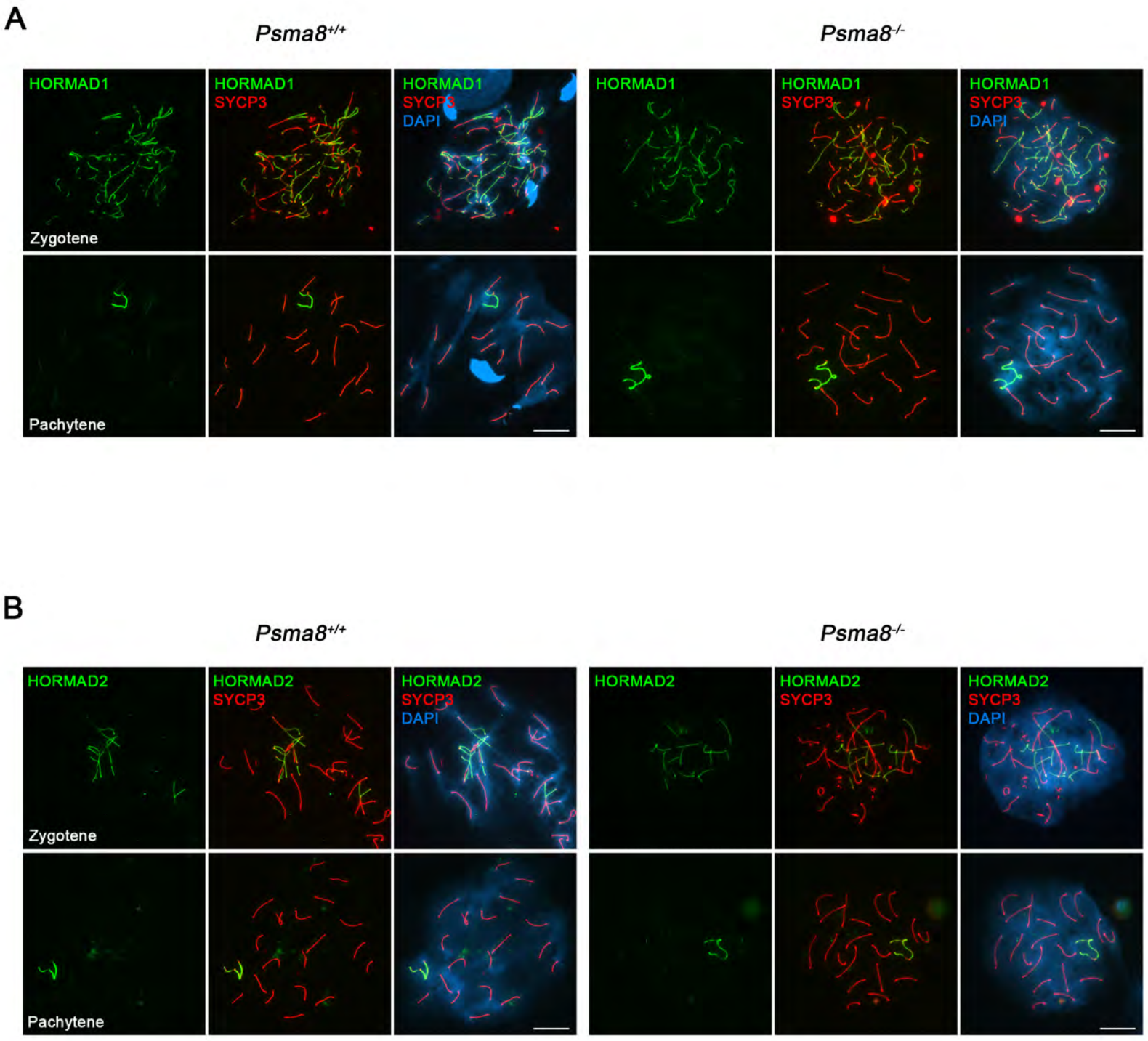

Table EVI

Name	Uniprot Accession ID	No of unique peptides			Sequence coverage			iBAQ Intensity			Ref.
		Ab1	Ab2	Control	Ab1	Ab2	Control	Ab1	Ab2	Control	
20 S Proteasome subunits											
PSMA1 (α1)	Q9R1P4	8	4	0	35.7	15.6	0	21249000	1213200	0	A
PSMA2 (α2)	P49722	7	1	0	41.5	6	0	12548000	163770	0	A
PSMA3 (α3)	O70435	7	4	1	33.3	19.6	4.7	20726000	1215300	79317	A
PSMA4 (α4)	Q9R1P0	7	2	1	38.7	10	3.8	29307000	452740	54041	A
PSMA5 (α5)	Q9Z2U1	9	5	0	49.8	24.1	0	21477000	1107800	0	A
PSMA6 (α6)	Q9QUM9	7	2	1	35.4	10.2	4.1	9870500	354100	28488	A
PSMA7 (α7)	Q9Z2U0	4	6	0	46.8	52.4	5.6	11999000	11121000	0	A
PSMA8 (α4s)	Q9CWH6	9	6	1	62	43.2	8.8	259210000	120340000	176410	A
PSMB1 (β1)	O09061	13	4	1	61.2	21.7	5.8	35406000	1344300	69458	A
PSMB2 (β2)	Q9R1P3	5	2	0	35.8	12.9	0	6124800	113520	0	A
PSMB3 (β3)	Q9R1P1	7	4	1	41.5	26.3	7.8	26797000	853790	66486	A
PSMB4 (β4)	P99026	5	2	0	35.6	13.3	0	8425400	263710	0	A
PSMB5 (β5)	O55234	13	6	2	57.2	23.1	8.7	26458000	1387200	91924	A
PSMB6 (β6)	Q60692	3	1	0	12.6	3.8	0	6322100	44701	0	A
PSMB7 (β7)	P70195	2	1	0	11.6	3.6	0	1435700	218870	0	A
Proteasome regulators											
19 S subunits											
PSMC1 (S4)	P62192	9	5	1	28.4	16.4	2.7	1670700	342000	62230	A
PSMC2 (S7)	P46471	8	4	4	23.3	10.6	11.3	1372900	289950	147590	A
PSMC3 (S6a)	A2AGN7	7	4	4	25.2	12.2	17.8	1011500	126150	172160	A
PSMC4 (S6b)	A0A140LIZ5	7	2	2	22.5	4.9	4.9	710210	136800	55476	A
PSMC5 (S8)	P62196	5	8	1	16.5	24.6	2.7	674310	255690	33610	A
PSMC6 (S10b)	P62334	9	5	5	29.6	15.2	16.2	1830300	176350	145970	A
PSMD1 (Rpn2/S1)	Q3TXS7	9	2	2	14.5	2.3	3.3	288850	15023	26996	A
PSMD2* (RPN1/S2)	Q8VDM4	7	7	11	10.7	8.8	13.9	439090	144410	263690	A
PSMD3 (Rpn3/S3)	P14685	8	5	5	17.9	11.1	11.7	1333400	156560	129110	A
PSMD4* (Rpn10/S5A)	O35226	1	1	0	4.8	3.2	0	246070	35322	0	A
PSMD5 (S5B)	Q8BJY1	2	2	1	5.6	3.6	1.8	106410	66715	18125	A
PSMD6* (Rpn7/S10)	Q99JI4	1	1	0	3.1	2.6	0	71743	15485	0	A
PSMD11 (Rpn6/S9)	Q8BG32	4	2	2	10.9	4	5.5	220960	42386	31410	A
PSMD13 (Rpn9/S11)	E9Q5I9	0	2	0	0	5.2	0	0	42839	0	A
Psmd14* (Rpn11)	O35593	1	1	1	4.2	4.2	4.2	175390	96458	47666	A
Other activators											
PSME3 (PA28γ)	A2A4J1	2	0	1	14.8	0	7.4	236880	0	33185	A
PSME4 (PA200)	Q5SSW2	3	1	0	1.7	0.7	0	25422	3386.8	0	A
Substoichiometric proteasome protein											
TXNL1	Q8CDN6	2	3	1	10	10.7	2.4	359900	110780	17998	B

A Wang, X., Chen, C. F., Baker, P. R., Chen, P. L., Kaiser, P., and Huang, L. (2007) Mass spectrometric characterization of the affinity-purified human 26S proteasome complex. Biochemistry 46, 3553–3565

B Andersen, K. M., Madsen, L., Prag, S., Johnsen, A. H., Semple, C. A., Hendil, K. B., & Hartmann-Petersen, R. (2009). Thioredoxin Txnl1/TRP32 Is a Redox-active Cofactor of the 26 S Proteasome. The Journal of Biological Chemistry, 284(22), 15246–15254. http://doi.org/10.1074/jbc.M900016200

Table EV1: Proteasome subunits and proteasome regulators coimmuniprecipitated with PSMA8 selected after analysis and filtering of the data.

*Due to their relevance, these proteins were also included in the present table as an “ad-hoc” selection to show their behavior in spite of them not passing our cut-off

Name	Uniprot Accession ID	No of unique peptides			Sequence coverage			iBAQ Intensity		
		Ab1	Ab2	Control	Ab1	Ab2	Control	Ab1	Ab2	Control
E3 ligases										
CAND1	Q6ZQ38	10	8	5	10	7.9	5.2	275300	143200	27601
CCT2	P80314	14	5	7	37.2	15	21.3	1713000	367550	184630
CUL3	Q9JLV5	3	6	1	6.8	9.6	1.3	104730	187950	6432.1
CUL9	E9QP09	3	2	0	1.1	0.6	0	20528	4934	0
NEDD4	P46935	2	0	0	4.7	0	0	68196	0	0
RAD18	E9Q392	3	0	0	43.7	0	0	20227000	0	0
RBX1	P62878	0	2	0	0	17.6	0	0	192900	0
SKP1	Q9WTX5	2	1	1	10.4	7.4	7.4	503960	136060	60179
TRIP12	A0A087WRV6	3	0	0	4.7	0	0	11882	0	0
TRIM36	E9Q3A0	5	1	0	9.3	2	0	237780	18278	0
UBR5	E9Q2H1	2	0	0	1.1	0	0	17518	0	0
UFL1	Q8CCJ3-1	2	0	0	3.8	0	0	57646	0	0
ZC3HC1	D3Z3D0	0	2	0	0	7.4	0	0	50351	0
Deubiquitinases										
USP5	Q3U4W8	1	2	0	1.9	4.1	0	3715.8	28815	0
USP7	F8VPX1	5	0	0	5.7	0	0	105410	0	0
USP9X	Q4FE56	10	2	0	4.9	1	0	121220	7683.3	0
USP14*	E9PYI8	0	1	0	0	5.2	0	0	32751	0
USP34	F6WJB7	6	0	0	2	0	0	41209	0	0
USP40*	Q8BWR4-3	1	1	0	1	1	0	22401	0	0
USP47	A0A1L1SV73	2	1	0	2.5	1.2	0	18169	2177.4	0
Chaperones										
AHSA1	Q8BK64	2	1	1	8.6	3	6.5	227160	2825.1	20386
CCT6B	Q61390	3	1	0	12.1	4.9	3.2	132900	25309	0
DNAJA1	P63037	2	1	0	8.1	3	0	1047200	67368	0
DNAJB9	Q9QYI6	1	2	0	4.5	11.3	0	66228	60676	0
DNAJC7	Q9QYI3	13	8	2	31.6	18.2	4	1376900	227200	25321
HSP90B1	P08113	17	8	9	28.8	12.2	14.5	4511300	1355800	619050
HSP90AB1	P11499	8	5	5	23.9	19.8	19.6	3171500	1127200	452050
HSPBP1	A0A0U1RPF2	2	0	0	6.9	0	0	46940	0	0
PSMG1 (PAC1)	Q9JK23	2	1	1	5.9	3.5	3.5	258480	35351	19395
TRAP1	Q9CQN1	4	5	0	6.9	8.1	0	143070	57267	0
Putative pips/ a priori unrelated / spermatogenesis related										
ADAD1	F8WI80	3	0	0	10	0	0	202110	0	0
BOLL	G3UYE8	3	1	1	11.7	3.2	3.2	400070	23474	37352
CAP1	P40124	0	2	2	0	4	6.8	0	46407	28930
CDK1	P11440	1	1	0	8.1	6.4	0	7093.3	41663	0
CDK5	P49615	3	1	2	12	6.5	6.5	542280	197000	29690
CDK16	Q04735-2	0	2	0	1.7	6.3	0	0	25675	0
DAZL	Q64368	3	3	0	13.4	15.4	0	473450	206150	0
MAEL	A0A0A6YWQ9	2	0	0	4.8	0	0	247850	0	0
RNF17	Q99MV7	8	4	1	5.7	2.9	0.7	161450	29164	4053.3

SHCBP1L	Q3TTP0	13	5	4	24.4	11	9.5	6787500	299050	173530
SMC4	E9Q2X6	4	1	0	3.6	0.7	0	130810	9056.2	0
SMC6	Q924W5	2	0	0	2.3	0	0	17639	0	0
SPAG1	Q80ZX8-3	4	3	0	8.1	6.1	0	290980	30285	0
SPATA5	A0A0G2JFY0	9	2	0	17.5	3.1	0	239890	13235	0
SPATA20	Q80YT5	7	7	3	11.6	12.4	4.1	1291900	234350	63556
SYCP1	Q62209	11	0	0	13.7	0	0	727550	0	0
TDRD1	Q99MV1	4	1	0	4.2	0.9	0	60474	3896.1	0
TDRD6	F2Z429	18	8	3	11.3	5	1.6	586920	46319	10974
TDRD9	Q14BI7	8	1	0	7.4	0.8	0	133480	5407.1	0
TDRKH	A0A0G2JFB2	4	2	0	9.4	4	0	384790	71610	0
TRIP13	Q3UA06	2	2	0	5.3	5.3	0	98523	41275	0

Table EV2: Selection of some of the proteasome-related proteins coimmuniprecipitated with PSMA8 selected after analysis and filtering of the data.

*Due to their relevance, these proteins were also included in the present table as an “ad-hoc” selection to show their behavior in spite of them not passing our cut-off.

Table EV3. Quantification of the percentage of metaphases I and metaphases II in the seminiferous tubules (number of metaphases relative to the number of prophases).

	MI - AI		MII - AII	
	WT	**KO**	**WT**	**KO**
Total	1.66 ± 0.50	6.75 ± 0.52	0.92 ± 1.03	8.32 ± 3.35
Apoptotic	0.09 ± 0.13	3.90 ± 0.53	0.00 ± 0.00	6.17 ± 4.05
n	855	1028	855	1028

Table EV4. Quantification of γH2AX levels and RAD51 foci

γH2AX		Mean (intensity)	SD	n
Leptotene	WT	82.23	19.64	27
	KO	81.58	26.69	27
Pachytene	WT	1.33	0.79	28
	KO	1.17	0.59	28

RAD51		Nº foci	SD	n
Leptotene	WT	104.13	19.80	23
	KO	111.53	18.79	18
Zygotene	WT	65.52	9.69	29
	KO	66.79	10.98	24
Pachytene	WT	9.90	3.39	29
	KO	10.55	3.23	22

A

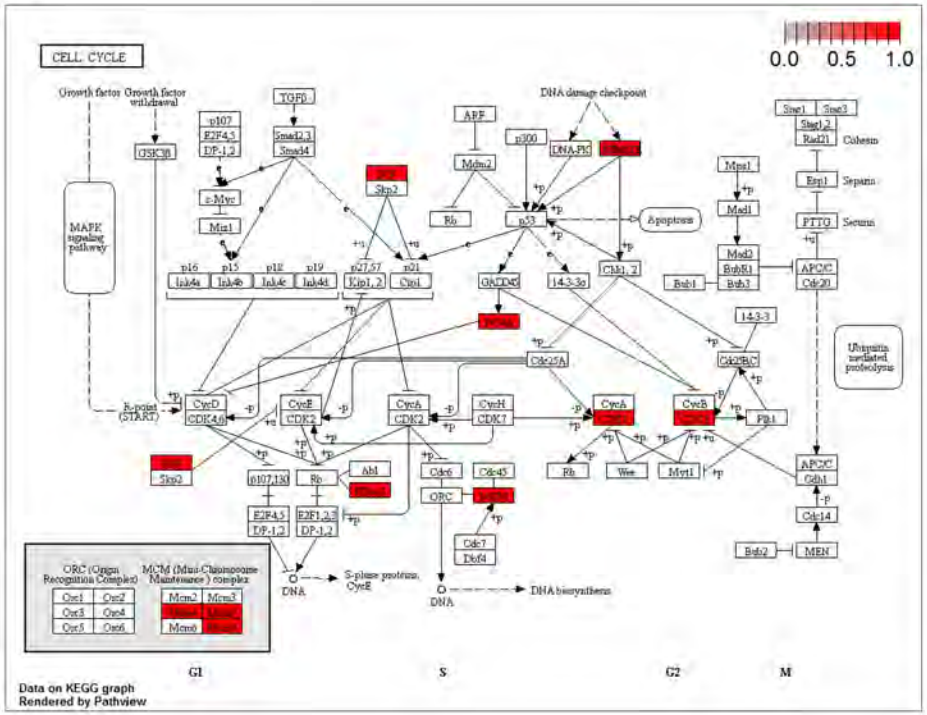

B

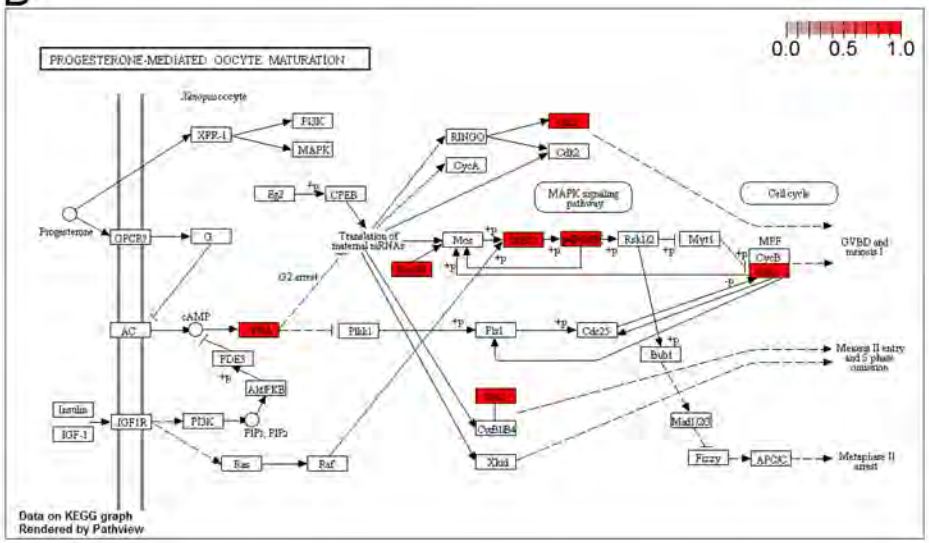

C

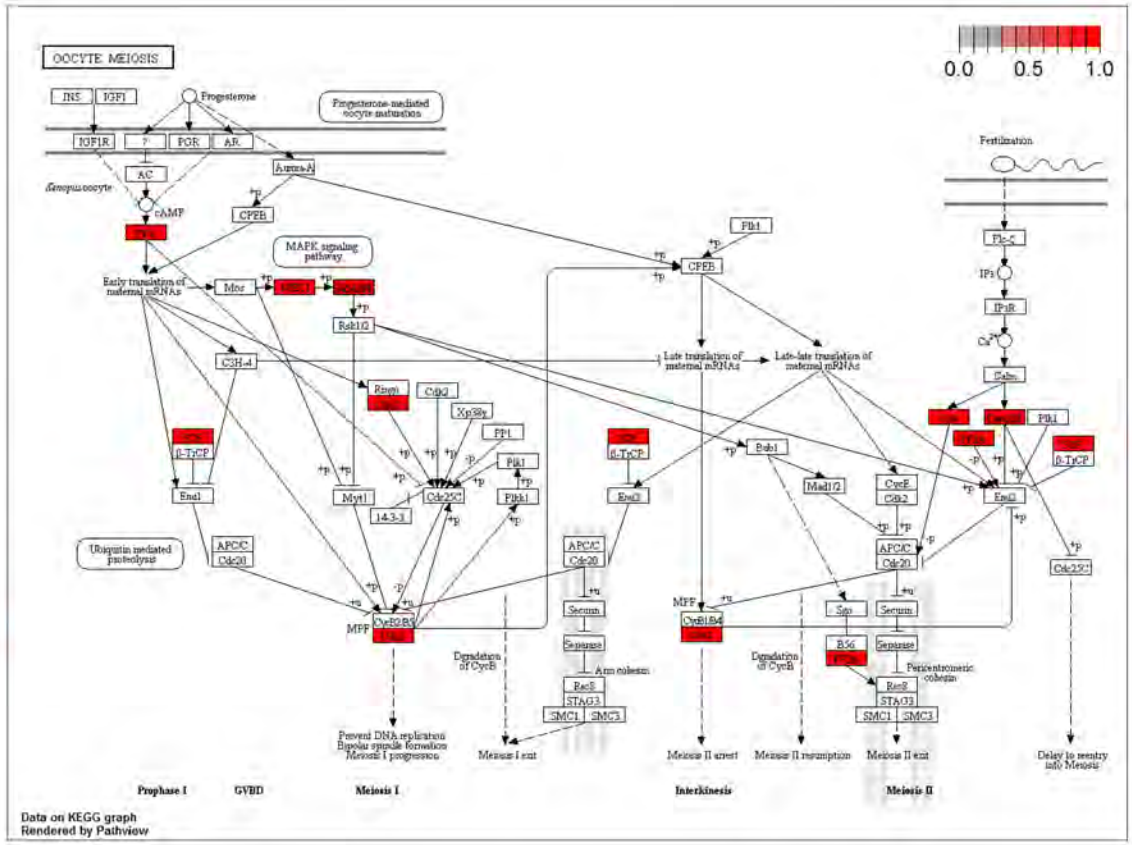

Exploratory representation of representative KEGG pathways.
a) Cell cycle (mmu04110)
b) Progesterone-mediated oocyte maduration (mmu04914).
c) Oocyte meosis (mmu04114)
In red, proteins detected in the coIP experiment over the stablished cut-off.

Name	Accession	Unique peptides RP1	Unique peptides RP2	Unique peptides IgG	Coverage RP1	Coverage RP2	Coverage IgG	Intensity RP1	Intensity RP2	Intensity IgG
Psma8	Q9CWH6	9	6	1	62	43.2	8.8	259210000	120340000	176410
Akr7a2	Q8CG76	13	3	3	41.7	10.4	10.4	203430000	1922700	143740
Hspa2	P17156	22	16	16	52.4	41.9	41.9	126310000	47492000	16229000
Sh3d21	Q7TSG5	33	4	2	54.6	9.8	5.8	80406000	153000	40492
Hadh	Q61425	14	5	1	61.8	20.7	3.2	64139000	7135200	32120
Gm8797	A0A0A6YW67	2	2	3	32.5	32.5	44.2	49406000	9117600	3730300
Prdx4	O08807	5	0	0	49.3	2.9	0	36224000	80086	0
Hspa8	P63017	15	11	14	42.9	32.4	35.6	36110000	8719000	3455800
Psmb1	O09061	13	4	1	61.2	21.7	5.8	35406000	1344300	69458
Atf7ip	Q7TT18	18	1	0	35.1	2.1	0	34376000	72907	0
Psma4	Q9R1P0	7	2	1	38.7	10	3.8	29307000	452740	54041
Psmb3	Q9R1P1	7	4	1	41.5	26.3	7.8	26797000	853790	66486
Psmb5	O55234	13	6	2	57.2	23.1	8.7	26458000	1387200	91924
Ldhc	P00342	12	6	7	44.9	26.5	28.3	22573000	7205200	3471000
Psma5	Q9Z2U1	9	5	0	49.8	24.1	0	21477000	1107800	0
Psma1	Q9R1P4	8	4	0	35.7	15.6	0	21249000	1213200	0
Psma3	O70435	7	4	1	33.3	19.6	4.7	20726000	1215300	79317
Rad18	E9Q392	3	0	0	43.7	0	0	20227000	0	0
Stk31	Q99MW1	37	23	6	47.7	30.3	7.4	18616000	3881400	59667
Ran	P62827	6	4	4	32.4	20.8	20.8	14907000	5073700	2980000
Gpx4	S4R1E5	6	2	3	36.9	13.4	22.3	13839000	1299000	770470
Psma2	P49722	7	1	0	41.5	6	0	12548000	163770	0
Setdb1	G5E8N3	28	7	0	21.1	5.4	0	12272000	198930	0
Psma7	Q9Z2U0	4	6	0	46.8	52.4	5.6	11999000	11121000	0
Pdia6	Q922R8	12	3	7	36.4	10.5	22	11933000	501830	905310
Rpl27	P61358	4	2	4	36	12.5	39.7	11587000	5531300	1610800
Cyp17a1	P27786	17	9	12	43.2	21.5	30.6	10917000	3014000	1389700
Rpl18	A0A1B0GQU8	5	3	1	29.6	22	6.9	9900000	1810300	158990
Psma6	Q9QUM9	7	2	1	35.4	10.2	4.1	9870500	354100	28488
Dynll1	P63168	2	0	0	62.9	12.4	12.4	9351700	80015	159090
Atp5c1	Q8C2Q8	7	4	6	25.2	16.8	24.1	9183400	1329800	924140
Atf7ip2	Q3UL97-2	9	3	0	39.2	14.1	0	8759700	227080	0
Psmb4	P99026	5	2	0	35.6	13.3	0	8425400	263710	0
Arl14ep	Q8BIX3	7	1	0	28.3	3.3	0	8158200	105270	0
Rps3	P62908	9	5	6	48.6	23	30.5	8148900	1738500	973730
Shcbp1l	Q3TTP0	13	5	4	24.4	11	9.5	6787500	299050	173530
Dcaf7	P61963	8	1	0	28.7	4.4	0	6748900	26450	0
Rpl14	Q9CR57	3	3	2	17.1	15.7	11.5	6644200	1042600	887710
Psmb6	Q60692	3	1	0	12.6	3.8	0	6322100	44701	0
Psmb2	Q9R1P3	5	2	0	35.8	12.9	0	6124800	113520	0
Rpl9	A0A140T8T4	4	1	3	22.9	5.2	15.6	6001700	705070	734640
Limd1	Q9QXD8	13	2	0	31	3.9	0	5913700	53416	0
Tcp1	P11983	16	15	11	37.9	32.7	25	5869500	1672200	759020
Rpl27a	P14115	2	2	1	15.5	15.5	7.4	5568600	1289800	793560
Hk2	O08528	24	4	2	36.5	6.2	3.9	5235400	83527	30653
Arl2bp	Q9D385-2	4	0	0	28.3	0	0	5064300	0	0
Cfap20	Q8BTU1	4	1	1	17.1	6.2	6.2	4993700	153700	43696
Eif3f	Q9DCH4	8	6	2	31.9	19.7	7.8	4809300	608340	74947
Hsp90b1	P08113	17	8	9	28.8	12.2	14.5	4511300	1355800	619050
Gm6576	A0A140T8L5	5	2	4	26.2	10.9	21.3	4483300	474110	589840
Rpl30	P62889	3	2	2	34.8	24.3	24.3	4244700	847770	760330
Vdac2	G3UX26	7	5	4	29.3	21.9	17.7	4231300	1424400	787330
Eif4a1	P60843	4	3	4	27.6	14.3	21.4	4179100	650230	553130
Pdhb	Q9D051	9	6	7	34	24	26.2	4121500	876220	822150
Eif3e	P60229	15	4	2	37.8	8.1	3.8	4096000	425920	28236
Ruvbl2	Q9WTM5	13	10	10	36.1	25.3	27	4079100	802120	586180
Rps16	P14131	4	2	3	27.4	13	22.6	3979500	572340	538710
Rps8	P62242	5	5	3	26.9	27.9	16.8	3894900	796960	100100
Hspa4l	P48722	19	11	10	37.2	18	17.2	3877700	1121700	291620
Eif3b	Q8JZQ9	20	6	6	29.4	11.5	11.7	3508700	137660	113440
Hnrnpf	Q9Z2X1	3	1	1	18.8	7.2	10.4	3481400	240540	434300
Adsl	P54822	9	4	4	24.4	9.1	9.1	3380500	151330	114480
Eif3l	Q8QZY1	15	4	3	28.5	8.2	5.5	3241200	170320	30257
Sdha	Q8K2B3	8	6	5	17.9	11.4	8.9	3218800	537700	209660
Dyrk1a	A1L341	11	0	0	19.5	0	0	3194400	0	0
Hsp90ab1	P11499	8	5	5	23.9	19.8	19.6	3171500	1127200	452050
Ruvbl1	P60122	7	7	7	20.6	20.6	20.6	2822700	392360	525660
Tekt3	Q6X6Z7	9	0	0	21.8	0	0	2810700	0	0
Eif3m	Q99JX4	9	6	0	24.9	16	0	2803400	216810	0
Prdx1	B1AXW5	4	4	2	23.7	27.8	10.7	2771100	792060	338700
Rpl21	Q9CQM8	2	0	2	20.6	0	20.6	2766400	0	375810
Dynll2	Q9D0M5	2	0	1	39.3	12.4	25.8	2734900	0	38034
Eif3i	Q9QZD9	6	3	2	22.2	9.5	6.5	2720000	264890	265200
Eif3c	Q8R1B4	11	8	4	14.1	10.4	4.3	2697200	240830	42086
Dars	Q922B2	16	8	10	40.7	18.4	21.8	2555000	464570	438240
Rab2a	P53994	4	2	3	27.8	9.9	15.1	2485700	77781	150860
Arf1	P84078	4	2	2	35.4	16	22.7	2454300	554230	270120
Ccdc116	Q80X53	4	0	0	13.5	0	0	2416800	0	0
Rpl18a	A0A1D5RME4	2	0	0	22	0	0	2385100	0	0
Srsf3	P84104-2	3	0	1	24.2	0	11.3	2331200	0	79359
Tufm	Q8BFR5	8	5	3	22.3	10	7.3	2319800	372640	169860
Hdac1	O09106	5	1	1	20.1	4.4	1.9	2315100	155130	0
Eif3k	Q9DBZ5	4	0	0	22.9	0	0	2235400	0	0
Erlin2	Q8BFZ9	7	2	1	34.4	13.5	9.7	2115200	379540	275030
Pcbp2	Q61990-3	3	2	3	17.5	17.2	15.5	2076300	493820	330530
Hnrnpm	Q9D0E1-2	13	6	7	24.5	10.4	13.2	2013500	223200	199580
Rps26	P62855	2	2	1	20.9	20.9	13	1968400	443970	59258
Slc25a5	P51881	4	3	3	28.9	11.1	13.8	1964600	728990	386330
Hnrnph1	Q8C2Q7	3	3	2	16.3	13.6	12.7	1925900	132260	182720
Hnrnpl	G3UY38	7	0	0	24.8	0	0	1887200	0	0

Pask	Q8CEE6	15	1	0	17.6	1.1	0	1834000	6125.2	0
Psmc6	P62334	9	5	1	29.6	15.7	1.6	1835600	126360	145970
Yy1	Q00899	5	4	0	20.5	0	0	1800200	0	0
Cct2	P80314	14	5	7	37.2	15	21.3	1713000	367550	184630
Lpp	Q8BFW7-4	5	1	0	17.6	3.1	0	1711600	26432	0
Atxn2l	Q3TGG2	11	5	7	13.8	6.2	8.5	1683900	113740	199310
Psmc1	P62192	9	5	1	28.4	16.4	2.7	1670700	342000	62230
Rab14	Q91V41	5	4	3	30.7	24.7	19.1	1665600	270910	208360
Rpl17	Q6ZWZ7	3	1	1	21.7	5.4	5.4	1609000	235380	198370
Znf608	Q56A10-2	9	1	0	8.5	1.1	0	1582700	16931	0
Fam76b	Q80XP8	3	0	0	10.3	0	0	1560400	0	0
Ddx39a	Q8VDW0	2	2	1	16.9	9.8	9.6	1535900	322840	270740
Rpl13a	A0A140T8K2	2	2	2	10.8	10.8	10.8	1515000	441420	220350
Tmpo	Q61033	8	0	0	24.8	0	0	1476400	0	0
Sar1a	Q99JZ4	2	1	1	11.6	6.1	6.1	1464100	61274	37099
Lancl1	O89112	3	2	1	7.3	5	3.3	1457400	1425900	90943
Ipo4	Q8VI75	2	2	2	1.9	1.8	2.6	1453100	175870	13831
Cope	O89079	6	2	4	30.5	10.1	21.1	1447700	86745	245740
Irgc1	D3Z720	10	10	5	28.3	24.8	13.8	1442300	744760	250070
Psmb7	P70195	2	1	0	11.6	3.6	0	1435700	218870	0
Dnajc7	Q9QYI3	13	8	2	31.6	18.2	4	1376900	227200	25321
Slc25a4	P48962	6	4	1	35.6	14.1	5.7	1373300	523170	100990
Psmc2	P46471	8	4	4	23.3	10.6	11.3	1372900	289950	147590
Gpt2	Q8BGT5	9	6	1	24.1	15.7	1.7	1362400	351130	36029
Acsbg1	Q99PU5	11	9	7	18.9	14.7	11.7	1344100	416440	239770
Psmd3	P14685	8	5	5	17.9	11.1	11.7	1333400	156560	129110
Eif3d	O70194	7	0	0	22.4	0	0	1317200	0	0
Tex101	Q9JMI7	4	5	2	23.6	29.2	12	1300900	729610	205940
Spata20	Q80YT5	7	7	3	11.6	12.4	4.1	1291900	234350	63556
Rpl23	P62830	2	2	1	25	20.7	14.3	1208400	189460	146690
Vdac3	A0A140T8V3	2	3	2	8.8	12.4	12	1201300	554910	115100
Mtch2	Q791V5	6	3	3	27.1	12.2	12.2	1184000	137350	205320
Slc25a1	Q8JZU2	3	3	2	10.3	10.3	7.7	1179900	209920	149980
Git1	Q5F258	7	0	2	12.2	0	2.9	1178500	0	44352
Gstp1	P19157	2	2	2	12.9	12.9	12.9	1147600	108970	190610
Dpysl3	Q3TT92	7	5	0	16.9	15.1	0	1138900	306150	0
Rbbp7	A2AFI9	2	0	0	7.8	2.1	0	1128000	5899.2	0
Erp44	Q9D1Q6	3	1	0	9.9	1.7	0	1125900	35407	0
Cse1l	Q9ERK4	5	4	0	6	5.4	0	1104200	36048	0
BC051142	Q80XD0	2	0	0	12.6	0	0	1095200	0	0
Rab18	P35293	6	3	1	37.4	15.5	5.3	1066900	307930	59884
Mta2	Q9R190	8	0	0	17.2	0	0	1058400	0	0
Fntb	Q8K2I1	4	0	0	9.8	0	0	1051300	0	0
Map2k1	P31938	4	0	0	11.2	0	0	1049800	0	0
Dnaja1	P63037	2	1	0	8.1	3	0	1047200	67368	0
Ppp2ca	P63330	3	1	1	12.9	3.6	3.6	1046900	55677	90802
Hnrnpc	Q9Z204-4	6	4	3	20.2	13.7	11.3	1035000	109350	150030
Psmc3	A2AGN7	7	4	4	25.2	12.2	17.8	1011500	126150	172160
Rps6	P62754	2	1	0	7.6	3.2	0	990500	214360	0
Txndc5	A0A0R4J1Y7	5	0	0	21.4	0	0	989240	0	0
Ppp3cb	E9Q6P2	4	0	0	14.3	2	2	978220	13761	15111
Ift122	E9Q9G8	13	7	3	13.7	7.3	3.1	940480	94143	29021
Dync1h1	Q9JHU4	63	19	17	17.5	4.6	4.5	933780	64150	46986
Etfb	Q9DCW4	5	4	2	26.7	16.1	7.1	918270	365300	104840
Vps35	Q9EQH3	12	6	8	19.2	9.4	14.4	909010	176410	175350
Dcp1b	B9EIX0	7	0	0	18.5	0	0	886220	0	0
Rtcb	Q99LF4	6	5	4	11.7	9.9	7.7	884290	256210	123290
Arl14epl	Q3UKZ7	3	0	0	27	0	0	881110	0	0
Ddx6	P54823	5	0	1	15.1	0	2.3	875720	0	25034
Acp1	Q9D358	2	3	1	12.7	24.1	7	870840	610780	121220
Rab6a	P35279-2	4	2	1	22.6	11.1	5.8	870320	162080	46001
Piwil1	Q9JMB7	14	4	4	18.8	5.9	5.9	857060	67907	49387
Abce1	P61222	8	5	1	17	9	1.7	855920	205550	0
Rpl4	Q9D8E6	4	2	1	12.6	6	2.9	855550	110570	59925
Sfxn3	Q3U4F0	5	3	2	31.7	16	10	830400	249240	137810
Dnaja2	Q9QYJ0	4	1	3	15.3	2.4	12.9	825270	99066	148270
Ropn1l	A0A0R4J1E7	2	3	2	12.4	17.4	12.4	807440	341040	129330
Prpf19	Q99KP6	5	1	0	14.3	1.8	0	807250	30263	0
Eif3h	Q91WK2	3	1	0	10.8	3.4	0	802430	19465	0
Gnb2l1	P68040	3	1	0	9.8	3.8	0	799790	68625	0
Dnaaf1	Q9D2H9	7	5	1	11.2	8.7	1.7	791540	168500	31362
Rab5a	Q9CQD1	1	1	0	10.7	10.7	0	786240	215040	0
Ddx4	Q3V086	6	2	2	12.5	6.5	4.3	778370	166830	105980
Eif3a	P23116	12	2	0	11.5	1.5	0	773730	18575	0
Aldh1b1	Q9CZS1	5	3	1	13.9	6.7	3.3	767540	205100	44445
Slc3a2	P10852	5	5	3	10.3	11.8	7	765020	274290	108820
Rab1b	Q9D1G1	2	2	1	40.3	36.3	13.4	758330	211050	69761
Fahd2	A0A0R4J094	4	2	2	18.8	8.3	8.3	728130	110430	105320
Sycp1	Q62209	11	0	0	13.7	0	0	727550	0	0
Gfpt1	P47856-2	9	3	1	16.2	5.4	2.2	724890	71042	11869
Dak	Q8VC30	7	5	4	19.7	14.2	11.6	722650	154410	138030
Kpna4	A0A0B4J1E7	3	0	0	9.8	0	0	714660	0	0
Cfap36	Q8C6E0	4	1	2	16	3.8	9.3	710280	93454	52663
Psmc4	A0A140LIZ5	7	2	2	22.5	4.9	4.9	710210	136800	55476
Tmem53	A0A0A0MQK8	4	0	0	19.4	0	0	707880	0	0
Mlec	Q6ZQI3	4	1	1	20.3	4.5	4.5	707080	131580	77949
Rpl3	P27659	3	1	0	8.2	3	0	707000	102420	0
Atp2a2	O55143	8	6	3	11.6	7.7	3.7	706940	225080	50155
Pycr2	Q922Q4	4	1	1	16.2	3.4	3.4	693220	38042	74553
Eif2s3y	Q9Z0N2	4	3	0	11.7	8.7	0	676760	190040	0
Psmc5	P62196	5	8	1	16.5	24.6	2.7	674310	255690	33610

Prdx2	D3Z4A4	3	1	0	24	5.5	0	673100	20892	0
Wdr5	P61965	4	1	0	17.1	8.7	0	667290	138580	0
Hnrnpa0	Q9CX86	3	2	1	14.6	9.6	5	655280	0	38033
Eif3g	Q9Z1D1	4	0	2	14.1	0	8.8	645750	0	23622
Mtmr9	Q9Z2D0	6	1	3	11.6	1.5	4.8	644760	6178.2	68376
Fxr1	A0A0G2JEP0	4	0	0	10.6	0	0	636960	0	0
Copz1	P61924	2	2	1	13.6	13.6	5.6	623540	270880	74104
Slc25a20	Q9Z2Z6	3	1	0	11	3.7	0	621420	92189	0
Dync1li2	Q6PDL0	4	3	2	11.8	8.1	6.3	617080	265970	54339
Tpi1	P17751	2	1	0	8.7	3.3	0	613070	37244	0
BC048507	Q80ZS7	2	0	0	40.4	0	0	609720	0	0
Hsd3b1	P24815	4	2	2	11	6.7	6.7	608220	22322	62818
Timm50	Q9D880	3	2	2	10.8	6.2	6.2	605120	277650	120550
Serpinb6a	K7E6F1	4	3	1	21.9	14	6.6	600730	152180	37770
Esd	H3BJP2	3	0	0	21.9	0	0	600010	0	0
Golga4	Q91VW5	20	0	0	11.6	0	0	590940	0	0
Tdrd6	F2Z429	18	8	3	11.3	5	1.6	586920	46319	10974
Tpp2	Q64514-2	11	10	4	11.4	10.6	3.9	584830	153750	42251
Dnah8	Q91XQ0	48	10	0	13.8	2.7	0	576490	30978	0
Ddx1	Q91VR5	8	3	1	12.7	4.5	2.6	565560	40173	9986.5
Pfkp	Q8C605	6	3	2	11	8.3	3.1	565310	140120	21730
Nufip2	Q5F2E7	3	1	0	7.1	1.9	0	563330	8193.8	0
Cep72	Q9D3R3	5	2	0	9.3	3.9	0	559980	40769	0
Cdk5	P49615	3	1	2	12	6.5	6.5	542280	197000	29690
Sdhb	Q9CQA3	4	3	1	17	11.7	3.5	526940	206910	24460
Prkar2a	A0A0A6YY28	2	1	0	16.5	4.5	0	519270	96380	0
Wdr92	Q8BGF3	2	1	0	10.6	3.4	0	518880	42659	0
Upf1	Q9EPU0-2	8	2	0	10.2	1.8	0	518240	17229	0
Skp1	Q9WTX5	2	1	1	10.4	7.4	7.4	503960	136060	60179
Palm2	Q8BR92	2	0	0	10.1	0	0	499920	0	0
Dpm1	A2BDX2	4	3	0	22.1	17.3	0	495810	143170	0
Ttc30a2	A2AKQ8	7	3	0	11.7	4.4	0	484370	58629	0
Pfkm	P47857	5	1	0	8.5	2.2	0	484000	22485	0
Prkra	Q9WTX2	2	0	0	7.3	0	0	479650	0	0
Dazl	Q64368	3	3	0	13.4	15.4	0	473450	206150	0
Klhdc10	Q6PAR0-2	4	1	2	13.7	3.2	6.8	472300	19463	49786
Rbm44	Q3V089	9	1	0	11.7	1.1	0	457030	6576.2	0
Copa	F8WHL2	12	6	1	12.4	5.7	0.8	448670	76723	13118
Slc16a1	P53986	3	3	1	8.5	8.5	2.6	445130	307410	43446
Pon3	Q62087	2	0	0	7.3	0	0	437880	0	0
Sbds	P70122	3	2	1	15.2	7.2	3.2	436250	106640	37294
Pcna	A0A140T8V5	2	1	0	13	7.3	0	433080	91202	0
Glrx3	Q9CQM9	3	3	2	7.4	10.4	7.1	432440	99865	74074
Ccdc88a	Q5SNZ0-3	13	0	0	9.2	0	0	429190	0	0
Lppr4	A0A0G2JGY9	5	0	0	7.8	0	0	426320	0	0
Dctn3	E9Q919	2	2	0	11.9	11.9	0	425430	176660	0
Arl1	F8WIB1	2	0	0	18.1	0	0	424340	0	0
Homer1	E9Q0I8	4	0	0	25	0	0	416720	0	0
Mtl5	Q9WTJ6	3	1	0	10.9	1.9	0	414160	7087.1	0
Pura	P42669	2	0	0	10.9	0	0	413350	0	0
Hsd17b10	Q99N15	3	2	1	16.9	9.2	7.7	412160	36357	11130
Piwil2	Q8CDG1	7	3	2	9.1	3.7	2.9	405820	33052	30541
Boll	G3UYE8	3	1	1	11.7	3.2	3.2	400070	23474	37352
Cbx3	Q9DCC5	2	0	0	14.8	0	0	399150	0	0
Ap2a1	P17426-2	9	3	2	16.8	3.4	4	394480	43529	14784
Impa1	Q924B0	3	3	1	15.5	11.9	4	392630	287750	48606
Myef2	A2ATP5	4	2	3	10.5	6.2	8.2	387690	36873	41314
Ddb1	Q3U1J4	9	2	2	8.1	1.7	2.5	387500	22567	14822
Tdrkh	A0A0G2JFB2	4	2	0	9.4	4	0	384790	71610	0
Ddhd1	F8WHP5	4	0	1	5	0	0.9	384100	0	7668.4
Dhrs7	Q9CXR1	3	1	1	9.5	3	3	379240	77205	56720
Ube2m	P61082	3	3	1	19.7	19.7	4.9	374540	177140	46367
Ppp2r3a	B2RXC8	4	0	0	4.9	0	0	373070	0	0
Otub2	Q9CQX0	2	1	2	9	4.7	10.3	372050	57692	59141
Dhx15	A0A0G2JG10	4	1	0	7.2	2.1	0	368290	37356	0
Rsph1	Q8VIG3	2	0	0	10.6	0	0	367090	0	0
Rsph3b	Q9DA80	5	2	1	13.1	5.1	2.8	366720	29809	26966
Faf2	Q3TDN2-2	5	2	2	17.4	5.6	5.6	364430	92582	70042
Ppp2r1a	Q76MZ3	4	0	1	12.6	0	1.7	363440	0	13410
Hnrnpa3	A2AL12	4	2	1	19.8	10.1	6.9	362830	76167	32688
Txnl1	Q8CDN6	2	3	1	10	10.7	2.4	359900	110780	17998
Eef2	P58252	7	2	2	13.4	2.1	3.8	359390	71959	52551
Copb1	Q9JIF7	5	1	0	6.9	1.9	0	352700	18540	0
Sccpdh	Q8R127	5	1	1	20.5	2.3	2.3	346370	57334	57658
Hsd17b12	O70503-2	3	0	0	22	0	0	336540	0	0
Rpap3	Q9D706	4	3	4	8.2	6.8	10.2	335190	49348	56312
Prkaca	P05132-2	2	1	2	7.3	3.5	7.3	334020	7143.4	63689
Hspa4	Q3U2G2	7	5	3	15.4	9.3	5	331840	72026	20918
Eif4g1	A0A0J9YUS5	6	1	0	6.6	1.2	0	330870	7924.8	0
Ppp3cc	P48455	3	3	1	11.3	9.6	3.9	327930	114480	17566
Ppp5c	F7BX26	3	0	0	9.5	0	0	326330	0	0
Nap1l1	Q3TF41	1	2	0	7.3	10.3	0	323780	153680	0
Lrrc46	Q9DAP0	2	2	1	7.4	7.4	4	318820	66027	35682
Vapa	Q9WV55	2	1	2	5.6	4.8	9.6	307250	54907	60028
Gm1141	B9EJU1	2	0	0	5.7	0	0	304310	0	0
Camk2g	Q923T9-3	2	2	1	8.3	4	4.6	298390	8613.4	35599
Hsd3b6	O35469	3	2	0	9.9	6.4	0	297150	42462	0
Fam49b	Q921M7	3	3	0	14.2	13.9	0	294550	135380	0
Spag1	Q80ZX8-3	4	3	0	8.1	6.1	0	290980	30285	0
Cbwd1	Q8VEH6	2	2	0	6.6	6.4	0	289890	94421	0
Psmd1	Q3TXS7	9	2	2	14.5	2.3	3.3	288850	15023	26996

Acads	Q07417	3	2	2	12.4	6.1	8	288670	102310	49595
Gkap1	Q9JM80	2	1	1	9.6	3.8	3.8	284690	23483	20598
Kif3b	Q61771	4	4	1	5.6	5	1.1	283560	117870	23225
Pygb	Q8CI94	6	5	2	8.8	5.9	2.1	280890	101420	43039
Wdr35	Q8BND3-2	10	3	1	12.1	2.7	0.8	280390	19254	7883.2
Sirt3	D3YVQ5	2	0	1	13.7	0	6	279700	0	54827
Cand1	Q6ZQ38	10	8	5	10	7.9	5.2	275300	143200	27601
Cnot7	Q60809	3	1	0	11.9	3.5	0	275070	5354.1	0
Nap1l4	B7ZNL2	2	3	1	10.1	14.5	2.8	273030	261560	0
Mark3	Q03141-2	7	0	0	13.3	0	0	271870	0	0
Crybg3	Q80W49	5	0	0	7.4	0	0	264910	0	0
Cpsf1	Q9EPU4	8	2	1	6	1.4	0.7	260070	6062.7	9855.8
Dld	O08749	2	2	1	5.3	5.3	2.6	259270	59387	32729
Cntrl	R4GML3	15	0	0	9	0	0	259050	0	0
Nlk	O54949	2	0	0	4	0	0	259050	0	0
Psmg1	Q9JK23	2	1	1	5.9	3.5	3.5	258480	35351	19395
Ctps1	P70698	4	5	2	8.5	10	3	258360	123640	20783
Ift140	E9Q682	6	4	2	5.4	3.4	1.5	258210	45418	26535
Fdps	A0A0G2JDJ5	2	0	1	23.1	0	12.4	257600	0	17584
Ppp2r2a	Q6P1F6	3	0	0	10.1	0	0	256040	0	0
Lrrc34	Q9DAM1	4	1	0	11.1	2.4	0	254610	0	0
Tcp11	Q5FWA2	2	0	1	4.3	0	1.8	254130	0	29894
Kpna2	P52293	3	2	0	8.5	5.1	0	251280	13443	0
Ranbp9	E9Q5D6	3	1	0	6.2	2	0	250650	7815.5	0
Mael	A0A0A6YWQ9	2	0	0	4.8	0	0	247850	0	0
Sae1	Q9R1T2-2	3	2	1	15.9	5.8	2.4	245020	75958	27300
Cpsf2	O35218	3	0	0	4.1	0	0	241940	0	0
Spata5	A0A0G2JFY0	9	2	0	17.5	3.1	0	239890	13235	0
Pfkl	P12382	4	1	1	9.4	5.5	1.9	238890	11129	12725
Trim36	E9Q3A0	5	1	0	9.3	2	0	237780	18278	0
Hdac2	A0A0R4J008	2	0	0	12.3	2.5	0	237200	0	0
Psme3	A2A4J1	2	0	1	14.8	0	7.4	236880	0	33185
Bag5	Q8CI32	3	1	0	6	1.8	0	235320	22304	0
Srsf6	Q3TWW8	1	1	0	5.3	5.3	0	235320	45476	0
Ap2b1	H3BKM0	4	2	2	10.2	3.7	3.5	233480	121610	29838
Tuba8	Q9JJZ2	2	1	1	33.9	15.4	23.8	227950	48755	13809
Memo1	Q91VH6	2	1	0	6.7	4.4	0	227370	35873	0
Ahsa1	Q8BK64	2	1	1	8.6	3	6.5	227160	2825.1	20386
Wdr62	Q3U3T8-3	7	3	3	5.9	2.3	2.3	226580	20886	24932
Ddx17	Q3U741	4	4	1	16	15.8	11.3	224510	52265	9686.9
Dnaaf2	Q8BPI1	4	3	1	9.8	4.3	1.2	223830	36053	5740.7
Cad	E9QAI5	12	6	1	8	3.5	0.6	222280	52548	5471.4
Psmd11	Q8BG32	4	2	2	10.9	4	5.5	220960	42386	31410
Cdc42	P60766	2	1	1	14.1	5.2	8.9	219500	188620	21874
Acsf2	Q8VCW8	3	4	2	7.5	8	5	218030	92766	40701
Hacd3	Q8K2C9	2	0	0	8.6	0	0	215640	0	0
Ythdc2	B2RR83	8	1	0	6.4	0.8	0	214670	7274.5	0
Samm50	Q8BGH2	3	0	1	7.7	0	3.8	214340	0	17521
Cnbp	P53996-2	2	0	0	17.1	0	0	211670	0	0
Bag2	Q91YN9	1	2	0	5.2	10	0	210820	85286	0
Slc25a11	Q5SX46	3	0	0	19.2	0	0	210070	0	0
Tgm2	P21981	3	3	1	6	5.7	1.7	208830	105310	9540.4
Kbtbd6	E9PYD7	3	0	0	6.4	0	0	208470	0	0
Atxn10	P28658	3	2	1	9.1	5.5	3.2	207550	40826	13762
Ttc21b	E9PVK4	5	4	2	6.1	4.2	1.8	203810	59131	22622
Adad1	F8WI80	3	0	0	10	0	0	202110	0	0
Ccnyl1	E9Q226	3	1	0	12.4	2.7	0	199020	17207	0
Tekt4	Q149S1	3	0	0	7.4	0	0	198690	0	0
Isyna1	Q9JHU9	3	0	1	7	0	2.9	198250	0	39557
Eif2s1	Q6ZWX6	3	0	0	11.1	0	0	195960	0	0
Zswim6	Q80TB7-2	4	0	0	5	0	0	195960	0	0
Ncl	P09405	4	2	1	6.4	3.1	1.3	195410	13639	6349.7
Rere	Q80TZ9	4	3	0	4	2.1	0	195200	59834	0
Wdr19	Q3UGF1-3	6	1	1	7.1	1.6	0.7	193870	12358	6047.5
Kif3a	Q3TET1	5	2	1	8.2	3	1.6	189240	41939	12334
Sec23a	E9Q1S3	2	1	1	7.5	1.5	1.8	189000	32133	6746.4
Gtf2h4	O70422	2	1	0	5.4	2.8	0	187670	28270	0
Ipo5	Q8BKC5-2	11	5	1	16	6.4	1	185270	75795	7677.2
Cdv3	A0A087WNP6	2	0	0	6.8	0	0	185140	0	0
Cpsf4	B2LVG5	2	0	0	8.2	0	0	184200	0	0
Atr	E9QPK4	4	4	0	2	2	0	183100	25634	0
Polr2b	Q8CFI7	7	2	1	7.2	1.6	0.8	181660	15678	6599.5
Mta1	F8WHY8	3	1	0	5	1.7	0	179000	2866.1	0
Pdxdc1	A0A0R4J034	3	1	1	4.6	1.4	1.4	178050	6034.6	5864.8
Drg1	P32233	4	1	1	12.5	3	3	177610	12588	33017
Arhgef7	D3Z0V2	2	0	0	6.8	0	0	176870	0	0
Ddx19a	Q61655	2	0	1	4.4	0	2.3	173620	0	6600.8
Larp7	Q05CL8	3	2	0	7.2	4.6	0	172750	19078	0
Mbd2	Q9Z2E1	2	0	0	7	0	0	171010	0	0
Akap12	Q9WTQ5-2	7	7	2	8	6.5	1.9	170590	66342	20853
Ncbp1	Q3UYV9	2	0	0	2.8	0	0	166040	0	0
Ssb	A2AR07	2	0	1	15.2	0	7.6	165690	0	18860
Atp6v1h	A0A0A6YX18	2	0	0	5.6	0	0	163630	0	0
Rnf17	Q99MV7	8	4	1	5.7	2.9	0.7	161450	29164	4053.3
Cpsf3	Q9QXK7	3	0	1	7.3	0	1.5	161340	0	4511.5
Vps26a	P40336	2	2	0	8.3	7.6	0	159140	39465	0
Nos1ap	Q9D3A8	4	0	0	7.8	0	0	158060	0	0
Tktl2	A0A0R4J2A3	3	2	1	6.9	4.6	2.4	156580	36250	7773.6
Eno4	A0A0J9YVG9	2	0	0	6.7	0	0	156500	0	0
Pih1d1	Q9CQJ2	2	0	0	9.3	0	0	156430	0	0
Acad8	D3YTT4	2	2	1	5.3	5.3	3.4	153130	44927	23960

Ppp3r2	Q63811	1	2	0	6.7	12.8	0	152260	109910	0
Ddx3x	Q62095	3	4	2	8.2	9.1	6.1	151650	243430	32088
Strap	Q9Z1Z2	2	3	0	7.4	10	0	148850	65140	0
Vps4a	Q8VEJ9	3	2	1	7.8	4.6	2.5	148880	19193	18613
Tuba4a	A0A0A0MQA5	3	0	0	43.2	11.9	21.6	145390	0	0
Trap1	Q9CQN1	4	5	0	6.9	8.1	0	143070	57267	0
Cdc5l	Q6A068	4	1	1	8.2	1.2	1.2	142120	5254.2	11743
Trim3	Q3TDT0	3	0	0	4.5	0	0	141550	0	0
Trafd1	Q3UDK1-2	2	1	0	3.3	1.7	0	140480	12267	0
Kif2a	F8VQ42	3	2	0	5.8	3.1	0	139200	15451	0
Kpnb1	P70168	5	2	3	6.1	3.1	4.1	137970	14127	24432
Copg2	Q9QXK3-4	3	2	0	7.7	3.4	1.4	137030	12674	2970.7
Nfatc2ip	O09130	2	0	0	8.7	0	0	136600	0	0
Golga1	Q9CW79	4	0	0	5.1	0	0	136190	0	0
Tdrd9	Q14BI7	8	1	0	7.4	0.8	0	133480	5407.1	0
Cct6b	Q61390	3	1	0	12.1	4.9	3.2	132900	25309	0
Rbm39	F7AA45	2	2	0	9	9	0	132480	38314	0
Dcaf5	Q80T85	5	0	0	6	0	0	131770	0	0
Sec24b	Q80ZX0	3	0	0	4.4	0	0	131750	0	0
Hnrnpul1	Q8VDM6-2	3	2	0	5.5	3.6	0	131200	27853	0
Smc4	E9Q2X6	4	1	0	3.6	0.7	0	130810	9056.2	0
Kif9	Q14BL9	3	0	0	7	0	0	126680	0	0
Nxn	P97346-2	3	1	0	9.2	2.3	0	125970	18839	0
Ap1m1	P35585	3	1	0	8.3	2.6	0	124980	7231.2	0
Serpinh1	P19324	2	1	1	6.5	2.9	2.9	122760	14970	13822
Cog6	Q8BRB0	4	0	0	6.9	0	0	122370	0	0
Usp9x	Q4FE56	10	2	0	4.9	1	0	121220	7683.3	0
Acaa1a	H3BKL5	2	0	0	8.3	0	0	120630	0	0
Arcn1	Q5XJY5	3	3	0	6.3	6.3	0	120020	19442	0
Eftud2	G3UZ34	4	1	0	5.4	1.2	1	118650	18337	0
Pdcd4	Q61823	2	1	1	6.8	2.3	2.3	117650	24683	13069
Nsf	P46460	4	3	1	5.9	4.8	1.7	116780	60492	13947
Hk1	G3UVV4	3	4	0	7.4	5.9	1.2	115950	81371	0
Gatad2a	A0A1I7Q4G8	2	0	0	3.9	0	0	115120	0	0
Lpcat3	Q91V01	2	0	0	5.1	0	0	114180	0	0
Mapk3	D3Z3G6	2	1	0	8.4	4.5	0	113360	36324	0
Setx	A2AKX3-2	5	2	0	3.3	1.1	0	113190	7251	0
Snrnp200	Q6P4T2	10	5	1	5.8	2.3	0.5	112810	22770	3551.8
Ankrd32	Q8R3P9	4	0	0	4.2	0	0	112710	0	0
Chd4	E9QAS4	6	0	0	3.3	0	0	110340	0	0
Axdnd1	J3QNG8	2	1	1	5.1	2.3	2.3	110270	4474.8	6949.4
Xpnpep1	S4R1I3	2	2	1	4.3	4.3	2.5	107720	26558	16217
Stkld1	Q80YS9	3	1	0	4.1	1.5	0	107490	4501.5	0
Nup93	Q8BJ71	4	2	1	7	2.8	1.3	106910	18232	9246.5
Psmd5	Q8BJY1	2	2	1	5.6	3.6	1.8	106410	66715	18125
Rhot1	Q8BG51	3	0	0	4.8	0	0	105920	0	0
Usp7	F8VPX1	5	0	0	5.7	0	0	105410	0	0
Mcm7	Q61881	4	1	0	7.9	2.4	0	105100	19153	0
Cul3	Q9JLV5	3	6	1	6.8	9.6	1.3	104730	187950	6432.1
Tbp	F6XYI9	2	1	0	12	4.8	0	104620	54880	0
Edc4	A0A0R4J1Q0	4	3	1	4.7	2.8	0.9	102190	33715	9754.5
Kctd19	Q562E2	4	0	0	4.2	0	0	100320	0	0
Ntpcr	D3YXL1	2	0	0	17.2	0	0	99917	0	0
Prune	Q8BIW1	2	1	0	6.4	3.3	0	99389	13298	0
Abcg2	S4R2E1	2	1	0	3.8	1.7	0	98756	33028	0
Trip13	Q3UA06	2	2	0	5.3	5.3	0	98523	41275	0
Aldh9a1	Q9JLJ2	2	4	1	4.7	9.5	2.2	97842	147000	16520
Morc3	A0A0J9YU83	2	0	0	2.8	0	0	97479	0	0
Dnah7b	L7N1Y0	3	0	0	4	1.4	0	95945	6181.1	0
Cfap70	D3Z1K9	3	0	0	3.9	0	0	94813	0	0
Gstz1	Q9WVL0	1	2	0	6	11.1	0	94777	84057	0
Scrib	Q80U72	5	0	0	3.3	0	0	94549	0	0
Ccnt1	Q9QWV9	2	0	0	3.9	0	0	92897	0	0
Rab11fip5	A0A0N4SW73	2	0	0	2.1	0	0	92862	0	0
Ogdh	Z4YJV4	4	1	1	4.5	0.9	0.9	92581	6521.4	8280.8
Fbln5	Q9WVH9	2	1	0	3.8	2	0	91860	18271	0
Ero1lb	Q8R2E9	2	0	0	6	0	0	91238	0	0
Sgk3	A0A087WR70	2	0	0	7.2	0	0	89785	0	0
Lrch3	B7ZWM8	3	1	0	5.8	1.7	0	88409	5478.6	0
Cnot1	B7ZWL1	8	3	5	3.9	1.4	2.2	86930	6917.2	13170
Dync1li1	Q8R1Q8	2	2	0	5.9	6.9	0	83447	34674	0
Wdr63	B2RY71	3	2	0	3.5	3.1	0	78378	18246	0
Cpt1a	P97742	3	1	0	5.2	1.2	0	78207	11780	0
Rnh1	A0A1B0GSG5	2	0	0	6.1	0	0	76932	0	0
Ccp110	Q7TSH4	2	1	0	3.6	1.7	0	76729	9870.9	0
Iars	Q8BU30	4	2	2	3.5	1.5	2.1	76197	19714	14759
Man2c1	E9PZ88	4	1	0	5.4	1	0	75318	9879.4	0
Ccdc170	F6ST92	2	0	0	3.5	0	0	73811	0	0
Pla2g6	P97819	4	1	1	7.7	1.5	1.5	70921	13457	6259
Stt3a	P46978	1	3	1	1	4.5	1.6	68258	123100	12137
Nedd4	P46935	2	0	0	4.7	0	0	68196	0	0
Ift172	Q6VH22	6	3	0	4.6	1.9	0	66988	13992	0
Lars	Q8BMJ2	5	8	0	5.1	8.8	0	66950	81840	0
Ccdc39	Q9D5Y1	4	2	0	4.4	2	0	66489	28133	0
Dnajb9	Q9QYI6	1	2	0	4.5	11.3	0	66228	60676	0
CXorf49	Q9D454	2	0	0	6	0	0	66049	0	0
Dnah17	E9Q7P0	14	2	0	4.3	1.1	0	65536	3926.3	0
2610020H08I	D3Z3J7	3	0	0	8.8	0	0	64770	0	0
Gtf2e1	Q9D0D5	2	0	0	8.2	0	0	62912	0	0
Gm20425	E9Q035	1	4	1	1.9	5.5	1.9	62605	58191	10148
Mcm4	P49717	2	1	0	3.2	1.5	0	62576	15361	0

Tdrd1	Q99MV1	4	1	0	4.2	0.9	0	60474	3896.1	0
Nrd1	A2A9Q3	2	1	0	1.9	0.9	0	59271	37613	0
Atp2b4	Q6Q477-2	2	2	0	3.2	2.4	0	58824	48365	0
Ufl1	Q8CCJ3-1	2	0	0	3.8	0	0	57646	0	0
Zmynd10	Q99ML0	2	1	0	7.3	2.5	0	57441	19531	0
Stat4	Q3V157	3	0	0	4.4	0	0	57358	0	0
Cdyl	Q9WTK2-2	3	1	0	7.2	2.6	0	56830	4383.4	0
Bbs1	Q3V3N7	3	0	0	6.7	0	0	55614	0	0
Ccdc65	Q8VHI7	2	2	0	4.5	3.2	0	55608	17939	0
Tfip11	Q9ERA6	2	0	0	2.3	0	0	53479	0	0
Rabl6	Q5U3K5	2	0	0	3.6	0	0	52979	0	0
Gars	Q9CZD3	3	0	0	7.4	0	0	52288	0	0
Cog7	A0A0R4J0Q9	1	2	0	1.2	2.5	0	51772	16075	0
Prpf8	Q99PV0	4	0	0	3	0.3	0	50289	1569.1	0
Ttc27	Q8CD92-2	2	1	0	2.7	1.7	0	50179	5007.9	0
Lrrc40	A0A0R4J0W6	3	2	1	4.7	3.3	1.7	50000	13109	5628.3
Ap2a2	P17427	2	1	0	6.1	1.2	1.9	49091	12920	0
Aldh1l1	Q8R0Y6	2	2	0	3.1	2.9	0	48148	9067.7	0
Hspbp1	A0A0U1RPF2	2	0	0	6.9	0	0	46940	0	0
Smarcc2	Q3UID0	2	1	1	3.2	1.9	1.3	46610	3605	7183.4
F13a1	Q8BH61	2	1	0	2.9	1.8	0	45541	10832	0
Alg2	Q9DBE8	1	2	0	3.9	5.3	0	45065	43899	0
Cep162	Q6ZQ06	3	0	0	2.1	0	0	44562	0	0
Cfap43	E9Q7R9	5	1	0	4.6	0.6	0	44532	9984.5	0
Flna	B7FAV1	4	3	2	2.3	1.5	1.2	44068	11629	8559.6
Efhd2	Q8C845	2	0	0	7.5	0	0	43924	0	0
Csnk1a1	H7BXB1	2	1	0	6.6	3.3	0	42046	64938	0
Nphp1	Q3TWM5	3	0	0	5.5	0	0	41800	0	0
Usp34	F6WJB7	6	0	0	2	0	0	41209	0	0
Sec23ip	G3X928	2	1	1	2.8	1	1	41041	6169.7	5116.2
Copb2	O55029	2	0	1	3.2	0	1	39965	0	6625.2
Mta3	Q3U3A7	2	0	0	4.9	0	0	39679	0	0
Odf2	A3KGV9	2	1	1	3.8	1.7	2	38756	9742.9	5876.7
Dnajc13	G3X922	5	1	3	3.3	0.6	1.5	38371	1681.6	4889.1
Pgm3	Q8BWW3	3	0	0	6	0	0	38182	0	0
Cab39	Q06138	2	0	0	5.9	0	0	36796	0	0
Wdr66	E9Q743	3	0	0	3.2	0	0	36334	0	0
Atp1a4	Q9WV27	2	2	0	2.5	2.5	0	36272	19114	0
Ppl	G5E898	7	0	0	4	0	0	35564	0	0
Ddx46	Q569Z5	2	3	0	1.9	3.1	0	35212	18628	0
Ttc26	Q8BS45	2	2	0	5.8	4.5	0	35047	33299	0
Mios	Q8VE19	3	0	0	3.7	0	0	34599	0	0
Nsun2	H3BKN0	2	0	0	3.9	0	0	33273	0	0
Dync2h1	Q45VK7	10	3	1	2.8	0.7	0.2	32680	3737.9	940.26
Ssr1	Q9CY50	1	2	0	5.2	9.1	0	32235	195720	0
Radil	D3YWJ9	3	0	0	4.4	0	0	31909	0	0
Ccdc136	E6Y2W7	2	0	0	3	0	0	31579	0	0
Skiv2l2	Q9CZU3	2	1	1	2.4	1	1.1	29891	8670	3164.3
Dnah12	Q3V0Q1	5	1	0	2.1	0.8	0	29816	2160.8	0
Hprt1	P00493	2	1	0	9.2	6	0	28933	48983	0
Dnah1	E9Q8T7	6	0	0	2	0.2	0	28729	0	0
Prpf6	Q91YR7	2	1	0	2.2	1.3	0	28301	0	0
Myo7a	A0A0U1RPX7	3	3	0	1.5	1.4	0	27244	7171.6	0
Dock11	A2AF47	4	0	0	2.1	0	0	26722	0	0
Ap3b1	Q9Z1T1	3	1	0	3	1	0	26254	1599.4	0
Fyco1	A0A140T8V9	2	0	0	2.5	0	0	26216	0	0
Psme4	Q5SSW2	3	1	0	1.7	0.7	0	25422	3386.8	0
Dnmt1	J3QNW0	3	0	0	1.9	0	0	23615	0	0
Akap4	Q60662-2	2	0	0	2.7	0	0	23497	0	0
Tfrc	Q62351	2	2	0	2.6	2.8	0	23486	23392	0
Gart	Q64737	3	0	0	4.4	0	0	23147	0	0
Ckap5	Z4YL78	3	3	0	2	1.9	0	21756	10433	0
Eps15	F6W2Q5	2	1	0	3.9	1.7	0	21254	12446	0
Plaa	P27612	1	2	0	2.5	3.4	0	20809	24636	0
Cul9	E9QP09	3	2	0	1.1	0.6	0	20528	4934	0
Npepps	F6QYF8	1	2	0	1	2.7	0	19833	17469	0
Clmn	Q8C5W0-2	2	1	0	2.9	1.8	0	19268	10965	0
Dock7	A0A0U1RNK7	3	4	0	1.8	2.1	0	18732	33026	0
Ssh2	Q5SW75	3	28	1	3.3	25.3	1.5	18474	2541200	4329.2
Usp47	A0A1L1SV73	2	1	0	2.5	1.2	0	18169	2177.4	0
Smc6	Q924W5	2	0	0	2.3	0	0	17639	0	0
Ubr5	E9Q2H1	2	0	0	1.1	0	0	17518	0	0
Mcm5	Q52KC3	1	3	0	1.5	5	0	17408	42438	0
Glmn	Q3T9A5	2	1	0	3.9	2.1	0	17220	3517.9	0
Vps13a	Q5H8C4-2	2	0	0	0.9	0	0	17018	0	0
Pakap	F7AA26	2	0	0	4.4	0	0	16750	0	0
Zw10	O54692	2	0	0	3.2	0	0	16683	0	0
Ide	F6RPJ9	2	1	0	2.4	1.2	0	16007	5823.4	0
Ahnak	E9Q616	3	3	1	5.4	6.5	3.4	15941	4625.2	3137.3
Kntc1	Q8C3Y4	4	0	0	2	0	0	15487	0	0
Arhgap31	A6X8Z5	2	0	0	2	0	0	15078	0	0
Lbr	Q3U9G9	1	3	0	3	5.3	0	13879	326000	0
Timm44	O35857	1	2	0	2.7	5.5	0	13736	22391	0
Myo6	E9Q175	1	5	0	0.9	4.8	0	13388	68514	0
Gcn1l1	E9PVA8	6	1	0	2.7	0.3	0	13234	901.05	0
Eefsec	A0A0N4SUV6	1	3	0	3	7.3	0	13091	35075	0
Trip12	A0A087WRV6	3	0	0	4.7	0	0	11882	0	0
Acaca	Q5SWU9	1	3	0	0.8	1.8	0	11324	15340	0
Dnah7c	A0A087WR13	2	0	0	3.8	1.4	0	10715	0	0
Dnah3	A0A140LIN9	3	3	0	1.1	1	0	10194	2413.4	0
Eif4g2	F7CBP1	2	0	0	2.1	0	0	9997.1	0	0

Uba1	Q02053	1	2	0	1.7	2	0	9898.3	3630.8	0
Sf3b1	G5E866	2	4	0	2.8	4.1	0	9759.3	0	0
Dnah6	E9Q0B6	1	1	0	0.6	0.5	0	8370.8	543.27	0
Cdk1	P11440	1	1	0	8.1	6.4	0	7093.3	41663	0
Cdc73	Q8JZM7	2	0	0	3.4	0	0	6357.8	0	0
Btaf1	E9QAE3	2	0	0	1.6	0	0	5740.5	0	0
Nbas	E9Q411	3	0	0	1.2	0	0	5442.9	0	0
Snx29	Q9D3S3	1	21	0	1.8	30.2	0	4321.8	5181600	0
Dock6	E9QPN7	2	0	0	1.3	0	0	3972.2	0	0
Usp5	Q3U4W8	1	2	0	1.9	4.1	0	3715.8	28815	0
Dnm1l	E9PUD2	1	2	0	1.4	2.7	0	3561	5640.7	0
Sptb	E9Q397	2	0	0	1.1	0	0	1715.4	0	0
Ppfia4	A0A087WPM7	0	3	0	0	8.4	0	0	51056	0
Abcd3	A0A0G2JDI9	0	3	0	0	9.5	0	0	46333	0
Lrrfip2	A0A0R4J169	0	4	0	0	10.8	0	0	445410	0
Tmcc1	A0A0N4SWB9	0	2	0	0	4	0	0	182350	0
Mthfd1	A0A1W2P733	0	2	0	0	3.2	0	0	29628	0
Elac2	B1ATP7	0	2	0	0	2.3	0	0	7118.3	0
Ppfia1	B2RXW8	0	3	0	0	7.1	0	0	50159	0
Ppfia2	B8QI34	0	17	0	0	23.6	0	0	2219500	0
Cit	F6SBR5	0	8	1	0	4.5	0.4	0	56966	0
Zc3hc1	D3Z3D0	0	2	0	0	7.4	0	0	50351	0
Adam3	E9QA56	0	2	0	0	18.1	0	0	118150	0
Uggt2	E9Q4X2	0	3	0	0	1.9	0	0	20927	0
Psmd13	E9Q5I9	0	2	0	0	5.2	0	0	42839	0
Kctd10	F8WGQ9	0	5	0	0	20.3	0	0	1042300	0
Armc8	G3X920	1	2	0	1.9	3.4	0	0	7961.5	0
Carkd	J3QN06	0	3	0	0	16.9	0	0	105280	0
Ptgis	Q8BXC0	0	2	0	0	3.3	0	0	52732	0
Tnfaip1	O70479	0	3	0	0	13.6	0	0	124120	0
Rbx1	P62878	0	2	0	0	17.6	0	0	192900	0
Naca	P70670	0	2	0	0	1.1	0	0	4777.4	0
Ppp4c	P97470	1	2	0	2.6	6.2	0	0	20715	0
Cdk16	Q04735-2	0	2	0	1.7	6.3	0	0	25675	0
Pnma5	Q5DTT8	0	4	0	0	8.3	0	0	198370	0
Capn11	Q6J756	0	2	0	0	2.5	0	0	6118.1	0
Pdcl2	Q78Y63-2	0	2	0	0	16.7	0	0	112950	0
Kctd13	Q8BGV7	0	5	0	0	22.2	0	0	853860	0
Bri3bp	Q8BXV2	0	2	0	0	13	0	0	237940	0
Spice1	Q8C804	0	2	0	0	3.3	0	0	13331	0
CX049	Q8CFE2	0	2	0	0	7.8	0	0	64455	0
Aldh4a1	Q8CHT0	0	2	0	0	5.5	0	0	38735	0
Grhpr	Q91Z53	0	2	0	0	6.1	0	0	84097	0
Cabyr	Q9D424	0	2	0	0	7.5	0	0	112910	0
Flii	Q9JJ28	0	8	0	0	7.6	0	0	123240	0
Cd2ap	Q9JLQ0	0	2	0	0	3.6	0	0	37269	0
Pacsin2	Q9WVE8	0	4	0	0	9.5	0	0	451210	0
Clic1	Q9Z1Q5	0	3	0	0	17.4	0	0	83915	0
Mthfd1l	Q3V3R1	0	3	1	0	3.8	1	0	27875	4522.5
Clpx	Q6P8N8	0	5	1	0	9.4	1.8	0	104310	8649.9
Ranbp1	P34022	0	2	1	0	10.8	5.4	0	2216000	88253